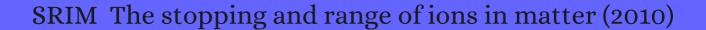
CITATION REPORT List of articles citing



DOI: 10.1016/j.nimb.2010.02.091 Nuclear Instruments & Methods in Physics Research B, 2010, 268, 1818-1823.

Source: https://exaly.com/paper-pdf/47860657/citation-report.pdf

Version: 2024-04-25

This report has been generated based on the citations recorded by exaly.com for the above article. For the latest version of this publication list, visit the link given above.

The third column is the impact factor (IF) of the journal, and the fourth column is the number of citations of the article.

#	Paper	IF	Citations
2242	On-state analytical modeling of IGBTs with local lifetime control. 2002 , 17, 815-823		11
2241	The human visual system: how is its design related to the physics of the natural environment?.		
2240	Impact of Proton Irradiation-Induced Bulk Defects on Gate-Lag in GaN HEMTs. 2009 , 56, 3192-3195		24
2239	. 2010 , 46, 2020-2023		16
2238	MetalSemiconductor FieldEffect Transistor (MESFET). 2010,		
2237	Deep levels induced by reactive ion etching in n- and p-type 4HBiC. 2010 , 108, 023706		32
2236	New Radiophotoluminescence Glass Dosimeter with Specialized Radiation-Sensitive Surface Layer. 2010 , 49, 116401		3
2235	Effect of Electron Flow Direction and Via Number on Electromigration Mechanism for Copper Dual Damascene Interconnects. 2010 , 49, 124201		1
2234	Evidence of nontermination of collective rotation near the maximum angular momentum in Rb75. 2010 , 82,		5
2233	Microscopic description of the thermalization process during pulsed laser deposition of aluminium in the presence of argon background gas. 2010 , 43, 425205		9
2232	Evidence of light guiding in ion-implanted diamond. 2010 , 105, 233903		46
2231	Research Activities in Fission Chamber Modeling in Support of the Nuclear Energy Industry. 2010 ,		12
2230	Monte Carlo simulation of the subsurface growth mode during pulsed laser deposition. 2011 , 110, 043	304	15
2229	4He+ ion beam irradiation induced modification of poly(dimethylsiloxane). Characterization by infrared spectroscopy and ion beam analytical techniques. 2011 , 27, 3842-8		30
2228	On the mechanisms of precipitation of graphene on nickel thin films. 2011 , 96, 46003		135
2227	Modification of the structure of diamond with MeV ion implantation. 2011 , 20, 774-778		21
2226	Locations of boundaries of outer and inner radiation belts as observed by Cluster and Double Star. 2011 , 116, n/a-n/a		26

2225	Ion Beam Shepherd for Contactless Space Debris Removal. 2011 , 34, 916-920		126
2224	Low energy focused ion beam milling of silicon and germanium nanostructures. 2011 , 22, 105304		19
2223	14 MeV Neutrons SEU Cross Sections in Deep Submicron Devices Calculated Using Heavy Ion SEU Cross Sections. 2011 , 58, 848-854		11
2222	Chemical control of the charge state of nitrogen-vacancy centers in diamond. 2011 , 83,		230
2221	Measurements of high energy loss rates of fast highly charged U ions channeled in thin silicon crystals. 2011 , 84,		4
2220	Effects of grain size and temperature on mechanical and failure properties of ultrananocrystalline diamond. 2011 , 20, 1303-1309		25
2219	Ion Beam Analysis: A Century of Exploiting the Electronic and Nuclear Structure of the Atom for Materials Characterisation. 2011 , 04, 41-82		33
2218	Electronic excitations of slow ions in a free electron gas metal: evidence for charge exchange effects. 2011 , 107, 163201		47
2217	Resonant charge transfer in low-energy ion scattering: Information depth in the reionization regime. 2011 , 605, 1913-1917		23
2216	Localized subsurface modification of materials using micro-low-energy multiple ion beamlets. 2011 , 1, 042150		7
2215	Sensitization of Solid State Nuclear Track Detector in Carbon Dioxide for Improved Fast Neutron Dosimeter. 2011 , 46, 163-167		4
2214	Investigation of boron implantation into silicon by quantitative energy-filtered transmission electron microscopy. 2011 , 326, 012053		1
2213	Ion irradiation of carbonaceous interstellar analogues. 2011 , 529, A146		60
2212	Quantum control of proximal spins using nanoscale magnetic resonance imaging. 2011 , 7, 687-692		100
2211	DNA damage response signaling in lung adenocarcinoma A549 cells following gamma and carbon beam irradiation. 2011 , 716, 10-9		19
221 0	EAGLEThe central European Array for Gamma Levels Evaluation at the Heavy Ion Laboratory of the University of Warsaw. 2011 , 659, 84-90		10
2209	Test of a micromegas detector with helium-based gas mixtures for active target time projection chambers utilizing radioactive isotope beams. 2011 , 660, 64-68		7
2208	Focused ion beam fabrication and IBIC characterization of a diamond detector with buried electrodes. <i>Nuclear Instruments & Methods in Physics Research B</i> , 2011 , 269, 2340-2344	1.2	28

2207	An empirical formula for calculation of range of charged particles with Z from 2 to 103 and energy from 2.5 MeV/nucleon to 500 MeV/nucleon in beryllium. <i>Nuclear Instruments & Methods in Physics</i> 1.2 <i>Research B</i> , 2011 , 269, 2145-2149	3
2206	Can swift heavy ions create latent tracks in silicon?. <i>Nuclear Instruments & Methods in Physics Research B,</i> 2011 , 269, 2649-2656	19
2205	Real-time in situ study of hydrogen diffusion in amorphous Si formed by ion implantation. <i>Nuclear Instruments & Methods in Physics Research B</i> , 2011 , 269, 2657-2661	4
2204	Sub-100keV ion beam generation with a Van De Graaff accelerator using an external DC voltage supply. <i>Nuclear Instruments & Methods in Physics Research B</i> , 2011 , 269, 2699-2702	1
2203	Comparison of the response of various TLDs to cosmic radiation and ion beams: Current results of the HAMLET project. 2011 , 46, 1680-1685	22
2202	Calculation of the relative efficiency of thermoluminescent detectors to space radiation. 2011 , 46, 1728-1731	9
2201	Feasibility study of solid-state microdosimetry for energetic protons and heavy ions with coincident particle identification. 2011 , 46, 1539-1542	2
2200	Chemical changes in PMMA as a function of depth due to proton beam irradiation. 2011 , 130, 702-707	34
2199	Steady-state neutronic analysis of converting the UK CONSORT reactor for ADS experiments. 2011 , 38, 2653-2660	2
2198	Radiolysis of sulfuric acid, sulfuric acid monohydrate, and sulfuric acid tetrahydrate and its relevance to Europa. 2011 , 215, 370-380	20
2197	Development of Monte Carlo Modeling for Neutron-Induced Failures of Trench FieldStop IGBT. 2011 , 58, 2748-2754	6
2196	Ion irradiation of novel yttrium/ytterbium-based pyrochlores: The effect of disorder. 2011 , 59, 7530-7537	39
2195	Practicality of the cyclotron production of radiolanthanide 142Pr: a potential for therapeutic applications and biodistribution studies. 2011 , 288, 937-942	23
2194	Noble gas diffusion mechanism in lunar soil simulant grains: Results from 4He+ implantation and extraction experiments. 2011 , 22, 566-577	2
2193	A fast numerical method for calculating the 3D proton dose profile in a single-ring wobbling spreading system. 2011 , 34, 317-25	2
2192	Gas-gain study of standard CERN GEM and Thick GEM in low-pressure He/CO2 mixed gas. 2011 , 625, 39-42	3
2191	Challenging measurement of the 16O+27Al elastic and inelastic angular distributions up to large angles. 2011 , 648, 46-51	37
2190	Trace element quantification in high-resolution Rutherford backscattering spectrometry. <i>Nuclear Instruments & Methods in Physics Research B</i> , 2011 , 269, 1284-1287	14

2189	Ion track structure calculations in silicon Epatial and temporal aspects. <i>Nuclear Instruments & Methods in Physics Research B</i> , 2011 , 269, 1630-1633	1.2	27
2188	The sputtering properties of artificial polymorphic AB binary compound crystals. 2011 , 257, 8864-8870		О
2187	& Methods in Physics Research B, 2011 , 269, 1425-1427	1.2	2
2186	Measurements of induced activity in concrete by secondary particles at forward direction produced by intermediate energy heavy ions on an Fe target. <i>Nuclear Instruments & Methods in Physics Research B</i> , 2011 , 269, 1929-1939	1.2	2
2185	TiNxOy/TiN dielectric contrasts obtained by ion implantation of $\{rm O\}_2^+$; structural, optical and electrical properties. 2011 , 44, 235501		6
2184	Ionodeterioration of the silicon nanocrystal photoluminescence. 2011 , 110, 114904		2
2183	Actinides and radiation effects: impact on the back-end of the nuclear fuel cycle. 2011 , 75, 2359-2377		38
2182	Direct observation of two protons in the decay of 54Zn. 2011 , 107, 102502		58
2181	Re-evaluation of neutron-He4 elastic scattering data near 20 MeV. 2011 , 83,		2
2180	Formation and annealing of dislocation loops induced by nitrogen implantation of ZnO. 2011 , 109, 0235	13	41
2179	Diamond processing by focused ion beamBurface damage and recovery. 2011 , 99, 183109		26
2178	The evolution of vacancy-type defects in silicon-on-insulator structures studied by positron annihilation spectroscopy. 2011 , 110, 016104		4
2177	. 2011,		
2176	Modification of Porous Silicon Formation by Varying the End of Range of Ion Irradiation. 2011 , 14, D45		5
2175	Sensing external spins with nitrogen-vacancy diamond. 2011 , 13, 055004		85
2174	Simulation of Proton Irradiation Damage for Fe-Ni Magnetic Alloy. 2012 , 503-504, 338-341		
2173	X-Ray Induced Depth Profiling of Ion Implantations into Various Semiconductor Materials. 2012 , 195, 274-276		1
2172	A multi-detector, digitizer based neutron depth profiling device for characterizing thin film materials. 2012 , 83, 073303		5

2171	Vacancy-type defects created by single-shot and chain ion implantation of silicon. 2012 , 14, 025007	3
2170	Interaction vertex imaging (IVI) for carbon ion therapy monitoring: a feasibility study. 2012 , 57, 4655-69	71
2169	The Effects of Femtosecond Laser Irradiation and Thermal Annealing on the Optoelectronic Properties of Silicon Supersaturated with Sulfur. 2012 , 29, 046101	3
2168	Spectroscopic measurement of the refractive index of ion-implanted diamond. 2012 , 37, 671-3	23
2167	Ion-Beam-Induced Luminescence Analysis as Diagnostic Tool for Microstructure Patterning on Diamond by Proton Beam Writing. 2012 , 51, 06FB07	5
2166	Formation of ZnO Nanoparticles by ZnO $^{-}$ and O $^{-}$ Dual Beam Ion Implantation and Thermal Annealing. 2012 , 51, 11PG03	1
2165	High-precision thickness regulation of graphene layers with low energy helium plasma implantation. 2012 , 23, 375303	3
2164	Combined helium ion beam and nanoimprint lithography attains 4 nm half-pitch dense patterns. 2012 , 30, 06F304	66
2163	Dopant effects on solid phase epitaxy in silicon and germanium. 2012 , 111, 034906	8
2162	Complex refractive index variation in proton-damaged diamond. 2012 , 20, 19382-94	21
2161	Structural recovery of ion implanted ZnO nanowires. 2012 , 111, 083524	12
2160	Fluorine passivation of vacancy defects in bulk germanium for Ge metal-oxide-semiconductor field-effect transistor application. 2012 , 101, 072104	39
2159	Impact of the surface-near silicon substrate properties on the microstructure of sputter-deposited AlN thin films. 2012 , 101, 221602	32
2158	Influence of ion source configuration and its operation parameters on the target sputtering and implantation process. 2012 , 83, 063304	
2157	Spin fluctuations of paramagnetic Rh clusters revealed by x-ray magnetic circular dichroism. 2012 , 109, 197204	14
2156	Inelastic energy loss of medium energy H and He ions in Au and Pt: Deviations from velocity proportionality. 2012 , 86,	21
2155	Reorientation-effect measurement of the <21+ E2 21+> matrix element in 10Be. 2012 , 86,	20
2154	Helium irradiation effects in polycrystalline Si, silica, and single crystal Si. 2012 , 111, 083527	15

2153	Depth profiling of residual activity of U237 fragments as a range verification technique for U238 primary ion beam. 2012 , 15,	3
2152	Atomic Excitation Exploited By Energetic-Beam Characterization Methods. 2012 , 1	1
2151	Resolution, masking capability and throughput for direct-write, ion implant mask patterning of diamond surfaces using ion beam lithography. 2012 , 22, 055005	11
2150	Effects of Displacing Radiation on Graphite Observed Using in situ Transmission Electron Microscopy. 2012 , 1383, 67	
2149	Radiochemical studies relevant to cyclotron production of the therapeutic radionuclide 167Tm. 2012 , 100, 915-918	1
2148	Mechanical Behavior of Ion-Irradiated Fe-Cr alloys Investigated by Spherical Indentation. 2012 , 1424, 1	2
2147	Radiation Damage of II, III, IV, V Pyrochlores - CaLnZrNbO7. 2012 , 1475, 571	
2146	On the Formation of 50 nm Diameter Free-Standing Silicon Wires Produced by Ion Irradiation. 2012 , 1, P66-P69	14
2145	Biological effectiveness on live cells of laser driven protons at dose rates exceeding 109 Gy/s. 2012 , 2, 011209	82
2144	Swift heavy ion-induced silicon dioxide nanostructuration: experimental observation of velocity effect. 2012 , 60, 10402	3
2143	Surface modifications of comet-exposed aerogel from the Stardust cometary collector. 2012 , 47, 1336-1346	1
2142	The isotopic composition and fluence of solar-wind nitrogen in a genesis B/C array collector. 2012 , 47, 1436-1448	8
2141	Hydrogen-induced defects in ion-implanted Si. 2012 , 86,	13
2140	Ion implantation induced modification of optical properties in single-crystal diamond studied by coherent acoustic phonon spectroscopy. 2012 , 101, 181904	11
2139	Ion-matter interaction: the three-dimensional version of the thermal spike model. Application to nanoparticle irradiation with swift heavy ions. 2012 , 45, 065302	72
2138	Three-dimensional silicon micromachining. 2012 , 22, 113001	22
2137	Single Particle Displacement Damage in Silicon. 2012 , 59, 3054-3061	45
2136	Optical and paramagnetic properties of polycrystalline CVD-diamonds implanted with deuterium ions. 2012 , 79, 600-609	2

2135	Effect of swift heavy ion irradiation on ethylenedhlorotrifluoroethylene copolymer. 2012, 81, 1741-1746	6
2134	Synthesis of buried layers of EsiC in Si by multiple energy carbon ion implantations and post thermal annealing. 2012 , 524, 35-38	1
2133	Pulse Shape Measurements by On-Chip Sense Amplifiers of Single Event Transients Propagating Through a 90 nm Bulk CMOS Inverter Chain. 2012 , 59, 2778-2784	17
2132	Characterization of ultra-shallow aluminum implants in silicon by grazing incidence and grazing emission X-ray fluorescence spectroscopy. 2012 , 27, 1432	32
2131	A compact dosimeter for space applications. 2012,	
2130	A Linear Mode Avalanche Photodiode for Ion Detection in the Energy Range 5250 keV. 2012 , 59, 2601-2607	12
2129	Overview of mercury radionuclides and nuclear model calculations of 195Hgm,g and 197Hgm,g to evaluate experimental cross section data. 2012 , 85,	12
2128	Sensitivity of the threshold displacement energy to temperature and time. 2012 , 86,	17
2127	Prototype AT-TPC: Toward a new generation active target time projection chamber for radioactive beam experiments. 2012 , 691, 39-54	55
2126	Pilot experiment on proton acceleration using the 25TW femtosecond Ti:Sapphire laser system at PALS. 2012 , 690, 48-52	1
2125	Statistical analysis of cross-section data for 12C(4He,4He)12C backscattering. <i>Nuclear Instruments & Methods in Physics Research B</i> , 2012 , 285, 116-124	5
2124	Depth-profiled characterization of complex refractive index of ion implanted optically transparent polymers using multilayer calculations and reflectance data. 2012 , 86, 1822-1827	8
2123	LEO protons on selected optical fibers. 2012 ,	
2122	Systematic calculation of threshold displacement energies: Case study in rutile. 2012 , 85,	42
2121	Structural response of A2TiO5 (A=La, Nd, Sm, Gd) to swift heavy ion irradiation. 2012 , 60, 4477-4486	36
2120	In situ measurements of the radiation stability of amino acids at 15🛭 40 K. 2012 , 220, 647-659	42
2119	Accelerated chemical aging of crystalline nuclear waste forms. 2012 , 16, 126-133	11
2118	Graphite grains in supernova ejecta Insights from a noble gas study of 91 individual KFC1 presolar graphite grains from the Murchison meteorite. 2012 , 76, 147-160	12

2117	electrochemical etching method. 2012 , 7, 416	19
2116	In-depth multi-technique characterization of chromium lilicon mixed oxides produced by reactive ion beam mixing of the Cr/Si interface. 2012 , 27, 390	3
2115	Integrative approaches for cellular cryo-electron tomography: correlative imaging and focused ion beam micromachining. 2012 , 111, 259-81	51
2114	Characterization of extended range Bonner Sphere Spectrometers in the CERF high-energy broad neutron field at CERN. 2012 , 694, 55-68	14
2113	Creation of nanodots on mica surfaces induced by highly charged xenon ions. <i>Nuclear Instruments & Methods in Physics Research B</i> , 2012 , 286, 299-302	10
2112	Thermal-to-fusion neutron convertor and Monte Carlo coupled simulation of deuteron/triton transport and secondary products generation. <i>Nuclear Instruments & Methods in Physics Research B</i> , 1.2 2012 , 287, 19-25	4
2111	Experimental study of the He stopping power into Al2O3 films. <i>Nuclear Instruments & Methods in Physics Research B</i> , 2012 , 287, 1-3	2
2 110	SEU due to electrons in silicon devices with nanometric sensitive volumes and small critical charge. Nuclear Instruments & Methods in Physics Research B, 2012, 287, 113-119	16
2109	Optical waveguides in Nd:GdVO4 crystals fabricated by swift N3+ ion irradiation. 2012 , 35, 310-313	7
2108	Influence of swift heavy ion beams and protons on the dielectric strength of polyimide. 2012 , 97, 2396-2402	8
2107	Isotope fractionation during ion beam formation in multi-collector inductively coupled plasma mass spectrometry. 2012 , 76, 126-132	17
2106	Accurate determination of quantity of material in thin films by Rutherford backscattering spectrometry. 2012 , 84, 6061-9	83
2105	Ion Beam Analysis. 2012 , 661-681	4
2104	Super-resolution fluorescence quenching microscopy of graphene. 2012 , 6, 9175-81	44
2103	Application of micro- and nanoprobes to the analysis of small-sized 3D materials, nanosystems, and nanoobjects. 2012 , 182, 287-321	5
2102	Electrical and microstructural analyses of 200 MeV Ag14+ ion irradiated Ni/GaN Schottky barrier diode. 2012 , 101, 153508	22
2101	Nanometer-thin solid-state nanopores by cold ion beam sculpting. 2012 , 100, 213104-2131044	32
2100	■otal□on Beam AnalysisBD Imaging of Complex Samples Using MeV Ion Beams. 2012 , 1	

2099 Elastic Recoil Detection Analysis. 2012 , 1	1
2098 Elastic Backscattering of Ions for Compositional Analysis. 2012 , 1	Ο
2097 An energy-loss model for low- and intermediate-energy carbon projectiles in water. 2012 , 88, 45-9	6
2096 Are nanoporous materials radiation resistant?. 2012 , 12, 3351-5	185
In vitro evaluation of combined temozolomide and radiotherapy using X rays and high-linear energy transfer radiation for glioblastoma. 2012 , 177, 651-62	27
2094 Temporal evolution of the radial plasma emissivity profile in HIPIMS plasma discharges. 2012 , 21, 035017	25
Ion multi-beam direct sputtering of Si imprint stamps and simulation of resulting structures. 2012 , 22, 055008	1
FIRST MEASUREMENTS OF THE COMPLETE HEAVY-ION CHARGE STATE DISTRIBUTIONS OF C, O, AND Fe ASSOCIATED WITH INTERPLANETARY CORONAL MASS EJECTIONS. 2012 , 751, 20	31
Study of focused-ion-beam[hduced structural and compositional modifications in nanoscale bilayer systems by combined grazing incidence x ray reflectivity and fluorescence. 2012 , 111, 044324	13
Depth profiling of NbxO/W multilayers: effect of primary ion beam species (O2+, Ar+ and Cs+). 2090 2012 , 44, 934-937	1
2089 Charge state manipulation of qubits in diamond. 2012 , 3, 729	152
2088 Study of Graphene Growth Mechanism on Nickel Thin Films. 2012 , 1-7	
2087 On the impact of the fissile coating on the fission chamber signal. 2012 , 681, 101-109	23
2086 In Situ Neutron Techniques for Studying Lithium Ion Batteries. 2012, 91-106	24
2085 THz Photoconductive Antennas Made From Ion-Bombarded Semiconductors. 2012 , 33, 455-473	14
A novel technique for simultaneous diagnosis and radioprotection by radioactive cerium oxide nanoparticles: study of cyclotron production of 137mCe. 2012 , 292, 53-59	24
2083 Alpha-particle energy distributions from thin sources measured with small solid angles. 2012 , 292, 571-577	4
$_{20}82$ Targetry and nuclear data for the cyclotron production of 55Fe via various reactions. 2012 , 293, 1-6	12

2081	Accelerator production of the positron emitter zirconium-89. 2012 , 41, 97-103		31
2 080	Energy limitation for models to simulate the buffer gas cooling. 2012 , 309, 44-48		4
2079	Effects of focused ion beam milling on electron backscatter diffraction patterns in strontium titanate and stabilized zirconia. 2012 , 246, 279-86		9
2078	Physico-chemical transformations in swift heavy ion modified poly(ethyleneterephthalate). 2012 , 81, 284-289		7
2077	Effect of irradiation on nonlinear optical recirculation cavity performance. 2012 , 664, 294-298		
2076	Development of a silicon detector monitor for the HIE-ISOLDE superconducting upgrade of the REX-ISOLDE heavy-ion linac. 2012 , 672, 21-28		3
2075	Biaxial texture development in the ion beam assisted deposition of magnesium oxide. <i>Nuclear Instruments & Methods in Physics Research B</i> , 2012 , 272, 28-32	1.2	13
2074	Magnetic properties of Co, Ni, Pt and their alloy nanoparticles formed in SiO2 by ion beam synthesis. <i>Nuclear Instruments & Methods in Physics Research B</i> , 2012 , 272, 70-73	1.2	6
2073	Heavy ion energy loss straggling data from Time of Flight stopping force measurements. <i>Nuclear Instruments & Methods in Physics Research B</i> , 2012 , 273, 6-10	1.2	10
2072	Reliability studies on NPN RF power transistors under swift heavy ion irradiation. <i>Nuclear Instruments & Methods in Physics Research B</i> , 2012 , 273, 36-39	1.2	15
2071	Information on ionBolid interactions obtained through magnetization measurements. <i>Nuclear Instruments & Methods in Physics Research B</i> , 2012 , 273, 72-75	1.2	1
2070	Developing the IBA equipment to increase the versatility of the CNA. <i>Nuclear Instruments & Methods in Physics Research B</i> , 2012 , 273, 218-221	1.2	2
2069	Single ion hit detection set-up for the Zagreb ion microprobe. <i>Nuclear Instruments & Methods in Physics Research B</i> , 2012 , 277, 140-144	1.2	8
2068	Nanometric transformation of the matter by short and intense electronic excitation: Experimental data versus inelastic thermal spike model. <i>Nuclear Instruments & Methods in Physics Research B</i> , 2012 , 277, 28-39	1.2	108
2067	Deuteron induced secondary electron emission from titanium deuteride surface. <i>Nuclear Instruments & Methods in Physics Research B</i> , 2012 , 280, 1-4	1.2	7
2066	Potassium-silicate glass exposed to low energy H+ beam. <i>Nuclear Instruments & Methods in Physics Research B</i> , 2012 , 280, 111-116	1.2	4
2065	Electric field gradient calculations in ZnO samples implanted with 111In(111Cd). 2012 , 152, 399-402		10
2064	Modeling reactive magnetron sputtering: Fixing the parameter set. 2012 , 206, 3666-3675		34

2063	Atom probe study of radiation induced grain boundary segregation/depletion in a Fe-12%Cr alloy. 2012 , 57, 14-19		15
2062	Simulation of thermally-induced processes of diffusion and phase formation in layered metal-metalloid systems. 2012 , 67, 263-268		1
2061	Measurement of the neutron capture cross-sections of 232Th at 5.9 MeV and 15.5 MeV. 2012 , 48, 1		17
2060	Cross sections for bare and dressed carbon ions in water and neon. 2013 , 58, 641-72		31
2059	Pre-equilibrium effects on proton, deuteron, and alpha induced reactions for the production of 72As as a PET imaging radioisotope. 2013 , 298, 501-512		10
2058	RIMS analysis of ion induced fragmentation of molecules sputtered from an enriched U3O8 matrix. 2013 , 296, 407-412		6
2057	Temperature measurements of fusion plasmas produced by Petawatt-Laser-Irradiated D2 - (3)He or CD4 - (3)He clustering gases. 2013 , 111, 055002		34
2056	Radiation damage in multiphase ceramics. 2013 , 443, 120-127		7
2055	A thousand-fold enhancement of photoluminescence in porous silicon using ion irradiation. 2013 , 114, 053517		6
2054	Detection of Alpha Particles and Low Energy Gamma Rays by Thermo-Bonded Micromegas in Xenon Gas. 2013 , 60, 3008-3013		3
2053	Calculation of Cross Section for Ion-Induced SEU Through Direct Ionization in Nanometric Silicon Devices With Small Critical Energy. 2013 , 60, 3092-3103		8
2052	A windowless hydrogen gas target for the measurement of 7Be(p,(gamma))8B with the recoil separator ERNA. 2013 , 49, 1		10
2051	Surface modification of Makrofol-DE induced by Eparticles. 2013 , 93, 4276-4285		9
2050	On the use of SRIM for computing radiation damage exposure. <i>Nuclear Instruments & Methods in Physics Research B</i> , 2013 , 310, 75-80	1.2	857
2049	The Genesis Solar Wind Concentrator: Flight and Post-Flight Conditions and Modeling of Instrumental Fractionation. 2013 , 175, 93-124		6
2048	Silicon and porous silicon mid-infrared photonic crystals. 2013 , 112, 517-523		13
2047	Ion beam synthesis and carrier dynamics of ZnO nanoparticles embedded in a SiO2 matrix. 2013 , 112, 801-806		2
2046	Anthology of the Development of Radiation Transport Tools as Applied to Single Event Effects. 2013 , 60, 1876-1911		71

(2013-2013)

2045	An Updated Perspective of Single Event Gate Rupture and Single Event Burnout in Power MOSFETs. 2013 , 60, 1912-1928	67
2044	Magneto-optical studies of Gd-implanted GaN: No spin alignment of conduction band electrons. 2013 , 103, 092401	4
2043	Depth Profiling of Electronic Transport Parameters in n-on-p Boron-Ion-Implanted Vacancy-Doped HgCdTe. 2013 , 42, 3108-3113	22
2042	A novel instrument for quantitative nanoanalytics involving complementary X-ray methodologies. 2013 , 84, 045106	75
2041	Ozone and carbon trioxide synthesis by low energy ion implantation onto solid carbon dioxide and implications to astrochemistry. 2013 , 139, 074706	12
2040	Simulation of the sputtering of Si nanoclusters with diameters of (2B) nm under bombardment with monatomic and cluster ions using the method of classical molecular dynamics. 2013 , 7, 201-210	1
2039	Evaluating focused ion beam induced damage in soft materials. 2013 , 50, 51-6	30
2038	Structural modifications of swift heavy ion irradiated PEN probed by optical and thermal measurements. 2013 , 88, 49-55	8
2037	Event identification in 3He proportional counters using risetime discrimination. 2013 , 717, 51-57	18
2036	Pulse shape discrimination at low energies with a double sided, small-pitch strip silicon detector. 2013 , 732, 87-90	9
2036		9
2035	2013, 732, 87-90 Swift heavy ion induced modification in morphological and physico-chemical properties of tin oxide	
2035	2013, 732, 87-90 Swift heavy ion induced modification in morphological and physico-chemical properties of tin oxide nanocomposites. <i>Nuclear Instruments & Methods in Physics Research B</i> , 2013, 315, 179-183	
2035	Swift heavy ion induced modification in morphological and physico-chemical properties of tin oxide nanocomposites. <i>Nuclear Instruments & Methods in Physics Research B</i> , 2013 , 315, 179-183 New Type of Neutron Image Scintillator based on H310BO3/ZnS(Ag). 2013 , 43, 216-222 Physical properties of epitaxial ZrN/MgO(001) layers grown by reactive magnetron sputtering.	10
2035 2034 2033	Swift heavy ion induced modification in morphological and physico-chemical properties of tin oxide nanocomposites. <i>Nuclear Instruments & Methods in Physics Research B</i> , 2013 , 315, 179-183 New Type of Neutron Image Scintillator based on H310BO3/ZnS(Ag). 2013 , 43, 216-222 Physical properties of epitaxial ZrN/MgO(001) layers grown by reactive magnetron sputtering. 2013 , 31, 061516 Analytical Method to Evaluate Soft Error Rate Due to Alpha Contamination. 2013 , 60, 4059-4066	10 1 39
2035 2034 2033 2032	Swift heavy ion induced modification in morphological and physico-chemical properties of tin oxide nanocomposites. Nuclear Instruments & Methods in Physics Research B, 2013, 315, 179-183 New Type of Neutron Image Scintillator based on H310BO3/ZnS(Ag). 2013, 43, 216-222 Physical properties of epitaxial ZrN/MgO(001) layers grown by reactive magnetron sputtering. 2013, 31, 061516 Analytical Method to Evaluate Soft Error Rate Due to Alpha Contamination. 2013, 60, 4059-4066	10 1 39 5
2035 2034 2033 2032 2031	Swift heavy ion induced modification in morphological and physico-chemical properties of tin oxide nanocomposites. <i>Nuclear Instruments & Methods in Physics Research B</i> , 2013 , 315, 179-183 New Type of Neutron Image Scintillator based on H310BO3/ZnS(Ag). 2013 , 43, 216-222 Physical properties of epitaxial ZrN/MgO(001) layers grown by reactive magnetron sputtering. 2013 , 31, 061516 Analytical Method to Evaluate Soft Error Rate Due to Alpha Contamination. 2013 , 60, 4059-4066 SEE Measurements and Simulations Using Mono-Energetic GeV-Energy Hadron Beams. 2013 , 60, 4142-4149 The Impact of Depletion Region Potential Modulation on Ion-Induced Current Transient Response.	10 1 39 5 13

2027	Glycine's radiolytic destruction in ices: first in situ laboratory measurements for Mars. 2013 , 13, 647-55	29
2026	Space-weathering of solar system bodies: a laboratory perspective. 2013 , 113, 9086-150	99
2025	. 2013 , 60, 4727-4736	5
2024	A setup for soft proton irradiation of X-ray detectors for future astronomical space missions. 2013 , 721, 65-72	6
2023	Influence of source composition and particle energy on the determination of gross alpha activity. 2013 , 82, 376-81	3
2022	Irradiation effects of 25MeV silicon ions on SiGe heterojunction bipolar transistors. <i>Nuclear Instruments & Methods in Physics Research B</i> , 2013 , 312, 77-83	14
2021	Annealing of ion irradiation damage in nuclear graphite. 2013 , 434, 334-346	19
2020	An analysis of 175 MeV Nickel ion irradiation and annealing effects on silicon NPN rf power transistors. 2013 , 13, 66-75	9
2019	Micromachining of commodity plastics by proton beam writing and fabrication of spatial resolution test-chart for neutron radiography. <i>Nuclear Instruments & Methods in Physics Research B</i> , 2013 , 306, 299-301	7
2018	Electrically active sodium-related defect centres in silicon. 2013 , 28, 105010	5
2017	Characterization of self-damaged (U,Pu)N fuel used in the NIMPHE program. 2013, 443, 491-496	2
2016	NEXAFS spectroscopy of CVD diamond films exposed to fusion relevant hydrogen plasma. 2013 , 34, 45-49	18
2015	Novel techniques of preparing TEM samples for characterization of irradiation damage. 2013 , 252, 251-7	3
2014	Radiation hardness of graphene and MoS2 field effect devices against swift heavy ion irradiation. 2013 , 113, 214306	67
2013	Molecular dynamics simulation of the initial stages of He bubbles formation in silicon. 2013 , 21, 065002	20
2012	Superplastic nanocrystalline ceramics at room temperature and high strain rates. 2013 , 69, 525-528	16
2011	In situ X-ray diffraction study of the growth of silver nanoparticles embedded in silica film by ion irradiation: The effect of volume fraction. <i>Nuclear Instruments & Methods in Physics Research B</i> , 2013 , 311, 5-9	5
2010	Effects of energetic ion irradiation on the magnetism of FeNi Invar alloy. <i>Nuclear Instruments & Methods in Physics Research B</i> , 2013 , 314, 103-106	1

2009 XRD monitoring of Belf-irradiation in uranium-americium mixed oxides. 2013 , 52, 14196-204		25
Sputtering of Al nanoclusters by 1¶3keV monatomic or polyatomic ions studied by Molecular Dynamics simulations. <i>Nuclear Instruments & Methods in Physics Research B</i> , 2013 , 303, 136-141	2	1
Structural and optical properties of porous silicon prepared by anodic etching of irradiated silicon. Nuclear Instruments & Methods in Physics Research B, 2013 , 315, 188-191	2	13
75MeV boron ion irradiation studies on Si PIN photodiodes. <i>Nuclear Instruments & Methods in Physics Research B</i> , 2013 , 316, 205-209	2	2
A compact biological cell irradiation system with a Van de Graaff accelerator. <i>Nuclear Instruments & Methods in Physics Research B</i> , 2013 , 315, 360-363	2	2
2004 . 2013,		1
2003 Fast Atom Beam Activated Wafer Bonds between n-Si and n-GaAs with Low Resistance. 2013 , 2, Q178-Q18	31	41
Ion beam engineered nano silver silicon substrates for surface enhanced Raman spectroscopy. 2013 , 44, 1014-1017		10
2001 Yield determination for a titanium neutron-forming target. 2013 , 113, 345-350		6
Influence of the ion synthesis and ion doping regimes on the effect of sensitization of erbium emission by silicon nanoclusters in silicon dioxide films. 2013 , 55, 2361-2367		
1999 Resonance triplet at E∄4.5 MeV in the 40Ca(⊞)44Ti reaction. 2013 , 88,		14
1998 Measuring and modelling cell-to-cell variation in uptake of gold nanoparticles. 2013 , 138, 7070-4		32
Size-controlled fluorescent nanodiamonds: a facile method of fabrication and color-center counting. 2013 , 5, 11776-82		21
Sputtering effect of low-energy ions on biological target: The analysis of sputtering product of urea and capsaicin. <i>Nuclear Instruments & Methods in Physics Research B</i> , 2013 , 308, 28-33	2	3
Proton and alpha particle induced changes in thermal and mechanical properties of Lexan polycarbonate. 2013 , 91, 1-6		20
Experimental study of fusion neutron and proton yields produced by petawatt-laser-irradiated DIIHe or CDIIHe clustering gases. 2013 , 88, 033108		15
1993 Analytical Models for Three-Dimensional Ion Implantation Profiles in FinFETs. 2013 , 32, 2004-2008		3
Optimization of DC Reactive Magnetron Sputtering Deposition Process for Efficient YSZ Electrolyte Thin Film SOFC. 2013 , 13, 279-288		18

1991	Evaluation of the neutron energy spectrum, angular distribution, and yield of the 9Be(d,n) reaction with a thick beryllium target. 2013 , 87,		11
1990	Positron study of alpha particles effect on oxide-dispersion-strengthened steels. 2013 , 443, 012016		
1989	Synthesis, thermal evolution and optical properties of CuZn alloy nanoparticles in SiO2 sequentially implanted with dual ions. 2013 , 549, 231-237		18
1988	LET effects on the hydrogen production induced by the radiolysis of pure water. 2013 , 82, 74-79		19
1987	L-shell X-ray production cross sections of selected lanthanoids by impact of 7Li2+ ions with energies between 3.50 MeV and 5.25 MeV. 2013 , 83, 48-53		5
1986	Deep levels generated by thermal oxidation in p-type 4H-SiC. 2013 , 113, 033705		14
1985	A modified Tersoff potential for pure and hydrogenated diamond-like carbon. 2013 , 67, 146-150		37
1984	A niobium water target for routine production of [IE] Fluoride with a MC 17 cyclotron. 2013, 72, 133-6		7
1983	Improved zircon fission-track annealing model based on reevaluation of annealing data. 2013 , 40, 93-10	6	13
1982	Evaluation of the cyclotron production of 165Er by different reactions. 2013 , 295, 923-928		8
1981	Oxidation of polyethylene implanted with low energy magnesium ions. <i>Nuclear Instruments & Methods in Physics Research B</i> , 2013 , 307, 624-629	1.2	2
1980	In situ TEM investigation of Xe ion irradiation induced defects and bubbles in pure molybdenum single crystal. 2013 , 437, 240-249		12
1979	Microstructural evolution of CANDU spacer material Inconel X-750 under in situ ion irradiation. 2013 , 443, 49-58		42
1978	Modeling of ion beam induced charge sharing experiments for the design of high resolution position sensitive detectors. <i>Nuclear Instruments & Methods in Physics Research B</i> , 2013 , 306, 169-175	1.2	3
1977	Tunnel junction sensors for HCI-surface measurements at low kinetic energies. <i>Nuclear Instruments & Methods in Physics Research B</i> , 2013 , 317, 66-71	1.2	2
1976	Characteristics of fast ions from laser-induced plasma and their applicability to shallow junction doping. <i>Nuclear Instruments & Methods in Physics Research B</i> , 2013 , 314, 162-165	1.2	
1975	Sputtering yield of amorphous 13C thin films under swift heavy-ion irradiation. <i>Nuclear Instruments & Methods in Physics Research B</i> , 2013 , 314, 34-38	1.2	7
1974	In gas laser ionization and spectroscopy experiments at the Superconducting Separator Spectrometer (S3): Conceptual studies and preliminary design. <i>Nuclear Instruments & Methods in Physics Research B</i> , 2013 , 317, 570-581	1.2	38

(2013-2013)

1973	Characterization of the lattice defects in Ge-ion implanted ZnO bulk single crystals by Rutherford Backscattering: Origins of low resistivity. <i>Nuclear Instruments & Methods in Physics Research B</i> , 2013 , 307, 366-369	1.2	4
1972	Measurement of fast neutron spectrum using CR-39 detectors and a new image analysis program (autoTRAK_n). 2013 , 729, 444-450		23
1971	On the formation of silicon wires produced by high-energy ion irradiation. <i>Nuclear Instruments & Methods in Physics Research B</i> , 2013 , 296, 32-40	1.2	12
1970	CVD diamond as a position sensitive detector using charge carrier transition time. <i>Nuclear Instruments & Methods in Physics Research B</i> , 2013 , 306, 186-190	1.2	1
1969	Thermal release rate studies of nuclear reaction products from polycrystalline metal matrices. <i>Nuclear Instruments & Methods in Physics Research B</i> , 2013 , 297, 86-93	1.2	4
1968	Nuclear model calculations of charged-particle-induced reaction cross section data for the production of the radiohalogen 34Clm. 2013 , 87,		6
1967	The study of Ga+ FIB implanting crystal silicon and subsequent annealing. <i>Nuclear Instruments & Methods in Physics Research B</i> , 2013 , 307, 253-256	1.2	18
1966	Opening windows into the cell: focused-ion-beam milling for cryo-electron tomography. 2013 , 23, 771-7	7	127
1965	UVIIisible and infrared spectroscopic studies of Li3+ and C5+ irradiated PADC polymer. 2013 , 3, 122-128	3	30
1964	The effect of gallium implantation on the optical properties of diamond. 2013 , 35, 47-52		7
1964 1963	The effect of gallium implantation on the optical properties of diamond. 2013 , 35, 47-52 Measurement of L X-ray production cross sections by impact of proton beams on Hf, Ir, and Tl. Nuclear Instruments & Methods in Physics Research B, 2013 , 316, 113-122	1.2	7
1963	Measurement of L X-ray production cross sections by impact of proton beams on Hf, Ir, and Tl.	1.2	
1963 1962	Measurement of L X-ray production cross sections by impact of proton beams on Hf, Ir, and Tl. <i>Nuclear Instruments & Methods in Physics Research B</i> , 2013 , 316, 113-122	1.2	14
1963 1962 1961	Measurement of L X-ray production cross sections by impact of proton beams on Hf, Ir, and Tl. <i>Nuclear Instruments & Methods in Physics Research B</i> , 2013 , 316, 113-122 Evaluation of freestanding GaN as an alpha and neutron detector. 2013 , 719, 13-16	1.2	14 24
1963 1962 1961	Measurement of L X-ray production cross sections by impact of proton beams on Hf, Ir, and Tl. Nuclear Instruments & Methods in Physics Research B, 2013, 316, 113-122 Evaluation of freestanding GaN as an alpha and neutron detector. 2013, 719, 13-16 The influence of CuNb interfaces on local vacancy concentrations in Cu. 2013, 69, 21-24	1.2	14 24 13
1963 1962 1961	Measurement of L X-ray production cross sections by impact of proton beams on Hf, Ir, and Tl. <i>Nuclear Instruments & Methods in Physics Research B</i> , 2013 , 316, 113-122 Evaluation of freestanding GaN as an alpha and neutron detector. 2013 , 719, 13-16 The influence of CuNb interfaces on local vacancy concentrations in Cu. 2013 , 69, 21-24 Improvement of trapped field in DyBaCuO bulk by proton irradiation. 2013 , 484, 117-119 Basic performance of a position-sensitive tissue-equivalent proportional chamber (PS-TEPC). 2013 ,	1.2	14 24 13
1963 1962 1961 1960	Measurement of L X-ray production cross sections by impact of proton beams on Hf, Ir, and Tl. Nuclear Instruments & Methods in Physics Research B, 2013, 316, 113-122 Evaluation of freestanding GaN as an alpha and neutron detector. 2013, 719, 13-16 The influence of CuNb interfaces on local vacancy concentrations in Cu. 2013, 69, 21-24 Improvement of trapped field in DyBaCuO bulk by proton irradiation. 2013, 484, 117-119 Basic performance of a position-sensitive tissue-equivalent proportional chamber (PS-TEPC). 2013, 732, 591-594	1.2	14 24 13 1

1955	Towards pumpprobe experiments of defect dynamics with short ion beam pulses. <i>Nuclear Instruments & Methods in Physics Research B</i> , 2013 , 315, 350-355	1.2	9
1954	Helium concentration in tungsten nano-tendril surface morphology using Elastic Recoil Detection. 2013 , 438, S913-S916		26
1953	Synthesis of optical waveguides in SiO2 by silver ion implantation. 2013 , 35, 927-934		18
1952	Degradation of thermal radiative properties of variable emissivity device based on manganese oxides in simulated space environment. 2013 , 71, 258-263		7
1951	Modelling surface restructuring by slow highly charged ions. <i>Nuclear Instruments & Methods in Physics Research B</i> , 2013 , 317, 149-153	1.2	3
1950	Nanoindentation of model Fell alloys with self-ion irradiation. 2013, 433, 174-179		53
1949	Effects of dose rate change under irradiation on hardening and microstructural evolution in A533B steel. 2013 , 50, 160-168		11
1948	Effect of 50-keV proton irradiation on the magnetism of a Fe66Ni34 Invar alloy. 2013 , 333, 13-17		3
1947	IBIC characterization of an ion-beam-micromachined multi-electrode diamond detector. <i>Nuclear Instruments & Methods in Physics Research B</i> , 2013 , 306, 181-185	1.2	19
1946	Palladium nanoparticles supported on nitrogen-doped HOPG: a surface science and electrochemical study. 2013 , 15, 2923-31		38
1945	Prediction of the thermal release of transactinide elements (112 🗷 🗈 16) from metals. 2013 , 101, 211-220)	3
1944	Erosion at the inner wall of JET during the discharge campaigns 2001\(\mathbb{Q}\)009. 2013 , 438, S780-S783		19
1943	Cu out-diffusion in kesterites transmission electron microscopy specimen preparation artifact. 2013 , 102, 051902		21
1942	Relative thermoluminescent efficiency of LiF detectors for proton radiation: Batch variability and energy dependence. 2013 , 56, 205-208		9
1941	Evaluation of the relative thermoluminescence efficiency of LiF:Mg,Ti and LiF:Mg,Cu,P TL detectors to low-energy heavy ions. 2013 , 51-52, 7-12		14
1940	Mask assisted fabrication of nanoislands of BiFeO3 by ion beam milling. 2013 , 113, 154101		18
1939	Noninvasive spatial metrology of single-atom devices. 2013 , 13, 1903-9		25
1938	Multi-scale simulation of structural heterogeneity of swift-heavy ion tracks in complex oxides. 2013 , 25, 135001		17

1937	Electrochemical behavior of N and Ar implanted highly oriented pyrolytic graphite substrates and activity toward oxygen reduction reaction. 2013 , 88, 477-487	47
1936	Reduced deuterium retention in self-damaged tungsten exposed to high-flux plasmas at high surface temperatures. 2013 , 53, 043003	24
1935	Ion impacts on graphene/Ir(111): interface channeling, vacancy funnels, and a nanomesh. 2013, 13, 1948-55	73
1934	Effects of irradiation temperature and dose rate on the mechanical properties of self-ion implanted Fe and FeIIr alloys. 2013 , 439, 33-40	81
1933	Effect of grain boundary orientation on radiation-induced segregation in a Fell 5.2at.% Cr alloy. 2013 , 61, 3490-3498	34
1932	Splitting of photoluminescent emission from nitrogenNacancy centers in diamond induced by ion-damage-induced stress. 2013 , 15, 043027	24
1931	Assessment of surface potential models by molecular dynamics simulations of atom ejection from (100)-Si surfaces. <i>Nuclear Instruments & Methods in Physics Research B</i> , 2013 , 303, 165-169	1
1930	Optical addressing of an individual erbium ion in silicon. 2013 , 497, 91-4	106
1929	A Monte Carlo track structure simulation code for the full-slowing-down carbon projectiles of energies 1[keV[u(-1)-10 MeV u(-1)] water. 2013 , 58, 673-701	23
1928	Ellipsometrical characterization of complex refractive index depth profile of 50 keV silicon ion implanted PMMA. 2013 , 94, 19-25	7
1927	Alpha localized radiolysis and corrosion mechanisms at the iron/water interface: Role of molecular species. 2013 , 433, 124-131	5
1926	Electron backscatter diffraction characterization of plasma immersion ion implantation effects in stainless steel. <i>Nuclear Instruments & Methods in Physics Research B</i> , 2013 , 295, 38-41	1
1925	Surface plasma pretreatment for enhanced diamond nucleation on AlN. 2013, 102, 201609	20
1924	Measurement of the MACS of at kT=30keV as a test of a method for Maxwellian neutron spectra generation. 2013 , 727, 1-6	16
1923	Amorphization and reduction of thermal conductivity in porous silicon by irradiation with swift heavy ions. 2013 , 114, 014903	30
1922	The Evolution of Neutron Straw Detector Applications in Homeland Security. 2013, 60, 1140-1146	15
1921	Defect enhanced funneling of diffusion current in silicon. 2013 , 102, 042102	11
1920	Hardening of self ion implanted tungsten and tungsten 5-wt% rhenium. 2013 , 432, 428-436	95

1919	Ion-Energy Dependency in Proton Irradiation Induced Chemical Processes of Poly(dimethylsiloxane). 2013 , 117, 25884-25889	18
1918	Pattern formation on Ge by low energy ion beam erosion. 2013 , 15, 103029	41
1917	Zn ion post-implantation-driven synthesis of CuZn alloy nanoparticles in Cu-preimplanted silica and their thermal evolution. 2013 , 5, 13055-62	11
1916	Direct graphene synthesis on SiO2/Si substrate by ion implantation. 2013 , 102, 193102	29
1915	Effects of He irradiation on Ti3AlC2: Damage evolution and behavior of He bubbles. 2013 , 440, 606-611	57
1914	Mechanical and Raman spectroscopic studies of multi-ion-beam irradiated 12,18Cr-oxide dispersion strengthened steels. <i>Nuclear Instruments & Methods in Physics Research B</i> , 2013 , 297, 35-38	10
1913	Resonant & Cattering of 6He: Limits of clustering in 10Be. 2013 , 87,	48
1912	Characterization of boron coated vitreous carbon foam for neutron detection. 2013 , 729, 346-355	7
1911	Characterization of the beam profile for the PIXE/PIGE beam line at the CRC proton cyclotron. 2013 , 63, 1291-1295	3
1910	Supply Voltage Dependent On-Chip Single-Event Transient Pulse Shape Measurements in 90-nm Bulk CMOS Under Alpha Irradiation. 2013 , 60, 2640-2646	9
1909	Materials modification using ions with energies below 1MeV/u. <i>Nuclear Instruments & Methods in Physics Research B</i> , 2013 , 317, 143-148	3
1908	Distribution and compositional variations of plasma ions in Mercury's space environment: The first three Mercury years of MESSENGER observations. 2013 , 118, 1604-1619	72
1907	Rapid prototyping of Fresnel zone plates via direct Ga(+) ion beam lithography for high-resolution X-ray imaging. 2013 , 7, 9788-97	42
1906	Laser-driven ion acceleration from relativistically transparent nanotargets. 2013 , 15, 085015	61
1905	Reflection of solar wind hydrogen from the lunar surface. 2013 , 118, 292-305	21
1904	Unlocking doping and compositional profiles of nanowire ensembles using SIMS. 2013 , 24, 045701	16
1903	Structure and phase transitions at the interface between 🖽 l2O3 and Pt. 2013 , 25, 232202	6
1902	Chemical evolution via beta decay: a case study in strontium-90. 2013 , 25, 065504	11

1901	Evaluation of resistless Ga+ beam lithography for UV NIL stamp fabrication. 2013, 24, 365302	3
1900	Application of proton beam writing for the direct etching of polytetrafluoroethylene for polydimethylsiloxane replica molding. 2013 , 31, 06F403	2
1899	Quasi-two-dimensional Ag nanoparticle formation in silica by Xe ion irradiation and subsequent Ag ion implantation. 2013 , 102, 133102	9
1898	Determination of thickness and composition of high-k dielectrics using high-energy electrons. 2013 , 103, 071911	10
1897	Long electron spin coherence in ion-implanted GaN: The role of localization. 2013 , 102, 192102	13
1896	Material Removal Property in Low Energy Ion Beam Etching. 2013 , 706-708, 142-147	
1895	Semiconductor Characterization by Scanning Ion Beam Induced Charge (IBIC) Microscopy. 2013 , 2013, 1-17	9
1894	Fast neutron production from lithium converters and laser driven protons. 2013 , 20, 053106	16
1893	Optimum laser intensity for the production of energetic deuterium ions from laser-cluster interaction. 2013 , 20, 093104	10
1892	Fabrication of nanopores in a graphene sheet with heavy ions: A molecular dynamics study. 2013 , 114, 234304	44
1891	Analytical modeling of thin film neutron converters and its application to thermal neutron gas detectors. 2013 , 8, P04020-P04020	36
1890	Epitaxial Ferroelectric Nanostructures Fabricated by FIB Milling. 2013, 23-43	2
1889	Formation of Co-implanted Silicon Ultra-Shallow Junctions for Low Thermal Budget Applications. 2013 , 30, 016101	2
1888	Process Prediction for Low-Energy Ion Beam Figuring Based on BH Modified Model. 2013 , 552, 238-243	
1887	Formation of single crystalline tellurium supersaturated silicon pn junctions by ion implantation followed by pulsed laser melting. 2013 , 34, 063001	
1886	Production and separation of 97Ru and coproduced 95Tc from 12C-induced reaction on yttrium target. 2013 , 101, 437-444	16
1885	SPICE-NIRS microbeam: a focused vertical system for proton irradiation of a single cell for radiobiological research. 2013 , 54, 736-47	40
1884	Measurement of the plasma astrophysical S factor for the 3He(d,p)4He reaction in exploding molecular clusters. 2013 , 111, 082502	36

1883 Lattice dependent motion of voids during electromigration. 2013 , 113, 134505	5
Heavy-ion-induced desorption yields of cryogenic surfaces bombarded with 1.4 MeV/u xeno 2013 , 16,	on ions.
1881 Micro/nanofabrication of poly(L-lactic acid) using focused ion beam direct etching. 2013 , 103	3, 163105 10
$_{ m 188o}$ Manipulation of the graphene surface potential by ion irradiation. 2013 , 102, 153103	41
1879 Cathodoluminescence characterization of suspended GaN nanomembranes. 2013 , 114, 0435	516 5
$_{ m 1878}$ Very bright, near-infrared single photon emitters in diamond. 2013 , 1, 032120	10
Comparison of proton microbeam and gamma irradiation for the radiation hardness testing silicon PIN diodes. 2013 , 8, P09003-P09003	of 2
First determination of the 8Li valence neutron asymptotic normalization coefficient using the 7Li(8Li,7Li)8Li reaction. 2013 , 88,	ne 9
1875 Effect of the substrate orientation on the formation of He-plates in Si. 2013 , 114, 193501	4
$_{1874}$ Excitation functions for production of Rf isotopes in the 248Cm+18O reaction. 2013 , 88,	9
1873 Defect formation and thermal stability of H in high dose H implanted ZnO. 2013 , 114, 08311	1 18
Effects of atomic collisions on the stoichiometry of thin films prepared by pulsed laser deposed 2013 , 111, 036101	sition. 29
1871 Ion beam irradiation induced fabrication of vertical coupling waveguides. 2013 , 102, 131112	5
Formation and optical absorption property of nanometer metallic colloids in Zn and Ag duall implanted silica: Synthesis of the modified Ag nanoparticles. 2013 , 113, 034304	ly ₁₁
1869 Radiation Damage of LaMgAl11O19 and CeMgAl11O19 Magnetoplumbite. 2013 , 96, 3325-33	332 3
A facility for soft proton irradiation of X-ray detectors and instrument testing for future spannissions. 2013 ,	ce
Fast atom beam-activated n-Si/n-GaAs wafer bonding with high interfacial transparency and electrical conductivity. 2013 , 113, 203512	29
The impact of negative oxygen ion bombardment on electronic and structural properties of magnetron sputtered ZnO:Al films. 2013 , 102, 242106	51

(2014-2013)

1865	Measurement or radiative proton capture on 18F and implications for oxygen-neon novae. 2013 , 110, 262502	17
1864	High Response in a Tellurium-Supersaturated Silicon Photodiode. 2013 , 30, 036101	11
1863	Direct measurement and modelling of internal strains in ion-implanted diamond. 2013 , 25, 385403	20
1862	A pixel detector system for laser-accelerated ion detection. 2013 , 8, P03008-P03008	9
1861	Measurement and modelling of anomalous polarity pulses in a multi-electrode diamond detector. 2013 , 104, 28005	6
1860	Graphical user interface for yield and doses estimations for cyclotron technetium production. 2013,	
1859	Specifications for hard condensed matter specimens for three-dimensional high-resolution tomographies. 2013 , 19, 726-39	17
1858	Study of the Spreading of Perfluoropolyether Lubricants on a Diamond-Like Carbon Film. 2013 , 56, 255-267	14
1857	Hydrogen Plasma-Driven Permeation through a Reduced Activation Ferritic Steel Alloy F82H. 2013 , 63, 361-363	15
1856	Radiological characteristics of charged particle interactions in the first clay-nanoparticle dichromate gel dosimeter. 2013 , 444, 012110	1
1855	Swift heavy ion irradiation of water ice from MeV to GeV energies. 2013 , 557, A97	47
1854	Digging gold: keV He(+) ion interaction with Au. 2013 , 4, 453-60	35
1853	Thin Film Polymer Composite Scintillators for Thermal Neutron Detection. 2013 , 2013, 1-8	9
1852	Scintillator diagnostics for the detection of laser accelerated ion beams. 2014 , 9, P09004-P09004	2
1851	Synthesis of embedded Au nanostructures by ion irradiation: influence of ion induced viscous flow and sputtering. 2014 , 5, 105-10	13
1850	Exploring the alpha cluster structure of nuclei using the thick target inverse kinematics technique for multiple alpha decays. 2014 , 66, 03005	2
1849	Enhancing Hydrogen Diffusion in Silica Matrix by Using Metal Ion Implantation to Improve the Emission Properties of Silicon Nanocrystals. 2014 , 2014, 1-8	1
1848	Direct-Write Ion Beam Lithography. 2014 , 2014, 1-26	41

1847	Fabrication of polydimethylsiloxane microlens arrays on a plastic film by proton beam writing. 2014 , 32, 06F506	3
1846	A study on the consequence of swift heavy ion irradiation of Zn-silica nanocomposite thin films: electronic sputtering. 2014 , 5, 1691-8	5
1845	References. 2014 , 14, 99-110	
1844	Solar particle event detected by ALTEA on board the International Space Station. 2014 , 4, A19	14
1843	Characterization of an Alternative Diamond Based Microdosimeter Prototype. 2014 , 61, 3479-3484	6
1842	Proton Radiation-Induced Void Formation in Ni/Au-Gated AlGaN/GaN HEMTs. 2014 , 35, 1194-1196	23
1841	TID and Displacement Damage Resilience of 1T1R \${rm HfO}_2/{rm Hf}\$ Resistive Memories. 2014 , 61, 2972-2978	17
1840	Comparison of total dose effects on SiGe heterojunction bipolar transistors induced by different swift heavy ion irradiation. 2014 , 23, 116104	2
1839	13 C(h) 16 O background in a liquid scintillator based neutrino experiment. 2014 , 38, 116201	4
1838	Deuterium retention and near-surface modification of ion-irradiated diamond exposed to fusion-relevant plasma. 2014 , 54, 073003	5
1837	Local formation of nitrogen-vacancy centers in diamond by swift heavy ions. 2014 , 116, 214107	13
1836	Nanomechanical and optical properties of yttrium thin films by magnetron sputtering. 2014 , 39, 3086-9	3
1835	Offline trapping of221Fr in a magneto-optical trap from implantation of an225Ac ion beam. 2014 , 9, P10013-P10013	4
1834	Improved spectral data unfolding for radiochromic film imaging spectroscopy of laser-accelerated proton beams. 2014 , 85, 043305	31
1833	Prediction of Spontaneous Plastic Deformation of Irradiated Metallic Glasses due to Thermal Spike-Induced Plasticity. 2014 , 2, 221-226	8
1832	Ionization effects coupled with the residual products of nuclear reactions induced by cosmic protons in the metallization layers of modern 3D integrated-circuit assemblies. 2014 , 8, 1265-1274	1
1831	Neutron dose estimation for 1H+9Be and 1H+12C reactions at 20 MeV proton energy via LET spectrometry using CR-39 detectors. 2014 , 302, 1289-1293	3
1830	A 14 MeV neutron generator as a source of various charged particles produced in fusion reactions. 2014 , T161, 014074	3

1829	Depth profiling of the modification induced by high-flux deuterium plasma in tungsten and tungstenEantalum alloys. 2014 , 54, 123013	23
1828	Relative nuclear abundance from C to Fe and integrated flux inside the Russian part of the ISS with the Sileye-3/Alteino experiment. 2014 , 41, 015202	3
1827	Microstructure evolution of zircaloy-4 during Ne ion irradiation and annealing: An in situ TEM investigation. 2014 , 23, 036102	6
1826	D and D/He plasma interactions with diamond: Surface modification and D retention. 2014 , 49, 103-110	6
1825	Track etch membranes (TEMs) for separation sciences from BARC-TIFR Pelletron accelerator. 2014 , 302, 947-950	1
1824	Irradiation-induced microstructural change in helium-implanted single crystal and nano-engineered SiC. 2014 , 453, 280-286	20
1823	Creation of deep blue light emitting nitrogen-vacancy center in nanosized diamond. 2014 , 104, 093101	7
1822	Stark shift and field ionization of arsenic donors in 28Si-silicon-on-insulator structures. 2014 , 104, 193502	15
1821	Nanoscale nuclear magnetic resonance with a 1.9-nm-deep nitrogen-vacancy sensor. 2014 , 104, 033102	111
1820	Material Stack Design With High Tolerance to Process-Induced Damage in Domain Wall Motion Device. 2014 , 50, 1-4	3
1819	Irradiation resistance of a nanostructured 316 austenitic stainless steel. 2014 , 63, 012121	11
1818	An apparatus to manipulate and identify individual Ba ions from bulk liquid Xe. 2014 , 85, 095114	11
1817	A compact proton spectrometer for measurement of the absolute DD proton spectrum from which yield and $\bf B$ are determined in thin-shell inertial-confinement-fusion implosions. 2014 , 85, 103504	13
1816	Thermal Desorption Studies of Ar+Implanted Silicon. 2014 , 125, 1400-1404	2
1815	Hydrogen accumulation in nanostructured as compared to the coarse-grained tungsten. 2014 , 453, 287-295	27
1814	Laser induced neutron production by explosion of the deuterium clusters. 2014 , 21, 013101	4
1813	Response function stability of single crystal diamond detectors to 14 MeV neutrons. 2014 , 85, 11D839	1
1812	Evaluation of mask repair strategies via focused electron, helium, and neon beam induced processing for EUV applications. 2014 ,	5

1811	Study of Oxide-Dispersion-Strengthened Ferritic Steels after Ion Implantation. 2014, 125, 741-743	1
1810	Acetone degradation by cosmic rays in the solar neighbourhood and in the Galactic Centre. 2014 , 444, 3792-3801	12
1809	Vacancy type defect formation in irradiated #Hron investigated by positron beam Doppler broadening technique. 2014 , 505, 012018	7
1808	Evaluation of EUV resist performance below 20nm CD using helium ion lithography. 2014 ,	9
1807	Dopant profile engineering using ArF excimer laser, flash lamp and spike annealing for junction formation. 2014 ,	2
1806	Degradation mechanisms of AlGaN/GaN HEMTs on sapphire, Si, and SiC substrates under proton irradiation. 2014 ,	6
1805	MeV-proton channeling in crystalline silicon. 2014 ,	O
1804	A study of buried channel formation in oxidized porous silicon. 2014 , 4, 57402-57411	7
1803	Extraction of thermalized projectile fragments from a large volume gas cell. 2014 , 763, 543-546	29
1802	The cryogenic gas stopping cell of SHIPTRAP. <i>Nuclear Instruments & Methods in Physics Research B</i> , 2014 , 338, 126-138	23
		12
	2014, 338, 126-138 Ion polished Cr/Sc attosecond multilayer mirrors for high water window reflectivity. 2014, 22, 26526-36 Metal-semiconductor-metal ion-implanted Si waveguide photodetectors for C-band operation	
1801	2014, 338, 126-138 Ion polished Cr/Sc attosecond multilayer mirrors for high water window reflectivity. 2014, 22, 26526-36 Metal-semiconductor-metal ion-implanted Si waveguide photodetectors for C-band operation.	12
1801 1800	Ion polished Cr/Sc attosecond multilayer mirrors for high water window reflectivity. 2014, 22, 26526-36 Metal-semiconductor-metal ion-implanted Si waveguide photodetectors for C-band operation. 2014, 22, 9150-8 Si+-implanted Si-wire waveguide photodetectors for the mid-infrared. 2014, 22, 27415-24	12
1801 1800 1799	Ion polished Cr/Sc attosecond multilayer mirrors for high water window reflectivity. 2014, 22, 26526-36 Metal-semiconductor-metal ion-implanted Si waveguide photodetectors for C-band operation. 2014, 22, 9150-8 Si+-implanted Si-wire waveguide photodetectors for the mid-infrared. 2014, 22, 27415-24 Optical depth localization of nitrogen-vacancy centers in diamond with nanometer accuracy. 2014,	12 12 18
1801 1800 1799 1798	Ion polished Cr/Sc attosecond multilayer mirrors for high water window reflectivity. 2014, 22, 26526-36 Metal-semiconductor-metal ion-implanted Si waveguide photodetectors for C-band operation. 2014, 22, 9150-8 Si+-implanted Si-wire waveguide photodetectors for the mid-infrared. 2014, 22, 27415-24 Optical depth localization of nitrogen-vacancy centers in diamond with nanometer accuracy. 2014, 22, 29986-95 Electrical properties and electronic structure of Si-implanted hexagonal boron nitride films. 2014,	12 12 18
1801 1800 1799 1798	Ion polished Cr/Sc attosecond multilayer mirrors for high water window reflectivity. 2014, 22, 26526-36 Metal-semiconductor-metal ion-implanted Si waveguide photodetectors for C-band operation. 2014, 22, 9150-8 Si+-implanted Si-wire waveguide photodetectors for the mid-infrared. 2014, 22, 27415-24 Optical depth localization of nitrogen-vacancy centers in diamond with nanometer accuracy. 2014, 22, 29986-95 Electrical properties and electronic structure of Si-implanted hexagonal boron nitride films. 2014, 105, 012104 A novel facility for 3D micro-irradiation of living cells in a controlled environment by MeV ions. 2014	12 12 18 9

1793	High-fidelity adiabatic inversion of a 31P electron spin qubit in natural silicon. 2014 , 104, 092115	18
1792	Empirical assessment of the detection efficiency of CR-39 at high proton fluence and a compact, proton detector for high-fluence applications. 2014 , 85, 043302	16
1791	Highly tunable formation of nitrogen-vacancy centers via ion implantation. 2014, 105, 063107	19
1790	Enhanced electrochemical etching of ion irradiated silicon by localized amorphization. 2014 , 104, 192108	2
1789	Cavity morphology in a Ni based superalloy under heavy ion irradiation with cold pre-injected helium. I. 2014 , 115, 103508	11
1788	Characterisation of deuterium spectra from laser driven multi-species sources by employing differentially filtered image plate detectors in Thomson spectrometers. 2014 , 85, 093303	26
1787	Position sensitive detection of neutrons in high radiation background field. 2014 , 85, 013304	8
1786	Hydrogen engineering via plasma immersion ion implantation and flash lamp annealing in silicon-based solar cell substrates. 2014 , 115, 064505	11
1785	Trace element content and magnetic properties of commercial HOPG samples studied by ion beam microscopy and SQUID magnetometry. 2014 , 4, 107142	22
1784	In situ growth and coalescence of He-filled bi-dimensional defects in Si by H supply. 2014 , 115, 223515	1
1783	Interaction of Sn atoms with defects introduced by ion implantation in Ge substrate. 2014 , 115, 173102	3
1782	Enhanced sputtering and incorporation of Mn in implanted GaAs and ZnO nanowires. 2014 , 47, 394003	22
1781	Creation and physical aspects of luminescent patterns using helium ion microscopy. 2014 , 115, 183502	10
1780	Chemical and physical effects induced by heavy cosmic ray analogues on frozen methanol and water ice mixtures. 2014 , 443, 2733-2745	14
1779	Micro-Raman study on the softening and stiffening of phonons in rutile titanium dioxide film: Competing effects of structural defects, crystallite size, and lattice strain. 2014 , 115, 143504	35
1778	Strength of the Ep=1.842 MeV resonance in the 40Ca(p,□)41Sc reaction reexamined. 2014 , 89,	7
1777	Comparison of the Edecay half-life of Po210 implanted in a copper matrix at 4.2 and 293 K. 2014 , 89,	8
1776	Edecay of the new neutron-deficient isotope 205Ac. 2014 , 89,	14

1775	Ultrashort pulsed neutron source. 2014 , 113, 184801		82
1774	Hybrid quantum circuit with implanted erbium ions. 2014 , 105, 162404		17
1773	The E3 center in zinc oxide: Evidence for involvement of hydrogen. 2014 , 104, 092111		16
1772	Criticality of Low-Energy Protons in Single-Event Effects Testing of Highly-Scaled Technologies. 2014 , 61, 2896-2903		24
1771	Ion irradiated graphite exposed to fusion-relevant deuterium plasma. <i>Nuclear Instruments & Methods in Physics Research B</i> , 2014 , 340, 21-26	1.2	4
1770	Integration of nano-scale components and supports in micromachined 3D silicon structures. 2014 , 24, 045008		3
1769	Understanding and engineering of NiGe/Ge junction formed by phosphorous ion implantation after germanidation. 2014 , 105, 062107		5
1768	Photonic crystals in lithium niobate by combining focussed ion beam writing and ion-beam enhanced etching. 2014 , 211, 2421-2425		17
1767	Effect of oxygen plasma and thermal oxidation on shallow nitrogen-vacancy centers in diamond. 2014 , 105, 042406		28
1766	Measurements of fusion reactions of low-intensity radioactive carbon beams on 12C and their implications for the understanding of X-ray bursts. 2014 , 112, 192701		27
1765	Dynamics of modification of Ni/n-GaN Schottky barrier diodes irradiated at low temperature by 200 MeV Ag14+ ions. 2014 , 104, 033507		15
1764	A new study of the 22Ne(p, [])23Na reaction deep underground: Feasibility, setup and first observation of the 186 keV resonance. 2014 , 50, 1		35
1763	Changes in the surface morphology induced by 1.0-MeV Au ion bombardment of Ti and Ti-6Al-4V. 2014 , 46, 314-320		1
1762	Invited article: Characterization of background sources in space-based time-of-flight mass spectrometers. 2014 , 85, 091301		19
1761	Double-resonant LA phonon scattering in defective graphene and carbon nanotubes. 2014 , 90,		18
1760	The Feasibility of direct measurement of the 44Ti(\mathbb{H} p)47V and 40Ca(\mathbb{H} p)43Sc reactions in forward kinematics at astrophysically relevant temperatures. 2014 , 50, 1		3
1759	Search for low-mass dark matter with CsI(Tl) crystal detectors. 2014 , 90,		20
1758	LIGHT-ELEMENT NUCLEOSYNTHESIS IN A MOLECULAR CLOUD INTERACTING WITH A SUPERNOVA REMNANT AND THE ORIGIN OF BERYLLIUM-10 IN THE PROTOSOLAR NEBULA. 2014 , 796, 124		18

1757	Surface morphology and deuterium retention of tungsten after low- and high-flux deuterium plasma exposure. 2014 , 54, 083014	49
1756	Origin of the lattice sites occupied by implanted Co in Si. 2014 , 29, 125006	4
1755	Plasma process induced physical damages on multilayered magnetic films for magnetic domain wall motion. 2014 , 53, 03DF03	4
1754	Evolution of isolated copper clusters under low-energy argon ion bombardment. 2014 , 56, 2568-2572	6
1753	Physical response of gold nanoparticles to single self-ion bombardment. 2014 , 29, 2387-2397	6
1752	Swift heavy ion track formation in Gd2Zr2IIi O7 pyrochlore: Effect of electronic energy loss. Nuclear Instruments & Methods in Physics Research B, 2014 , 336, 102-115	44
1751	Preliminary production of 211At at the Texas A&M University Cyclotron Institute. 2014 , 107, 1-9	4
1750	APPLICATION OF THE S3M AND MCNPX CODES IN PARTICLE DETECTOR DEVELOPMENT. 2014 , 27, 1460153	1
1749	Guided-wave phase-matched second-harmonic generation in KTiOPO 4 waveguide produced by swift heavy-ion irradiation. 2014 , 53, 117102	9
1748	Fluence measurement of fast neutron fields with a highly efficient recoil proton telescope using active pixel sensors. 2014 , 161, 41-5	4
1747	Helium Implantation of Ultrafine Grained Tungsten within a TEM. 2014 , 1645, 1	
1746	Evidence for age-related performance degradation of (241)Am foil sources commonly used in UK schools. 2014 , 34, 347-61	О
1745	Passive tailoring of laser-accelerated ion beam cut-off energy by using double foil assembly. 2014 , 21, 023119	6
1744	Structural modifications of swift-ion-bombarded metallic glasses studied by high-energy X-ray synchrotron radiation. 2014 , 80, 309-316	30
1743	High efficiency proton beam generation through target thickness control in femtosecond laser-plasma interactions. 2014 , 104, 214101	45
1742	Nanoscale lithography of LaAlOØsrTiO®wires using silicon stencil masks. 2014 , 25, 445301	8
1741	Generation of 3D nanopatterns with smooth surfaces. 2014 , 25, 315302	7
1740	Confinement in MeV Au 2+ implanted Si: a Raman scattering study. 2014 , 5, 015002	4

1739	Development of a PIXE method at high energy with the ARRONAX cyclotron. 2014 , 302, 895-901		4
1738	Swift Heavy Ion-Induced Decomposition and Phase Transformation in Nanocrystalline SnO2. 2014 , 1715, 13		Ο
1737	High resistivity isolation for AlGaN/GaN HEMT using Al double-implantation. 2014, 1635, 9-14		2
1736	Attosecond broadband multilayer mirrors for the water window spectral range. 2014,		1
1735	Potku [New analysis software for heavy ion elastic recoil detection analysis. <i>Nuclear Instruments & Methods in Physics Research B</i> , 2014 , 331, 34-41	1.2	88
1734	Proton stopping power measurements using high intensity short pulse lasers produced proton beams. 2014 , 740, 105-106		9
1733	Behavioral modeling of SRIM tables for numerical simulation. <i>Nuclear Instruments & Methods in Physics Research B</i> , 2014 , 322, 2-6	1.2	19
1732	Proximity gettering of slow diffuser contaminants in CMOS image sensors. 2014 , 91, 91-99		37
1731	Shielding data for hadron-therapy ion accelerators: Attenuation of secondary radiation in concrete. <i>Nuclear Instruments & Methods in Physics Research B</i> , 2014 , 319, 154-167	1.2	6
1730	The shape of ion tracks in natural apatite. <i>Nuclear Instruments & Methods in Physics Research B</i> , 2014 , 326, 117-120	1.2	17
1729	Resistance to He2+ induced irradiation damage in metallic glass Zr64Cu17.8Ni10.7Al7.5. 2014 , 444, 342	2-348	18
1728	Measurements of (186)Re production cross section induced by deuterons on (nat)W target at ARRONAX facility. 2014 , 41 Suppl, e16-8		8
1727	Fish gelatin thin film standards for biological application of PIXE. <i>Nuclear Instruments & Methods in Physics Research B</i> , 2014 , 332, 37-41	1.2	6
1726	Modifications of structural, optical and chemical properties of Li3+ irradiated polyurethane and polyetheretherketone. 2014 , 96, 181-185		23
1725	Ion-beam simulation of radiation damage produced by fast neutrons in heterophase structures. <i>Nuclear Instruments & Methods in Physics Research B</i> , 2014 , 326, 41-44	1.2	9
1724	Metallic conduction behavior in selenium-hyperdoped silicon. 2014 , 17, 134-137		6
1723	High energy (MeV) ion fluence dependent nano scale free volume defects studies of PMMA films. <i>Nuclear Instruments & Methods in Physics Research B</i> , 2014 , 320, 64-69	1.2	16
1722	Radial distribution of dose within heavy charged particle tracks [Models and experimental verification using LiF:Mg,Cu,P TL detectors. 2014 , 71, 242-246		5

1721	A comparative study of the effect of Ni9+ and Au8+ ion beams on the properties of poly(methacrylic acid) grafted gum ghatti films. 2014 , 97, 253-261		11	
1720	Corrosion and wear mechanisms of aluminum alloys surface reinforced by multicharged N-implantation. 2014 , 310, 311-316		10	
1719	Modifications in structure and optical property of Cu nanoparticles in SiO2 by post heavy ion irradiation. <i>Nuclear Instruments & Methods in Physics Research B</i> , 2014 , 326, 28-32	1.2	2	
1718	Study of physical and chemical modifications induced by 50 MeV Li3+ ion beam in polymers. 2014 , 94, 54-57		19	
1717	Sputtering yields exceeding 1000 by 80keV Xe irradiation of Au nanorods. <i>Nuclear Instruments & Methods in Physics Research B</i> , 2014 , 341, 17-21	1.2	14	
1716	(232)Th(d,4n)(230)Pa cross-section measurements at ARRONAX facility for the production of (230)U. 2014 , 41 Suppl, e19-22		11	
1715	60MeV Ni ion induced modifications in nano-CdS/polystyrene composite films. 2014 , 94, 49-53		21	
1714	Modeling detector response function of alpha particles for neutron depth profiling. 2014 , 57, 35-38		2	
1713	Evaluation of 500 keV proton irradiation of bilayer graphene on SiC by the use of SRIM code, a Monte Carlo simulation method for stopping and range of ions in matter. 2014 , 299, 13-17		4	
1712	ENMR. 2014 , 225, 173-182		31	
1711	Measurement of thermal conductivity in proton irradiated silicon. <i>Nuclear Instruments & Methods in Physics Research B</i> , 2014 , 325, 11-14	1.2	27	
1710	The production of radionuclides for nuclear medicine from a compact, low-energy accelerator system. 2014 , 41 Suppl, e7-15		2	
1709	Simulation of the direct production of 99mTc at a small cyclotron. <i>Nuclear Instruments & Methods in Physics Research B</i> , 2014 , 329, 18-21	1.2	13	
1708	Accurate Simulations of (^{206})Pb Recoils in SuperCDMS. 2014 , 176, 937-942		3	
1707	Effect of ion doping on the dislocation-related photoluminescence in Si+-implanted silicon. 2014 , 48, 199-203		7	
1706	Cross sections for energetic heavy-ion impact on protonated water clusters. 2014 , 114, 251-255		1	
1705	Chemically Induced Phase Transformation in Austenite by Focused Ion Beam. 2014 , 45, 1189-1198		21	
1704	Measurement of proton induced I-ray emission cross sections on Al from 2.5 to 4.1MeV. <i>Nuclear Instruments & Methods in Physics Research B</i> , 2014 , 332, 355-358	1.2	14	

1703	Extended X-ray absorption fine structure analysis of the local structure of iron nanoparticles. 2014 , 114, 19-21	2
1702	Post-annealing effects on structural and magnetic properties of MnN codoped ZnO thin films. 2014 , 21, 52-57	5
1701	TRI3DYN © Collisional computer simulation of the dynamic evolution of 3-dimensional nanostructures under ion irradiation. <i>Nuclear Instruments & Methods in Physics Research B</i> , 2014 , 322, 23-33	72
1700	Neutron depth profiling of Li-ion cell electrodes with a gas-controlled environment. 2014 , 248, 489-497	18
1699	Production cross sections of niobium and tantalum isotopes in proton-induced reactions on (nat)Zr and (nat)Hf up to 14 MeV. 2014 , 90, 149-57	8
1698	Optical switching and photoluminescence in erbium-implanted vanadium dioxide thin films. 2014 , 115, 093107	25
1697	Addressing single nitrogen-vacancy centers in diamond with transparent in-plane gate structures. 2014 , 14, 2359-64	32
1696	Influence of silicon dangling bonds on germanium thermal diffusion within SiO2 glass. 2014 , 104, 111901	9
1695	Fabrication of tapered graded-refractive-index micropillars using ion-implanted-photoresist as an etch mask. 2014 , 32, 021305	
1694	Irradiation behaviour of ₹ and □ phases in He ion implanted titanium aluminide alloy. 2014, 50, 28-33	11
1693	Influence of Ar/Kr ratio and pulse parameters in a Cr-N high power pulse magnetron sputtering process on plasma and coating properties. 2014 , 32, 021513	6
1692	Single and multiple profile fitting of AES and XPS intensity-depth profiles for analysis of interdiffusion in thin films. 2014 , 46, 1057-1063	9
1691	Quantifying defects in N-layer graphene via a phenomenological model of Raman spectroscopy. Nuclear Instruments & Methods in Physics Research B, 2014 , 319, 71-74	15
1690	Two shallow donors related to Zn interstitial in S-ion implanted ZnO epitaxial film. 2014 , 188, 12-14	3
1689	Ion irradiation of Allende meteorite probed by visible, IR, and Raman spectroscopies. 2014 , 237, 278-292	43
1688	Deuterium accumulation in tungsten under low-energy high-flux plasma exposure. 2014 , 8, 234-238	3
1687	A review of nuclear batteries. 2014 , 75, 117-148	137
1686	Plasticity and fracture of sapphire at room temperature: Load-controlled microcompression of four different orientations. 2014 , 40, 2083-2090	46

1685	Evaluation of radiation hardening in ion-irradiated Fe based alloys by nanoindentation. 2014, 444, 1-6	50
1684	Optical spectroscopy and imaging of colour centres in lithium fluoride crystals and thin films irradiated by 3MeV proton beams. <i>Nuclear Instruments & Methods in Physics Research B</i> , 2014 , 326, 72-75 ^{1.2}	9
1683	DFT study of the hyperfine parameters and magnetic properties of ZnO doped with 57Fe. 2014 , 185, 25-29	2
1682	Improved depth resolution of secondary ion mass spectrometry profiles in diamond: A quantitative analysis of the delta-doping. 2014 , 557, 222-226	21
1681	Measurement of fast neutron spectra from the interaction of 20MeV protons with thick Be and C targets using CR-39 detector. <i>Nuclear Instruments & Methods in Physics Research B</i> , 2014 , 318, 237-240	11
1680	Photoluminescence of focused ion beam implanted Er3+:Y2SiO5 crystals. 2014 , 8, 880-884	8
1679	Chains of quantum dot molecules grown on Si surface pre-patterned by ion-assisted nanoimprint lithography. 2014 , 105, 153106	7
1678	Interface and Bulk Charge Localization in Manganite Thin Films. 2014 , 1, 1400079	2
1677	Numerical estimation of self-sputtering effect in ionized physical vapor deposition system. 2014,	
1676	Measurements of fission product yield in the neutron-induced fission of 238U with average energies of 9.35 MeV and 12.52 MeV. 2014 , 65, 18-24	1
1675	Fine phantom image from laser-induced proton radiography with a spatial resolution of several h. 2014 , 65, 6-11	5
1674	Determination of the nitrogen abundance in organic materials by NanoSIMS quantitative imaging. 2014 , 29, 512	32
1673	First observation of HOIreactivity in water under high energy ions at elevated temperature. 2014 , 16, 23975-84	4
1672	Application of HOPG and CVD graphene as ion beam detectors. <i>Nuclear Instruments & Methods in Physics Research B</i> , 2014 , 340, 81-84	3
1671	Biophysical Basis of Ionizing Radiation. 2014 , 65-104	4
1670	Plasma-Induced Erosion on Ceramic Wall Structures in Hall-Effect Thrusters. 2014 , 30, 690-695	17
1669	High accuracy traceable Rutherford backscattering spectrometry of ion implanted samples. 2014 , 6, 120-129	22
1668	Irradiated rare-earth-doped powellite single crystal probed by confocal Raman mapping and transmission electron microscopy. 2014 , 45, 383-391	12

1667	A Facility for Soft Proton Irradiation and Instrument Testing for Future Space Missions. 2014 , 61, 1937-1942	1
1666	Comparison of YBatut Films Irradiated With Helium and Neon Ions for the Fabricationof Josephson Devices. 2014 , 24, 1-5	10
1665	Radiolytic Corrosion of Uranium Dioxide: Role of Molecular Species. 2014 , 118, 1071-1080	13
1664	Relative TL and OSL efficiency to protons of various dosimetric materials. 2014 , 161, 112-5	7
1663	Effects of high temperature annealing on defects and luminescence properties in H implanted ZnO. 2014 , 47, 342001	7
1662	Buried centimeter-long micro- and nanochannel arrays in porous silicon and glass. 2014 , 14, 2081-9	12
1661	In situ TEM ion irradiation and implantation effects on Au nanoparticle morphologies. 2014 , 50, 7593-6	9
1660	A time-dependent model for reactive sputter deposition. 2014 , 47, 235302	40
1659	Fabrication of silicon molds with multi-level, non-planar, micro- and nano-scale features. 2014 , 25, 375301	3
1658	Peculiarities of temperature dependent ion beam sputtering and channeling of crystalline bismuth. 2014 , 25, 305302	
1657	Graphical user interface for yield and dose estimations for cyclotron-produced technetium. 2014 , 59, 3337-52	4
1656	An array of ferromagnetic nanoislands nondestructively patterned via a local phase transformation by low-energy proton irradiation. 2014 , 8, 4698-704	17
1655	Solid state detectors based on point defects in lithium fluoride for advanced proton beam diagnostics. 2014 , 156, 170-174	30
1654	Excitation energy dependence of the total kinetic energy release in 235U(n,f). 2014 , 89,	12
1653	Effect of irradiation damage on the shear strength of CuNb interfaces. 2014, 90-91, 29-32	18
1652	Effect of dislocation density on improved radiation hardening resistance of nano-structured tungstenthenium. 2014 , 611, 388-393	32
1651	Ion implantation in diamond for quantum information processing (QIP): doping and damaging. 2014 , 36-67	2
1650	The origin of conductivity in ion-irradiated diamond-like carbon Phase transformation and atomic ordering. 2014 , 80, 677-690	31

1649	On the formation of the porous structure in nanostructured a-Si coatings deposited by dc magnetron sputtering at oblique angles. 2014 , 25, 355705	32
1648	A broad angular-range measurement of elastic and inelastic scatterings in the 16O on 27Al reaction at 17.5MeV/u. 2014 , 763, 314-319	43
1647	Radiation induced microstructures in ODS 316 austenitic steel under dual-beam ions. 2014 , 455, 242-247	13
1646	An analytical model for the mechanical deformation of locally graphitized diamond. 2014 , 48, 73-81	8
1645	Emulation of reactor irradiation damage using ion beams. 2014 , 88, 33-36	158
1644	Development of position-sensitive time-of-flight spectrometer for fission fragment research. 2014 , 764, 53-58	8
1643	Irradiation effects of high-energy proton beams on MoS2 field effect transistors. 2014 , 8, 2774-81	82
1642	Experimental study of pyrolytic boron nitride at high temperature with and without proton and VUV irradiations. 2014 , 314, 415-425	5
1641	Oxygen depth profiling with subnanometre depth resolution. <i>Nuclear Instruments & Methods in Physics Research B</i> , 2014 , 337, 27-33	4
1640	An Analytical Model to Quantify Decay Chain Disequilibrium Application to the Thorium Decay Chain. 2014 , 61, 1414-1419	2
1639	Pd Nanoparticles deposited on nitrogen-doped HOPG: New Insights into the Pd-catalyzed Oxygen Reduction Reaction. 2014 , 141, 89-101	39
1638	Positron studies of interaction between yttrium atoms and vacancies in bcc iron with relevance for ODS nanoparticles formation. 2014 , 455, 398-401	8
1637	Thermoluminescent Properties of Undoped and Ce-Doped Lutetium Orthosilicate and Yttrium Orthosilicate Single Crystals and Single Crystalline Films Scintillators. 2014 , 61, 276-281	6
1636	Impact of bias conditions on performance degradation in SiGe HBTs irradiated by 10MeV Br ion. 2014 , 54, 2728-2734	2
1635	Solid state field-cycling NMR relaxometry: instrumental improvements and new applications. 2014 , 82, 39-69	84
1634	Investigation of gold nanoparticle radiosensitization mechanisms using a free radical scavenger and protons of different energies. 2014 , 59, 6431-43	55
1633	Hydrogen detection near surfaces and shallow interfaces with resonant nuclear reaction analysis. 2014 , 69, 196-295	88
1632	Study of the inter-strip gap effects on the response of Double Sided Silicon Strip Detectors using proton micro-beams. 2014 , 767, 99-111	14

1631	Deformation of nanoporous nanopillars by ion beam-induced bending. 2014 , 49, 5598-5605		18
1630	Profiling lithium distribution in Sn anode for lithium-ion batteries with neutrons. 2014 , 301, 277-284		20
1629	Application of alpha particle transport to the modelization of efficiency curves in proportional counters. 2014 , 302, 297-302		2
1628	Ion beam irradiation of ZnS dispersed in PMMA and its photocatalytic application. 2014 , 302, 819-824		3
1627	Influence of Light Ion Irradiation on the Current-Voltage Characteristics of Electrochemical Anodization of p-Type Silicon. 2014 , 161, E97-E103		1
1626	Defect accumulation in ThO2 irradiated with swift heavy ions. <i>Nuclear Instruments & Methods in Physics Research B</i> , 2014 , 326, 169-173	1.2	35
1625	Dependence of the thermoluminescent high-temperature ratio (HTR) of LiF:Mg,Ti detectors on proton energy and dose. 2014 , 71, 39-42		8
1624	Measurements and 3D Monte Carlo simulation of MeV ion transmission through conical glass capillaries. <i>Nuclear Instruments & Methods in Physics Research B</i> , 2014 , 330, 11-17	1.2	20
1623	Measurement of the Half-Life of the T=12 Mirror Decay of Ne19 and its Implication on Physics Beyond the Standard Model. 2014 , 112,		18
1622	Simulation of the characteristics of low-energy proton induced single event upset. 2014 , 57, 1902-1906		3
1621	Size-induced moment formation on isolated Fe atoms embedded in a nanocrystalline Ta matrix: Experiment and theory. 2014 , 89,		5
1620	Solid state detectors based on luminescent point defects in lithium fluoride for proton beam diagnostics. 2014 ,		
1619	Thoron detection with an active Radon exposure meterfirst results. 2014 , 85, 022106		8
1618	Substrate-Dependent Effects on the Response of AlGaN/GaN HEMTs to 2-MeV Proton Irradiation. 2014 , 35, 826-828		65
1617	Concurrent in situ ion irradiation transmission electron microscope. <i>Nuclear Instruments & Methods in Physics Research B</i> , 2014 , 338, 56-65	1.2	82
1616	A solid target system with remote handling of irradiated targets for PET cyclotrons. 2014 , 94, 294-301		7
1615	Effects of helium implantation on the tensile properties and microstructure of Ni73P27 metallic glass nanostructures. 2014 , 14, 5176-83		50
1614	Transmission Electron Microscope-Based Spectroscopy. 2014 , 231-244		2

1613	The excitation functions of (100)Mo(p,x)(99)Mo and (100)Mo(p,2n)(99m)Tc. 2014 , 94, 344-348		25
1612	Printing nearly-discrete magnetic patterns using chemical disorder induced ferromagnetism. 2014 , 14, 435-41		65
1611	Luminescence studies of 100[MeV Si8+ ion irradiated nanocrystalline Y2O3. 2014 , 71, 518-523		12
1610	Effect of neutron irradiation on charge collection efficiency in 4H-SiC Schottky diode. 2014 , 735, 218-22	22	19
1609	Swift heavy ions induced surface modifications in Ag-polypyrrole composite films synthesized by an electrochemical route. <i>Nuclear Instruments & Methods in Physics Research B</i> , 2014 , 323, 7-13	1.2	9
1608	The Dark Matter Time Projection Chamber 4Shooter directional dark matter detector: Calibration in a surface laboratory. 2014 , 755, 6-19		9
1607	Improved physics in SIMNRA 7. Nuclear Instruments & Methods in Physics Research B, 2014, 332, 176-180	1.2	138
1606	Investigation of pyridine carboxylic acids in CM2 carbonaceous chondrites: Potential precursor molecules for ancient coenzymes. 2014 , 136, 1-12		34
1605	Dynamic microstructural evolution of graphite under displacing irradiation. 2014 , 68, 273-284		22
1604	Optical characterization and laser damage of fused silica optics after ion beam sputtering. 2014 , 125, 756-760		6
1603	Effect of swift heavy ion irradiation on single- and multiwalled carbon nanotubes. <i>Nuclear Instruments & Methods in Physics Research B</i> , 2014 , 326, 33-36	1.2	12
1602	Temperature effects on the behavior of carbon 14 in nuclear graphite. <i>Nuclear Instruments & Methods in Physics Research B</i> , 2014 , 332, 106-110	1.2	7
1601	Musett: A segmented Si array for Recoil-Decay-Tagging studies at VAMOS. 2014 , 747, 69-80		9
1600	Nuclear reaction analysis of Ge ion-implanted ZnO bulk single crystals: The evaluation of the displacement in oxygen lattices. <i>Nuclear Instruments & Methods in Physics Research B</i> , 2014 , 332, 11-14	1.2	
1599	Modelling of hydrogen isotope retention in the tungsten divertor of EAST during ELMy H-mode. 2014 , 89, 2214-2219		9
1598	Electronic stopping force of 12C, 28Si and 63Cu ions in HfO2 and SiO2 dielectric films. <i>Nuclear Instruments & Methods in Physics Research B</i> , 2014 , 322, 54-58	1.2	9
1597	Under-response correction for EBT3 films in the presence of proton spread out Bragg peaks. 2014 , 30, 454-61		40
1596	Reflection and implantation of low energy helium with tungsten surfaces. 2014 , 447, 254-270		34

1595	Conceptual design and optimization of a plastic scintillator array for 2D tomography using a compact D-D fast neutron generator. 2014 , 86, 63-70	8
1594	Slow positron beam and nanoindentation study of irradiation-related defects in reactor vessel steels. 2014 , 451, 249-254	22
1593	Nonlinear refraction of lithium niobate crystal doped with different metal nanoparticles. 2014 , 123, 35-37	17
1592	On ion implantation and damage effect in Li2TiO3 as a fusion breeder blanket: A technological approach for degradation testing. 2014 , 89, 1529-1533	8
1591	Measuring the fusion cross-section of light nuclei with low-intensity beams. 2014 , 743, 5-13	11
1590	Swift heavy ion irradiation-induced amorphization of La2Ti2O7. <i>Nuclear Instruments & Methods in Physics Research B</i> , 2014 , 326, 145-149	19
1589	Fabrication of fine imaging devices using an external proton microbeam. <i>Nuclear Instruments & Methods in Physics Research B</i> , 2014 , 332, 238-241	0
1588	Oxidation smoothening of silicon machined micro- and nano-scale structures. 2014 , 121, 156-161	3
1587	Temperature dependent formation of ZnO and Zn2SiO4 nanoparticles by ion implantation and thermal annealing. <i>Nuclear Instruments & Methods in Physics Research B,</i> 2014 , 332, 359-363	7
1586	Surface morphology and phase stability of titanium foils irradiated with 136MeV 136Xe. <i>Nuclear Instruments & Methods in Physics Research B</i> , 2014 , 328, 78-83	5
1585	Application of slow positron beam for study of commercial oxide-dispersion-strengthened steels. 2014 , 450, 99-103	9
1584	Investigation of structural stability and magnetic properties of Fe/Ni multilayers irradiated by 300keV Fe10+. 2014 , 452, 31-36	17
1583	Raman study of damage extent in graphene nanostructures carved by high energy helium ion beam. 2014 , 72, 233-241	46
1582	Dosimetry measurements using Timepix in mixed radiation fields induced by heavy ions; comparison with standard dosimetry methods. 2014 , 55, i141-i142	3
1581	Self-irradiation and oxidation effects on americium sesquioxide and Raman spectroscopy studies of americium oxides. 2014 , 217, 159-168	10
1580	Room-temperature control of the residual stress gradient in titanium micro-cantilever beams by helium ion implantation. 2014 , 216, 116-122	6
1579	Effect of proton irradiation on the friction and wear properties of polyimide. 2014 , 316, 30-36	29
1578	Ion-beam-induced thin film stress in lithium niobate. 2014 , 47, 265302	5

1577	Numerical study of the effects of physical parameters on the dynamic fuel retention in tungsten materials. 2014 , 455, 111-115		5
1576	Continuous observation of polarization effects in thin SC-CVD diamond detector designed for heavy ion microbeam measurement. <i>Nuclear Instruments & Methods in Physics Research B</i> , 2014 , 1. 331, 113-116	.2	20
1575	TOF SIMS characterization of SEI layer on battery electrodes. <i>Nuclear Instruments & Methods in Physics Research B</i> , 2014 , 332, 368-372	.2	18
1574	Analysis of the background of the Jena 14C-AMS facility. <i>Nuclear Instruments & Methods in Physics Research B</i> , 2014 , 331, 238-242	.2	3
1573	The LILIA (laser induced light ions acceleration) experiment at LNF. <i>Nuclear Instruments & Methods in Physics Research B</i> , 2014 , 331, 15-19	.2	14
1572	Proton irradiation effects on the precipitate in a Zrū.6Snū.6Nbū.2Feū.1Cr alloy. 2014 , 452, 335-342		30
1571	Emission channeling studies on transition-metal doped GaN and ZnO: Cation versus anion substitution. <i>Nuclear Instruments & Methods in Physics Research B</i> , 2014 , 332, 143-147	.2	3
1570	Energy spectra and LET spectra of protons behind shielding. <i>Nuclear Instruments & Methods in Physics Research B</i> , 2014 , 333, 46-51	.2	8
1569	Structural dependence of threshold displacement energies in rutile, anatase and brookite TiO2. 2014 , 147, 311-318		27
1568	Kink Band Formation in Graphite under Ion Irradiation at 100 and 298 K. 2014 , 55, 447-450		5
1567	Irradiation Induced Chemical and Physical Effects in Silicones. 2014 , 75-84		2
1566	Carbon ion irradiation of the human prostate cancer cell line PC3: a whole genome microarray study. 2014 , 44, 1056-72		28
1565	ENMR of 8Li+ in rutile TiO2. 2014 , 551, 012032		2
1564	First Wall Particle Flux Measurements by an F82H Permeation Probe in QUEST. 2014 , 9, 3405041-3405041		3
1563	Current Status of Beryllium Materials for Fusion Blanket Applications. 2014 , 66, 28-37		21
1562	Vacancy defects study in Fe based alloys induced by irradiation under various conditions. 2014 , 505, 01200	07	2
1561	Direct Imaging of Cl- and Cu-Induced Short-Circuit Efficiency Changes in CdTe Solar Cells. 2014 , 4, 1400454	4	58
1560	MEASUREMENT OF 230Pa AND 186Re PRODUCTION CROSS SECTIONS INDUCED BY DEUTERONS AT ARRONAX FACILITY. 2014 , 27, 1460149		

1559	Toward site-specific dopant contrast in scanning electron microscopy. 2014 , 20, 1312-7		1
1558	Study on annealing effects of irradiated Ga0.5In0.5P/GaAs/Ge solar cell by 170 keV proton. 2014 ,		
1557	Tracking subsurface ion radiation damage with metal®xide®emiconductor device encapsulation. 2015 , 30, 1413-1421		8
1556	The application of proton spectrometers at the SG-III facility for ICF implosion areal density diagnostics. 2015 , 3,		7
1555	Measurement of the angle, temperature and flux of fast electrons emitted from intense laserBolid interactions. 2015 , 81,		21
1554	Transmission electron microscopy with in situ ion irradiation. 2015 , 30, 1214-1221		11
1553	Examination of the impact of electronphonon coupling on fission enhanced diffusion in uranium dioxide using classical molecular dynamics. 2015 , 30, 1485-1494		12
1552	In situ characterization of ion-irradiation enhanced creep of third generation Tyranno SA3 SiC fibers. 2015 , 30, 1572-1582		7
1551	Thermal conductivity measurements via time-domain thermoreflectance for the characterization of radiation induced damage. 2015 , 30, 1403-1412		37
1550	Characterization of ion-induced radiation effects in nuclear materials using synchrotron x-ray techniques. 2015 , 30, 1366-1379		27
1549	Electron Beam Effects during In-Situ Annealing of Self-Ion Irradiated Nanocrystalline Nickel. 2015 , 1809, 13-18		6
1548	Multi-Sampling Ionization Chamber (MUSIC) for measurements of fusion reactions with radioactive beams. 2015 , 799, 197-202		21
1547	Semi-empirical relationships for the energy loss and straggling of 100 keV hydrogen ions passing through thin carbon foils. <i>Nuclear Instruments & Methods in Physics Research B</i> , 2015 , 359, 115-119	1.2	14
1546	Development of a new in-air micro-PIXE set-up with in-vacuum charge measurements in Atomki. <i>Nuclear Instruments & Methods in Physics Research B</i> , 2015 , 362, 167-171	1.2	8
1545	Radiolytic corrosion of uranium dioxide induced by He2+ localized irradiation of water: Role of the produced H2O2 distance. 2015 , 467, 832-839		3
1544	Challenges to the use of ion irradiation for emulating reactor irradiation. 2015 , 30, 1158-1182		128
1543	Distribution of D1 dislocation luminescence centers in Si+-implanted silicon and the photoluminescence model. 2015 , 1, 33-37		1
1542	Production of scandium-44 m and scandium-44 g with deuterons on calcium-44: cross section measurements and production yield calculations. 2015 , 60, 6847-64		37

(2015-2015)

1541	IM3D: A parallel Monte Carlo code for efficient simulations of primary radiation displacements and damage in 3D geometry. 2015 , 5, 18130	36
1540	Electronic stopping power in a narrow band gap semiconductor from first principles. 2015 , 91,	40
1539	Threshold displacement energies in graphene and single-walled carbon nanotubes. 2015 , 92,	19
1538	Modification of Pt/Co/Pt film properties by ion irradiation. 2015 , 92,	8
1537	Phase transformations in Ln2O3 materials irradiated with swift heavy ions. 2015 , 92,	32
1536	Energy-dependent fragmentation cross sections of relativistic C12. 2015 , 92,	21
1535	High-precision half-life measurements for the superallowed Fermi ⊞ emitter Ne18. 2015 , 92,	13
1534	Hot fusion-evaporation cross sections of Sc45-induced reactions with lanthanide targets. 2015 , 92,	5
1533	Strengths of the resonances at 436, 479, 639, 661, and 1279 keV in the Ne22(p, DNa23 reaction. 2015 , 92,	21
1532	Hot fusion-evaporation cross sections of Ca44-induced reactions with lanthanide targets. 2015 , 92,	1
1531	Evidence for survival of the Æluster structure in light nuclei through the fusion process. 2015 , 92,	9
1530	Sub-barrier radioactive ion beam investigations using a new methodology and analysis for the stacked target technique. 2015 , 92,	13
1529	Predictions for the energy loss of light ions in laser-generated plasmas at low and medium velocities. 2015 , 92, 053109	19
1528	Uniform heating of materials into the warm dense matter regime with laser-driven quasimonoenergetic ion beams. 2015 , 92, 063101	22
1527	Inverse Kinematic Study of the (26g)Al(d,p)(27)Al Reaction and Implications for Destruction of (26)Al in Wolf-Rayet and Asymptotic Giant Branch Stars. 2015 , 115, 062701	20
1526	Limit on Tensor Currents from ^{8}Li Decay. 2015 , 115, 182501	22
1525	Three New Low-Energy Resonances in the $^{22}Ne(p,D)^{23}Na$ Reaction. 2015 , 115, 252501	42
1524	Collectivity in the light radon nuclei measured directly via Coulomb excitation. 2015 , 91,	8

1523	Non-Contact Measurement of Thermal Diffusivity in Ion-Implanted Nuclear Materials. 2015 , 5, 16042	59
1522	Nuclear model calculations on cyclotron production of 51Cr. 2015 , 80, 569-574	1
1521	The plasma oxidation mechanism of Al coatings on Si substrates. 2015 , 4, 42-47	
1520	Degradation mechanisms of 2 MeV proton irradiated AlGaN/GaN HEMTs. 2015 , 107, 083504	26
1519	Visualization of expanding warm dense gold and diamond heated rapidly by laser-generated ion beams. 2015 , 5, 14318	26
1518	On the Structural and Chemical Characteristics of Co/Al2O3/graphene Interfaces for Graphene Spintronic Devices. 2015 , 5, 14332	7
1517	Cryogenic micro-calorimeters for mass spectrometric identification of neutral molecules and molecular fragments. 2015 , 118, 104503	9
1516	From a non-magnet to a ferromagnet: Mn+ implantation into different TiO2 structures. 2015 , 107, 242405	12
1515	Radiation Defects Formed in Ion-Irradiated 316L Stainless Steel Model Alloys with Different Si Additions. 2015 , 56, 1549-1552	4
1514	Ion irradiation of the Murchison meteorite: Visible to mid-infrared spectroscopic results. 2015 , 577, A41	46
1513	Calibration of BAS-TR image plate response to high energy (3-300 MeV) carbon ions. 2015 , 86, 123302	22
1512	Ion-beam synthesis of GaN in silicon. 2015 , 643, 012082	2
1511	THz photomixers based on nitrogen-ion-implanted GaAs. 2015 , 118, 183102	2
1510	Elimination of carbon vacancies in 4H-SiC epi-layers by near-surface ion implantation: Influence of the ion species. 2015 , 118, 175701	23
1509	Self-organized titanium oxide nano-channels for resistive memory application. 2015 , 118, 224903	19
1508	Molecular dynamics simulation of radiation damage cascades in diamond. 2015 , 117, 245901	21
1507	Spectroscopic properties and radiation damage investigation of a diamond based Schottky diode for ion-beam therapy microdosimetry. 2015 , 118, 184503	20
1506	Photoluminescence of radiation-induced color centers in lithium fluoride thin films for advanced diagnostics of proton beams. 2015 , 106, 261108	24

1505	Single proton counting at the RIKEN cell irradiation facility. 2015 , 86, 085103		1
1504	Tuned NV emission by in-plane Al-Schottky junctions on hydrogen terminated diamond. 2014 , 4, 3634		31
1503	The effect of irradiation with H+ and Ne+ ions on resistive switching in metalinsulator thetal memristive structures based on SiO x. 2015 , 41, 957-960		1
1502	DPA damage analysis for 14-MeV neutrons on PFC materials. 2015 , 66, 1841-1844		
1501	Damage buildup in Ar-ion-irradiated 3C-SiC at elevated temperatures. 2015 , 118, 105705		14
1500	Direct Depth- and Lateral- Imaging of Nanoscale Magnets Generated by Ion Impact. 2015 , 5, 16786		29
1499	Instability of Ferromagnetic Nanoclusters in Fe Implanted Amorphous SiO2. 2015 , 75, 565-571		2
1498	Thermal decomposition and desorption of PFPE Zdol on a DLC substrate using quartic bond interaction potential. 2015 , 5, 69651-69659		1
1497	Direct measurement of neon production rates by (﴿) reactions in minerals. 2015, 148, 130-144		9
1496	Energy loss and straggling of 150 keV H, He, C, N, and O ions passing through few layer graphene. Nuclear Instruments & Methods in Physics Research B, 2015, 358, 223-228	1.2	4
1495	Swift heavy ion modifications of astrophysical water ice. <i>Nuclear Instruments & Methods in Physics Research B</i> , 2015 , 365, 472-476	1.2	16
1494	Track Reconstruction Progress from the DMTPC Directional Dark Matter Experiment. 2015 , 61, 39-44		6
1493	Argon diffusion in Apollo 16 impact glass spherules: Implications for 40Ar/39Ar dating of lunar impact events. 2015 , 148, 251-268		14
1492	A dedicated AMS setup for 53Mn/60Fe at the Cologne FN tandem accelerator. <i>Nuclear Instruments & Methods in Physics Research B</i> , 2015 , 361, 95-99	1.2	4
1491	A detection system for charged-particle decay studies with a continuous-implantation method. 2015 , 804, 1-7		18
1490	Swift heavy ion irradiation and annealing studies on the IIV characteristics of N-channel depletion MetalBxideIemiconductor field-effect transistors. 2015 , 89, 943-950		1
1489	Reference-free, depth-dependent characterization of nanolayers and gradient systems with advanced grazing incidence X-ray fluorescence analysis. 2015 , 212, 523-528		15
1488	Impact of Swift Heavy Ions and Gamma Radiation upon Optical, Structural, and Chemical Properties of Polypropylene Polymer Films. 2015 , 34, n/a-n/a		2

1487	Influence of ion irradiation on the resistive switching parameters of SiOx-based thin-film structures. 2015 , 643, 012094	2
1486	Synthesis of Layer-Tunable Graphene: A Combined Kinetic Implantation and Thermal Ejection Approach. 2015 , 25, 3666-3675	38
1485	Ion-Beam Deposition/Etching Using EMIM-N(CN)2 Ionic Liquid Ion Source. 2015, 40, 87-90	2
1484	Characterization of the ion-amorphization process and thermal annealing effects on third generation SiC fibers and 6H-SiC. 2015 , 1, 8	9
1483	Fabrication of Microstructures Embedded in SC-CVD Diamond with a Focused Proton Microbeam. 2015 , 643, 15-19	
1482	A Comparative Study of the Effects of Oxygen Ions Upon the Free Volume and Physico-Chemical Properties of Makrofol (KG & N) Polycarbonate. 2015 , 357, 86-98	
1481	Nanostructuring graphene by dense electronic excitation. 2015 , 26, 465302	31
1480	Krypton ion irradiation-induced amorphization and nano-crystal formation in pyrochlore Lu 2 Ti 2 O 7 at room temperature. 2015 , 24, 126103	7
1479	Water radiolysis with heavy-ion beams at GANIL. Back to 20 years of investigations. 2015 , 629, 012009	1
1478	Transient and Post-irradiation Response of Optoelectronic Devices to Ionizing Radiation. 2015 , 574, 012019	1
1477	Monte Carlo simulation of prompt ⊡ray emission in proton therapy using a specific track length estimator. 2015 , 60, 8067-86	6
1476	Near Surface Changes Due to 700lkeV Si+ Irradiation of Titanium Silicon Carbide. 2015 , 98, 4050-4057	6
1475	Effect of irradiation by He+ and Ga+ ions on the 2D-exciton susceptibility of InGaAs/GaAs quantum-well structures. 2015 , 252, 1950-1954	8
1474	Direct Observation of Li-Ion Transport in Electrodes under Nonequilibrium Conditions Using Neutron Depth Profiling. 2015 , 5, 1500498	65
1473	Cellular localization of uranium in the renal proximal tubules during acute renal uranium toxicity. 2015 , 35, 1594-600	24
1472	In situ E-SEM and TEM observations of the thermal annealing effects on ion-amorphized 6H-SiC single crystals and nanophased SiC fibers. 2015 , 252, 149-152	6
1471	Scanning reflection ion microscopy in a helium ion microscope. 2015 , 6, 1125-37	9
1470	Ion Preparation Systems for Low-Energy Experiments at SLOWRI. 2015 ,	

1469 Investigating energy dissipation through nucleon transfer reactions. **2015**, 91, 00010

1468 S-Fact	or measurement of the12C(p,[])13N reaction in inverse kinematics. 2015 , 93, 03012	2
1467 A labo	ratory study of ion-induced erosion of ice-covered carbon grains. 2015, 575, A76	15
1466 lon im	plantation for manufacturing bent and periodically bent crystals. 2015 , 107, 064102	7
	observation and atomic resolution imaging of the ion irradiation induced amorphisation of ene. 2014 , 4, 6334	49
Relati 14 ⁶⁴ 182, 1	ng surface chemistry and oxygen surface exchange in LnBaCo2O(5+🎚air electrodes. 2015 , 45-57	27
14 ⁶ 3 Calibra 164, 4	ation of modified Liulin detector for cosmic radiation measurements on-board aircraft. 2015 , 89-92	2
1462 Perfor	mance of timing Resistive Plate Chambers with protons from 200 to 800 MeV. 2015 , 10, C01043-C010	436
	on of Blue Light Emitting Color Centers in Nanosized Diamond for Different Applications. 93-101	1
1460 Cyclot	ron production of (44)Sc: From bench to bedside. 2015 , 42, 745-51	66
1459 Sputte	ering of cubic metal crystals by low-energy xenon-ions. 2015 , 107, 102-109	3
	mination of deuteron characteristic channeling parameters by simulation of RBS spectrum Si . 2015 , 79, 19-23	1
1457 Impac	t of Radiation on Electronics. 2015 , 79-111	
	ferromagnetic semiconductors prepared by the combination of ion implantation with pulse nelting. 2015 , 48, 263001	17
1455 On the	e influence of etch pits in the overall dissolution rate of apatite basal sections. 2015 , 42, 629-640	2
1454 Soft p	roton scattering efficiency measurements on x-ray mirror shells. 2015 , 39, 343-365	15
1453 Develo	opment of neutron depth profiling at CMRR. 2015 , 788, 1-4	7
1452 Towar	ation of hard-coated optical absorbers with microstructured surfaces using etched ion tracks: ad broadband ultra-low reflectance. <i>Nuclear Instruments & Methods in Physics Research B</i> , 2015 1.2 357, 154-159	8

1451	Nanomechanical and in situ TEM characterization of boron carbide thin films on helium implanted substrates: Delamination, real-time cracking and substrate buckling. 2015 , 639, 54-64	6
1450	Simulations of the fission-product stopping efficiency in IGISOL. 2015 , 51, 1	17
1449	Synchrotron x-ray diffraction analysis of gadolinium and lanthanum titanate oxides irradiated by xenon and tantalum swift heavy ions. 2015 , 1743, 26	2
1448	Edecay properties of the new isotope U216. 2015 , 91,	24
1447	On radiation damage in FIB-prepared softwood samples measured by scanning X-ray diffraction. 2015 , 22, 267-72	4
1446	Dark Current Spectroscopy on Alpha Irradiated CMOS Image Sensors. 2015 ,	2
1445	3D Silicon Microdosimetry and RBE Study Using \$^{12}{rm C}\$ Ion of Different Energies. 2015 , 62, 3027-3033	28
1444	Post-acceleration of laser-induced ion beams. 2015 , 170, 290-302	1
1443	Charge Collection Mechanisms of Ge-Channel Bulk \$p\$ MOSFETs. 2015 , 62, 2725-2731	7
1442	SEU Rate in Avionics: From Sea Level to High Altitudes. 2015 , 62, 3369-3380	7
1441	Comparative Response of Microchannel Plate and Channel Electron Multiplier Detectors to Penetrating Radiation in Space. 2015 , 62, 2283-2293	8
1440	Effect of recrystallization on ion-irradiation hardening and microstructural changes in 15Cr-ODS steel. <i>Nuclear Instruments & Methods in Physics Research B</i> , 2015 , 365, 313-318	12
1439	Focused ion-beam writing of channel waveguides in bismuth germanate crystal for telecommunication bands. 2015 , 54, 057108	2
1438	Thermal annealing behavior of Al2O3 scintillation screens. <i>Nuclear Instruments & Methods in Physics Research B</i> , 2015 , 365, 548-552	3
1437	Stability of Silicon Carbide Particle Detector Performance at Elevated Temperatures. 2015 , 62, 2360-2366	13
1436	Electron multiplication CCD detector technology advancement for the WFIRST-AFTA coronagraph. 2015 ,	1
1435	H trapping and mobility in nanostructured tungsten grain boundaries: a combined experimental and theoretical approach. 2015 , 55, 113009	25
1434	Modifications in optical and electrical properties of selenium nanowire arrays using ion beam irradiation. 2015 , 121, 571-579	6

1433	Effect of simultaneous helium implantation on the microstructure evolution of Inconel X-750 superalloy during dual-beam irradiation. 2015 , 95, 3933-3949	6
1432	. 2015,	
1431	A study of the CR-39 track detector sensitivity to heavy charged particles of space radiation. 2015 , 58, 794-798	3
1430	Defect recovery and damage reduction in borosilicate glasses under double ion beam irradiation. 2015 , 112, 36002	29
1429	Characterisation of Defects in ZnO Implanted by Hydrogen. 2015 , 365, 49-54	
1428	. 2015 , 62, 2912-2918	20
1427	Micro- and nano-scale damage on the surface of W divertor component during exposure to high heat flux loads with He. 2015 , 466, 357-361	4
1426	Comparison of irradiated and hydrogen implanted German RPV steels using PAS technique. <i>Nuclear Instruments & Methods in Physics Research B</i> , 2015 , 365, 222-224	2
1425	Reprint of: Determination of deuteron characteristic channeling parameters by simulation of RBS spectrum along Si . 2015 , 83, 68-72	
1424	Depth-Resolved Imaging of Radiation-Induced Doping Changes in Silicon. 2015 , 4, P462-P467	3
1423	Determination of migration of ion-implanted Ar and Zn in silica by backscattering spectrometry. 2015 , 170, 229-237	3
1422	Interface effect in pentacene field-effect transistors from high energy proton beam irradiation. 2015 , 27, 240-246	6
1421	Sub-Micron Resolution of Localized Ion Beam Induced Charge Reduction in Silicon Detectors Damaged by Heavy Ions. 2015 , 62, 2919-2925	1
1420	The solution of the positron diffusion trapping model tested for profiling of defects induced by proton implanted in stainless steel. 2015 , 121, 289-295	9
1419	Spatially dependent cluster dynamics model of He plasma surface interaction in tungsten for fusion relevant conditions. 2015 , 55, 013014	24
1418	An intermetallic forming steel under radiation for nuclear applications. 2015 , 458, 361-368	8
1417	The influence of cross-linking and clustering upon the nanohole free volume of the SHI and Gradiation induced polymeric material. 2015 , 328, 482-490	20
1416	Compaction of porous ices rich in water by swift heavy ions. 2015 , 250, 222-229	34

1415	Effective implantation of light emitting centers by plasma immersion ion implantation and focused ion beam methods into nanosized diamond. 2015 , 328, 577-582		10
1414	Determination of energy loss of 1200 keV deuterons along axial and planar channels of Si. <i>Nuclear Instruments & Methods in Physics Research B</i> , 2015 , 345, 9-14	1.2	3
1413	Helium bubble formation in ultrafine and nanocrystalline tungsten under different extreme conditions. 2015 , 458, 216-223		100
1412	Defective Solid-Phase Epitaxial Growth of Si. 2015 , 123-163		1
1411	In situ measurements of a homogeneous to heterogeneous transition in the plastic response of ion-irradiated <1 1 1> Ni microspecimens. 2015 , 88, 121-135		23
1410	Ion-irradiation-induced clustering in WRe and WReDs alloys: A comparative study using atom probe tomography and nanoindentation measurements. 2015 , 87, 121-127		95
1409	Production of medical isotopes from a thorium target irradiated by light charged particles up to 70 MeV. 2015 , 60, 931-46		22
1408	Proton beam lithography in negative tone liquid phase PDMS polymer resist. <i>Nuclear Instruments & Methods in Physics Research B</i> , 2015 , 348, 213-217	1.2	8
1407	Role of developing L10chemical order on the (0 0 1)-texture formation of (Fe1 \(\text{LUx} \))Pt films grown on amorphous substrates. 2015 , 48, 085001		5
1406	Ion implantation for isolation of AlGaN/GaN HEMTs using C or Al. 2015 , 212, 1162-1169		22
1405	Stopping force of Ti for 6? Z? 29 ions measured by time of flight spectrometry. <i>Nuclear Instruments & Methods in Physics Research B</i> , 2015 , 349, 1-5	1.2	6
1404	Sensitivity changes of LiF:Mg,Ti and LiF:Mg,Cu,P TL detectors after proton exposures. 2015 , 74, 26-30		5
1403	Fabrication of three-dimensional SU-8 microchannels by proton beam writing for microfluidics applications: Fluid flow characterisation. <i>Nuclear Instruments & Methods in Physics Research B</i> , 2015 , 348, 223-228	1.2	7
1402	Influence of SHI upon nanohole free volume and micro scale level surface modifications of polyethyleneterephthalate polymer films. 2015 , 337, 19-26		18
1401	Ion beam irradiation of nanostructures: sputtering, dopant incorporation, and dynamic annealing. 2015 , 30, 033001		40
1400	Ion Beam Analysis for the provenance attribution of lapis lazuli used in glyptic art: The case of the Collezione Mediceall Nuclear Instruments & Methods in Physics Research B, 2015, 348, 278-284	1.2	20
1399	Generation of ensembles of individually resolvable nitrogen vacancies using nanometer-scale apertures in ultrahigh-aspect ratio planar implantation masks. 2015 , 15, 1751-8		33
1398	Characterization of the RisITL/OSL DA-20 reader for application in TL dosimetry. 2015 , 74, 1-5		18

1397	Identification of photoluminescence P line in indium doped silicon as InSi-Sii defect. 2015 , 5, 017101		3
1396	Three-dimensional micro/nano-scale structure fabricated by combination of non-volatile polymerizable RTIL and FIB irradiation. 2014 , 4, 3722		20
1395	Realization of a diamond based high density multi electrode array by means of Deep Ion Beam Lithography. <i>Nuclear Instruments & Methods in Physics Research B</i> , 2015 , 348, 199-202	1.2	17
1394	Redox response of actinide materials to highly ionizing radiation. 2015 , 6, 6133		64
1393	Investigation of in-depth and surface properties of polyethyleneterephthalate thin films after SHI and gamma radiation treatment by means of PALS and AFM studies. 2015 , 115, 31-38		12
1392	Focused particle beam nano-machining: the next evolution step towards simulation aided process prediction. 2015 , 26, 050501		1
1391	Calculations and measurements of the scintillator-to-water stopping power ratio of liquid scintillators for use in proton radiotherapy. 2015 , 776, 15-20		5
1390	Experimental and computational techniques for the analysis of proton beam propagation through a target stack. <i>Nuclear Instruments & Methods in Physics Research B</i> , 2015 , 345, 48-52	1.2	5
1389	Non-crystallization and enhancement of field emission of cupric oxide nanowires induced by low-energy Ar ion bombardment. 2015 , 329, 94-103		10
1388	Spectroscopy of surface-induced noise using shallow spins in diamond. 2015 , 114, 017601		136
1387	Studies of dense electronic excitation-induced modification in crystalline Fe-doped SnO2 thin films. 2015 , 332, 726-735		25
1387 1386			
,	2015, 332, 726-735 Raman Scattering in Natural Diamond Crystals Implanted with High-Energy Ions and Irradiated with		25
1386	2015, 332, 726-735 Raman Scattering in Natural Diamond Crystals Implanted with High-Energy Ions and Irradiated with Fast Neutrons. 2015, 81, 969-977 Atomistic modeling of radiation-induced disordering and dissolution at a Ni/Ni3Al interface. 2015,		25 9
1386 1385	2015, 332, 726-735 Raman Scattering in Natural Diamond Crystals Implanted with High-Energy Ions and Irradiated with Fast Neutrons. 2015, 81, 969-977 Atomistic modeling of radiation-induced disordering and dissolution at a Ni/Ni3Al interface. 2015, 30, 1456-1463 Accurate Monte Carlo modeling of cyclotrons for optimization of shielding and activation		25 9 10
1386 1385 1384	Raman Scattering in Natural Diamond Crystals Implanted with High-Energy Ions and Irradiated with Fast Neutrons. 2015, 81, 969-977 Atomistic modeling of radiation-induced disordering and dissolution at a Ni/Ni3Al interface. 2015, 30, 1456-1463 Accurate Monte Carlo modeling of cyclotrons for optimization of shielding and activation calculations in the biomedical field. 2015, 116, 231-236		25 9 10 18
1386 1385 1384 1383	Raman Scattering in Natural Diamond Crystals Implanted with High-Energy Ions and Irradiated with Fast Neutrons. 2015, 81, 969-977 Atomistic modeling of radiation-induced disordering and dissolution at a Ni/Ni3Al interface. 2015, 30, 1456-1463 Accurate Monte Carlo modeling of cyclotrons for optimization of shielding and activation calculations in the biomedical field. 2015, 116, 231-236 Cryo-focused-ion-beam applications in structural biology. 2015, 581, 122-30		25 9 10 18 76

1379	Radiation effects on microstructure and hardness of a titanium aluminide alloy irradiated by helium ions at room and elevated temperatures. 2015 , 459, 284-290		11
1378	Performance Study of an Integrated \$Delta {hbox{E}}{hbox{B}{hbox{E}}}\$ Silicon Detector Telescope using the Lohengrin Fission Fragment Separator at ILL, Grenoble. 2015 , 62, 264-271		2
1377	In-situ TEM/heavy ion irradiation on ultrafine-and nanocrystalline-grained tungsten: Effect of 3 MeV Si, Cu and W ions. 2015 , 99, 68-76		40
1376	The first interdisciplinary experiments at the IMP high energy microbeam. <i>Nuclear Instruments & Methods in Physics Research B</i> , 2015 , 348, 18-22	2	4
1375	Geometric optimization of a neutron detector based on a lithium glasspolymer composite. 2015 , 784, 168-171		20
1374	Lattice swelling and modulus change in a helium-implanted tungsten alloy: X-ray micro-diffraction, surface acoustic wave measurements, and multiscale modelling. 2015 , 89, 352-363		101
1373	TDPAC studies of interaction between He and A = 140 elements in Fe. 2015 , 230, 187-193		
1372	Investigation of EBT2 and EBT3 films for proton dosimetry in the 4-20 MeV energy range. 2015 , 54, 71-79		37
1371	Deposition of CVD diamond onto Zirconium. 2015 , 1734, 13		
1370	Mechanisms of material removal and mass transport in focused ion beam nanopore formation. 2015 , 117, 085304		8
1369	Application of PIGE, BS and NRA techniques to oxygen profiling in steel joints using deuteron beam. <i>Nuclear Instruments & Methods in Physics Research B</i> , 2015 , 348, 165-169	2	8
1368	Radiation tolerance of nanocrystalline ceramics: insights from Yttria Stabilized Zirconia. 2015 , 5, 7746		56
1367	Benchmark measurements of non-Rutherford proton elastic scattering cross section for boron. Nuclear Instruments & Methods in Physics Research B, 2015, 343, 70-76	2	11
1366	Selective etching of focused gallium ion beam implanted regions from silicon as a nanofabrication method. 2015 , 26, 265304		5
1365	Measurement of 23Na(p)26Mg at Energies Relevant to 26Al Production in Massive Stars. 2015 , 115, 052702		11
1364	Precipitate stability in CuAgW system under high-temperature irradiation. 2015, 97, 348-356		19
1363	Characterization of ion-irradiated ODS Fettralloys by doppler broadening spectroscopy using a positron beam. 2015 , 464, 140-146		14
1362	The influence of ion beam rastering on the swelling of self-ion irradiated pure iron at 450 $^{\circ}$ C. 2015 , 465, 343-348		61

1	361	Defects induced ferromagnetism in hydrogen irradiated 3CBiC thin films. 2015 , 156, 54-57	6
1	360	Irradiation-induced structural transitions in Ti2AlC. 2015 , 98, 197-205	42
1	359	Surface structural changes, surface energy and antiwear properties of polytetrafluoroethylene induced by proton irradiation. 2015 , 85, 162-168	16
1	358	Influence of the interface on the magnetic properties of NiZn ferrite thin films treated by proton irradiation. <i>Nuclear Instruments & Methods in Physics Research B</i> , 2015 , 358, 1-5	1
1	357	Scintillation efficiency for low energy nuclear recoils in liquid xenon dark matter detectors. 2015 , 61, 56-61	8
1	356	Radon backgrounds in the DEAP-1 liquid-argon-based Dark Matter detector. 2015 , 62, 178-194	17
1	355	The radiation stability of glycine in solid CO2 IIn situ laboratory measurements with applications to Mars. 2015 , 252, 466-472	11
1	354	Mn fraction substitutional site and defects induced magnetism in Mn-implanted 6H-SiC. 2015 , 632, 760-765	10
1	353	Effects of non-amorphizing hydrogen ion implantation on anisotropy in micro cutting of silicon. 2015 , 225, 439-450	35
1	352	Dynamic fuel retention in tokamak wall materials: An in situ laboratory study of deuterium release from polycrystalline tungsten at room temperature. 2015 , 467, 432-438	30
1	351	Copper thin films by ion beam assisted deposition: Strong texture, superior thermal stability and enhanced hardness. 2015 , 98, 17-28	23
1	350	An RF-only ion-funnel for extraction from high-pressure gases. 2015 , 379, 110-120	23
1	349	Studies of dense electronic excitation induced modification in cobalt doped SnO2 thin films prepared by RF sputtering technique. 2015 , 648, 550-558	19
1	348	Use of proton elastic scattering techniques to determine carbonaceous fractions in atmospheric aerosols collected on Teflon filters. 2015 , 89, 85-95	9
1	347	Effects of fluence and fluence rate of proton irradiation upon magnetism in Fe65Ni35 Invar alloy. 2015 , 394, 491-495	2
1	346	Depth-Resolved Structural and Compositional Characterization of Ion-Implanted Polystyrene that Enables Direct Covalent Immobilization of Biomolecules. 2015 , 119, 16793-16803	17
1	345	Proton-induced direct and indirect damage of plasmid DNA. 2015 , 54, 343-52	30
1	344	Particle-Based Imaging Techniques. 2015 , 69, 315-337	5

1343	Helium bubble evolution in a ZrBnNbBellr alloy during post-annealing: An in-situ investigation. 2015 , 107, 309-316		10
1342	Temperature dependence of helium-implantation-induced lattice swelling in polycrystalline tungsten: X-ray micro-diffraction and Eigenstrain modelling. 2015 , 107, 96-99		28
1341	Resonance parameters of the reaction 12C(d,p[))13C in the vicinity of 1450 keV for accelerator energy calibration. <i>Nuclear Instruments & Methods in Physics Research B</i> , 2015 , 342, 184-187	1.2	2
1340	Equilibrium and non-equilibrium charge-state distributions of 2.0 MeV/u carbon ions passing through carbon foils. <i>Nuclear Instruments & Methods in Physics Research B</i> , 2015 , 354, 172-176	1.2	12
1339	Ion beam effects of 26.0 MeV Cu7+ ions in thin metallic and insulating films during Heavy Ion ERDA measurements. <i>Nuclear Instruments & Methods in Physics Research B</i> , 2015 , 349, 79-84	1.2	
1338	On the traceably accurate voltage calibration of electrostatic accelerators. <i>Nuclear Instruments & Methods in Physics Research B</i> , 2015 , 349, 173-183	1.2	25
1337	Development of additive [11C]CO2 target system in the KOTRON-13 cyclotron and its application for [11C]radiopharmaceutical production. <i>Nuclear Instruments & Methods in Physics Research B</i> , 2015 , 356-357, 1-7	1.2	5
1336	Palladium contamination in silicon. 2015 , 106, 68-77		1
1335	An integrated time-of-flight versus residual energy subsystem for a compact dual ion composition experiment for space plasmas. 2015 , 86, 054501		5
1334	In situdefect annealing of swift heavy ion irradiated CeO2and ThO2using synchrotron X-ray diffraction and a hydrothermal diamond anvil cell. 2015 , 48, 711-717		22
1333	Role of the 19/2 orbital in the development of collectivity in the ABO region: The case of Co61. 2015 , 91,		5
1332	Nuclear model calculation and targetry recipe for production of 110mln. 2015 , 104, 60-6		3
1331	Cross-section scaling for track structure simulations of low-energy ions in liquid water. 2015 , 166, 15-8		10
1330	Neutralization and wake effects on the Coulomb explosion of swift H2+ ions traversing thin films. 2015 , 91,		6
1329	Maximum likelihood analysis of low energy CDMS II germanium data. 2015 , 91,		8
1328	Giant-planet chemistry: Ammonium hydrosulfide (NH4SH), its IR spectra and thermal and radiolytic stabilities. 2015 , 258, 181-191		13
1327	Molecular-dynamics simulation of threshold displacement energies in BaTiO3. <i>Nuclear Instruments & Methods in Physics Research B</i> , 2015 , 358, 142-145	1.2	7
1326	Radiochromic film diagnostics for laser-driven ion beams. 2015,		3

1325	Radiation effects in Zr and Hf containing garnets. 2015 , 462, 508-513	3
1324	Decomposition and CO2 evolution of an aliphatic polymer under bombardment with high energy heavy ions. 2015 , 119, 132-138	O
1323	Response of GaN to energetic ion irradiation: conditions for ion track formation. 2015 , 48, 325304	32
1322	Disassembly time of deuterium-cluster-fusion plasma irradiated by an intense laser pulse. 2015 , 92, 013102	8
1321	Nanoscale Ehuclear magnetic resonance depth imaging of topological insulators. 2015 , 112, E3645-50	15
1320	Response of Gd2Ti2O7 and La2Ti2O7 to swift-heavy ion irradiation and annealing. 2015 , 93, 1-11	43
1319	Fabrication of porous silicon based tunable distributed Bragg reflectors by anodic etching of irradiated silicon. <i>Nuclear Instruments & Methods in Physics Research B,</i> 2015 , 358, 105-111	9
1318	Improved calibration of mass stopping power in low density tissue for a proton pencil beam algorithm. 2015 , 60, 4243-61	6
1317	Improving Room-Temperature Ferromagnetism in Mn-Implanted Si by High-Temperature Annealing. 2015 , 51, 1-4	
1316	Atomic-scale thermocapillary flow in focused ion beam milling. 2015 , 27, 052003	2
1315	p-type conduction in Zn-ion implanted InN films. 2015 , 48, 215102	2
1314	Research on anisotropy of fusion-produced protons and neutrons emission from high-current plasma-focus discharges. 2015 , 86, 013502	5
1313	Note: fast neutron efficiency in CR-39 nuclear track detectors. 2015 , 86, 036103	5
1312	The local environment of cobalt in amorphous, polycrystalline and epitaxial anatase TiO2:Co films produced by cobalt ion implantation. 2015 , 117, 183901	15
1311	Development and characterization of a diamond-insulated graphitic multi electrode array realized with ion beam lithography. 2014 , 15, 515-28	19
1310	Elemental distribution and sample integrity comparison of freeze-dried and frozen-hydrated biological tissue samples with nuclear microprobe. <i>Nuclear Instruments & Methods in Physics</i> 1.2 <i>Research B</i> , 2015 , 348, 147-151	24
1309	The role of ion-neutral collisions in Titan?s magnetospheric interaction. 2015 , 108, 73-86	10
1308	Irradiation-induced formation of a spinel phase at the FeCr/MgO interface. 2015 , 93, 87-94	7

1307	Electroluminescence from a diamond device with ion-beam-micromachined buried graphitic electrodes. <i>Nuclear Instruments & Methods in Physics Research B</i> , 2015 , 348, 187-190	1.2	10
1306	Reduced plasma-induced damage to near-surface nitrogen-vacancy centers in diamond. 2015 , 15, 2887	-91	27
1305	Temperature-dependent electrical characterization of high-voltage AlGaN/GaN-on-Si HEMTs with Schottky and ohmic drain contacts. 2015 , 111, 12-17		15
1304	Proton irradiation energy dependence of defect formation in graphene. 2015 , 344, 52-56		18
1303	The SPIDER fission fragment spectrometer for fission product yield measurements. 2015 , 788, 59-66		26
1302	Simulation of particle impact on protective coating of high-level waste storage packages. 2015 , 81, 196	-202	2
1301	Ion beam induced fluorescence imaging in biological systems. <i>Nuclear Instruments & Methods in Physics Research B</i> , 2015 , 348, 131-136	1.2	6
1300	Displacement cross sections of electron irradiated graphene and carbon nanotubes. <i>Nuclear Instruments & Methods in Physics Research B</i> , 2015 , 350, 20-25	1.2	5
1299	A comparison of 100 MeV oxygen ion and 60Co gamma irradiation effects on advanced 200 GHz SiGe heterojunction bipolar transistors. 2015 , 89, 789-796		4
1298	3-D tracking in a miniature time projection chamber. 2015 , 788, 95-105		16
1297	Formation of donor centers upon the annealing of silicon light-emitting structures implanted with oxygen ions. 2015 , 49, 406-408		1
1296	Further improvement for 10Be measurement on an upgraded compact AMS radiocarbon facility. <i>Nuclear Instruments & Methods in Physics Research B</i> , 2015 , 361, 178-182	1.2	1
1295	Structural manipulation in Ge by swift heavy ions governed by electronphonon coupling strength. 2015 , 2, 045903		10
1294	Ion implantation induced phase transformation and enhanced crystallinity of as deposited copper oxide thin films by pulsed laser deposition. 2015 , 84, 24-35		13
1293	Accurate electronics calibration for particle backscattering spectrometry. 2015 , 7, 3096-3104		15
1292	Certified ion implantation fluence by high accuracy RBS. 2015 , 140, 3251-61		14
1291	Influence of the physical data to calibrate TEPCs. 2015 , 166, 238-41		2
1290	Antibacterial properties of Au doped polycarbonate synthesized by gamma radiation assisted diffusion method. 2015 , 112, 97-103		11

1289	Effect of helium ion beam treatment on the etching rate of silicon nitride. <i>Nuclear Instruments & Methods in Physics Research B</i> , 2015 , 349, 90-95	7
1288	Heavy ion irradiation of crystalline water ice. 2015 , 576, A125	53
1287	Effects of crystallographic plane and co-deposited element on the growth of ion-sputter induced Si nano-cone arrays: a mechanism study. 2015 , 119, 1033-1038	3
1286	Experimental and Monte Carlo study on production of 110mIn via natCd(p,xn) reaction. 2015 , 306, 423-427	3
1285	Single atom devices by ion implantation. 2015 , 27, 154204	50
1284	3D mapping of lithium in battery electrodes using neutron activation. 2015 , 287, 226-230	14
1283	Thermoluminescence of solgel derived Y2O3:Nd3+ nanophosphor exposed to 100MeV Si8+ ions and gamma rays. 2015 , 637, 564-573	23
1282	A multiphase interfacial model for the dissolution of spent nuclear fuel. 2015 , 462, 135-146	11
1281	Hyperdoping silicon with selenium: solid vs. liquid phase epitaxy. 2015 , 5, 8329	39
1280	A comparison between the codes SRIM and AlfaMC in the Monte Carlo simulation of alpha-particle backscattering. 2015 , 305, 479-485	1
1279	Coatings synthesised by the pulsed laser ablation of a B4C/W2B5 ceramic composite. 2015 , 593, 5-9	5
1278	Impact of implanted phosphorus on the diffusivity of boron and its applicability to silicon solar cells. 2015 , 118, 045702	2
1277	Swift heavy ion irradiation damage in TiBALEV and TiBALEVIB: Study of the microstructure and mechanical properties. <i>Nuclear Instruments & Methods in Physics Research B</i> , 2015 , 365, 515-521	6
1276	Dynamics of Atomic Clusters Under Intense Femtosecond Laser Pulses. 2015 , 65-87	
1275	Nanometer-scale isotope analysis of bulk diamond by atom probe tomography. 2015 , 60, 60-65	7
1274	On the use of averaging stopping power of recoiled nuclei for determining maximum neutron energy of 241Am B e by superheated drop detectors. 2015 , 83, 31-35	2
1273	New recoil transfer chamber for thermalization of heavy ions produced in fusion apporation reactions. 2015 , 798, 52-61	1
1272	In situ TEM observation of helium bubble evolution in V/Ag multilayer during annealing. 2015 , 467, 537-543	19

Multiphase Structure of Tantalum Oxynitride TaOxNy Thin Films Deposited by Reactive Magnetron Sputtering. 2015, 119, 23559-23571 Surface damage and mechanical properties degradation of Cr/W multilayer films irradiated by Xe20+. 2015, 357, 1225-1230 Fabrication of Thermoresponsive Nanoactinia Tentacles by a Single Particle Nanofabrication Technique. 2015, 31, 11692-700 9	
Xe20+. 2015 , 357, 1225-1230 Fabrication of Thermoresponsive Nanoactinia Tentacles by a Single Particle Nanofabrication	
1267 The Efficiency of Hydrogen-Doping as a Function of Implantation Temperature. 2015 , 242, 175-183	
1266 Thin-Film Gallium Antimonide for Room-Temperature Radiation Detection. 2015 , 44, 3288-3293	
Active charge state control of single NV centres in diamond by in-plane Al-Schottky junctions. 2015 , 5, 12160	
1264 Effect of Ar+ ion irradiation on the microstructure of pyrolytic carbon. 2015 , 117, 115101	
1263 Radiation tolerant nanocrystalline ZrN films under high dose heavy-ion irradiations. 2015 , 117, 145901 17	
Suppression of spin pumping between Ni80Fe20 and Cu by a graphene interlayer. 2015 , 117, 213907 5	
1261 Time constant of defect relaxation in ion-irradiated 3C-SiC. 2015 , 106, 202102	
Primary and aggregate color centers in proton irradiated LiF crystals and thin films for luminescent solid state detectors. 2015 , 80, 012018	
Surface state reconstruction in ion-damaged SmB6. 2015 , 91,)
SHI irradiation of metal doped zinc sulfide polymer nanocomposites synthesized using micro emulsion method. <i>Nuclear Instruments & Methods in Physics Research B</i> , 2015 , 358, 258-262	
ECORCE: A TCAD Tool for Total Ionizing Dose and Single Event Effect Modeling. 2015 , 62, 1516-1527 12	
On the pressure effect in energetic deposition of Cu thin films by modulated pulsed power magnetron sputtering: A global plasma model and experiments. 2015 , 117, 203302	
1255 Calibration of time of flight detectors using laser-driven neutron source. 2015 , 86, 073308	
TEM study of the nucleation of bubbles induced by He implantation in 316L industrial austenitic	

1253	Comparative investigations of the relative thermoluminescent efficiency of LiF detectors to protons at different proton therapy facilities. 2015 , 82, 8-13	20
1252	Revisited water radiolysis at elevated pH by accounting O3Ikinetics at low and high LET. 2015 , 5, 89244-89253	3
1251	Study on structural recovery of graphite irradiated with swift heavy ions at high temperature. Nuclear Instruments & Methods in Physics Research B, 2015, 365, 522-524	5
1250	Influence of defects and displacements in sapphire doped with Ag+ ions. 2015 , 357, 1231-1235	1
1249	Ion-beam-assisted fabrication and manipulation of metallic nanowires. 2015 , 10, 334-338	5
1248	Defect studies of H+ implanted niobium. 2015 , 645, S69-S71	9
1247	Differential cross section measurements of 27Al(p,p/[])27Al and 27Al(p,])24Mg reactions in the energy range of 1.6B.0 MeV. <i>Nuclear Instruments & Methods in Physics Research B</i> , 2015 , 362, 138-141	3
1246	Synthesis of heterostructured SiC and CBiC nanotubes by ion irradiation-induced changes in crystallinity. 2015 , 95, 279-285	9
1245	Effect of low-damage inductively coupled plasma on shallow nitrogen-vacancy centers in diamond. 2015 , 107, 073107	53
1244	Reduction of graphene oxide by 100 MeV Au ion irradiation and its application as H2O2sensor. 2015 , 48, 365105	38
1243	Transmittance Measurement of Accelerated Ions and Electrons in Divergent Gas-Puff \$Z\$ -Pinch Plasma. 2015 , 43, 2492-2496	1
1242	Ion beam analysis of Cu(In,Ga)Se 2 thin film solar cells. 2015 , 356, 631-638	15
1241	Enhanced sputter yields of ion irradiated Au nano particles: energy and size dependence. 2015 , 26, 325301	18
1240	ProtonBilicon interaction potential extracted from high-resolution measurements of crystal rainbows. <i>Nuclear Instruments & Methods in Physics Research B</i> , 2015 , 360, 23-29	16
1239	Effects of surface conditions on the plasma-driven permeation behavior through a ferritic steel alloy observed in VEHICLE-1 and QUEST. 2015 , 463, 1066-1070	14
1238	Positron study of steel NF 709 after irradiation and thermal strain. <i>Nuclear Instruments & Methods in Physics Research B</i> , 2015 , 365, 309-312	2
1237	Macroscopic rate equation modeling of trapping/detrapping of hydrogen isotopes in tungsten materials. 2015 , 467, 424-431	43
1236	Irradiation of low energy ions damage analysis on multilayers. 2015 ,	1

1235	Ion beam induced luminescence analysis of defect evolution in lithium fluoride under proton irradiation. 2015 , 49, 1-5		7
1234	The study of the carriers[transport mechanism of GaAs/Ge solar cells based on irradiation damage model. <i>Nuclear Instruments & Methods in Physics Research B</i> , 2015 , 360, 64-67	1.2	3
1233	PALS and physico-chemical study of swift heavy ions and gamma radiation irradiated polyamide nylon 66 polymer. 2015 , 121, 177-186		6
1232	Modification of the microstructure and electronic properties of rutile TiO2 thin films with 79 MeV Br ion irradiation. <i>Nuclear Instruments & Methods in Physics Research B</i> , 2015 , 365, 553-559	1.2	8
1231	Cross section measurements of deuteron induced nuclear reactions on natural titanium up to 34 MeV. 2015 , 103, 160-5		0
1230	Sub-micrometer 20MeV protons or 45MeV lithium spot irradiation enhances yields of dicentric chromosomes due to clustering of DNA double-strand breaks. 2015 , 793, 30-40		10
1229	Time dependence of silica optical properties during the implantation of fast hydrogen ions: Theory. <i>Nuclear Instruments & Methods in Physics Research B</i> , 2015 , 362, 182-186	1.2	3
1228	Structural modifications induced by ion irradiation and temperature in boron carbide B4C. <i>Nuclear Instruments & Methods in Physics Research B</i> , 2015 , 365, 30-34	1.2	19
1227	Swift heavy ion-induced radiation damage in isotropic graphite studied by micro-indentation and in-situ electrical resistivity. <i>Nuclear Instruments & Methods in Physics Research B</i> , 2015 , 365, 509-514	1.2	8
1226	Cross section measurements of deuteron induced nuclear reactions on natural tungsten up to 34 MeV. 2015 , 97, 52-58		19
1225	Cyclotron production of 52Mn and Monte Carlo benchmarking. 2015 , 304, 669-674		6
1224	Cell death induced by ozone and various non-thermal plasmas: therapeutic perspectives and limitations. 2014 , 4, 7129		47
1223	In-situ TEM observation of the response of ultrafine- and nanocrystalline-grained tungsten to extreme irradiation environments. 2014 , 4, 4716		111
1222	Study of the Ion-Irradiation Behavior of Advanced SiC Fibers by Raman Spectroscopy and Transmission Electron Microscopy. 2015 , 98, 675-682		17
1221	Advanced characterization of MIMAS MOX fuel microstructure to quantify the HBS formation. 2015 , 281, 79-87		5
1220	Understanding the effects of ion irradiation using nanoindentation techniques. 2015 , 462, 391-401		72
1219	High-temperature corrosion of helium ion-irradiated Ni-based alloy in fluoride molten salt. 2015 , 91, 1-6		46
1218	Design study of the ESS-Bilbao 50 MeV proton beam line for radiobiological studies. <i>Nuclear Instruments & Methods in Physics Research B</i> , 2015 , 344, 33-38	1.2	2

1217	Cross-sections for (p,x) reactions on natural chromium for the production of $(52,52m,54)$ Mn radioisotopes. 2015 , 96, 154-161	25	5
1216	Temperature dependent surface modification of T91 steel under 3.25MeV Fe-ion implantation. 2015 , 326, 1-6	13	3
1215	Plume propagation and Pt film growth during shadow-masked pulsed laser deposition in a buffer Ar gas. <i>Nuclear Instruments & Methods in Physics Research B</i> , 2015 , 343, 52-61	2	
1214	Dose rate effect on micro-structure and hardness of Hastelloy-N irradiated by Xe ions. 2015 , 52, 829-836	2	
1213	Studying localized corrosion using liquid cell transmission electron microscopy. 2015 , 51, 168-71	53	3
1212	Structural changes and tribological performance of thermosetting polyimide induced by proton and electron irradiation. 2015 , 107, 171-177	13	3
1211	Prediction of production of 22Na in a gas-cell target irradiated by protons using Monte Carlo tracking. <i>Nuclear Instruments & Methods in Physics Research B</i> , 2015 , 342, 244-248	7	
1210	Behaviour of P, Si, Ni impurities and Cr in self ion irradiated Fell alloys Comparison to neutron irradiation. 2015 , 456, 471-476	80	0
1209	IonBolid interactions at the extremes of electronic energy loss: Examples for amorphous semiconductors and embedded nanostructures. 2015 , 19, 29-38	2 1	1
1208	Physical assembly of Ag nanocrystals on enclosed surfaces in monocrystalline Si. 2014 , 4, 6744	5	
1207	Influence of edge effects on single event upset susceptibility of SOI SRAMs. <i>Nuclear Instruments & Methods in Physics Research B</i> , 2015 , 342, 286-291	2	
1206	Polymerization of room-temperature ionic liquid monomers by electron beam irradiation with the aim of fabricating three-dimensional micropolymer/nanopolymer structures. 2015 , 31, 4281-9	2.	4
1205	Radiation response of amorphous metal alloys: Subcascades, thermal spikes and super-quenched zones. 2015 , 83, 419-430	38	8
1204	Resistance to He2+ irradiation damage in metallic glass Fe80Si7.43B12.57. <i>Nuclear Instruments & Methods in Physics Research B</i> , 2015 , 342, 221-227	12	4
1203	Ionization yield from nuclear recoils in liquid-xenon dark matter detection. 2015, 62, 108-114	5	
1202	Radiolytic yield of ozone in air for low dose neutron and x-ray/gamma-ray radiation. 2015 , 106, 95-98	3	
1201	Effects of O7+ and Ni9+ swift heavy ions irradiation on polyacrylamide grafted Gum acacia thin film and sorption of methylene blue. 2015 , 111, 73-82	2.	4
1200	Investigation of ionoluminescence of semiconductor materials using helium ion microscopy. 2015 , 157, 321-326	12	2

1199	Quantitative comparison of sink efficiency of CuNb, CuV and CuNi interfaces for point defects. 2015 , 82, 328-335	50
1198	Study of phase transitions in NbN ultrathin films under composite ion beam irradiation. 2016 , 130, 012046	3
1197	Investigation of radiation-induced transformations in thin NbN films by analytical electron microscopy. 2016 , 130, 012058	
1196	Thin-Film Optics. 2016 , 99-125	1
1195	Modelling and analysis of nucleon emission from deuteron-induced reactions at incident energies up to 100 MeV. 2016 , 122, 04004	5
1194	Cosmic-ray slowing down in molecular clouds: Effects of heavy nuclei. 2016 , 585, A15	14
1193	Hydration of magnesia cubes: a helium ion microscopy study. 2016 , 7, 302-9	11
1192	A novel method to recover DD fusion proton CR-39 data corrupted by fast ablator ions at OMEGA and the National Ignition Facility. 2016 , 87, 11D812	1
1191	Active and fast charge-state switching of single NV centres in diamond by in-plane Al-Schottky junctions. 2016 , 7, 1727-1735	5
1190	Atom Probe Sample Preparation. 2016 , 97-121	18
1189	First measurement of nuclear recoil head-tail sense in a fiducialised WIMP dark matter detector. 2016 , 11, P10019-P10019	16
1188	Modeling of Fission-Gas Induced Swelling of Nuclear Fuels. 2016,	
1187	80 MeV C6+ ion irradiation effects on the DC electrical characteristics of silicon NPN power transistors. 2016 ,	
1186	Auger electron-based targeted radioimmunotherapy with 58mCo, a feasibility study. 2016,	5
1185	Simulation for thick-target yields of transmutation reactions on radioactive targets, based on inverse kinematics. 2016 , 122, 07003	
1184	Search for mixed-symmetry states in212Po. 2016 , 724, 012023	
1183	Search for mixed-symmetry states of nuclei in the vicinity of the double-magic nucleus208Pb. 2016 , 107, 03004	1
1182	Monitoring of Hadrontherapy Treatments by Means of Charged Particle Detection. 2016 , 6, 177	19

1181	Ar+-Implanted Si-Waveguide Photodiodes for Mid-Infrared Detection. 2016 , 3, 46	3
1180	Alpha contamination assay, dosimetry and spectrometry using charge coupled devices. 2016 ,	O
1179	Characteristics of Protons Exiting from a Polyethylene Converter Irradiated by Neutrons with Energies between 1 keV and 10 MeV. 2016 , 11, e0157627	6
1178	Molecular Dynamics Simulations of Platinum Plasma Sputtering: A Comparative Case Study. 2016 , 4,	8
1177	High repetition-rate neutron generation by several-mJ, 35 fs pulses interacting with free-flowing D2O. 2016 , 109, 144102	11
1176	Radiation-Damage Resistance in Phyllosilicate Minerals from First Principles and Implications for Radiocesium and Strontium Retention in Soils. 2016 , 64, 108-114	6
1175	Layered Structure Induced Anisotropic Low-Energy Recoils in Ti3SiC2. 2016 , 99, 2693-2698	9
1174	Evaluation of neon focused ion beam milling for TEM sample preparation. 2016 , 264, 59-63	17
1173	Irradiation effects in CaF2 probed by Raman scattering. 2016 , 47, 978-983	9
1172	Molybdenum and Tungsten Contamination in MOS Capacitors. 2016 , 5, P203-P210	3
1171	Structural and antibacterial properties of a Dradiation-assisted, in situ prepared silverpolycarbonate matrix. 2016 , 133,	3
1170	Softening the ultra-stiff: Controlled variation of Young modulus in single-crystal diamond by ion implantation. 2016 , 116, 95-103	21
1169	Fluence-based dosimetry of proton and heavier ion beams using single track detectors. 2016 , 61, 1021-40	13
1168	In Situ Electrical Characteristics of 150 MeV Ag9+Ion Beam Induced Damage in Si Photo Detector. 2016 , 5, P384-P388	3
1167	Temperature dependent dispersoid stability in ion-irradiated ferritic-martensitic dual-phase oxide-dispersion-strengthened alloy: Coherent interfaces vs. incoherent interfaces. 2016 , 116, 29-42	48
1166	Irradiation effects in 6HBiC induced by neutron and heavy ions: Raman spectroscopy and high-resolution XRD analysis. 2016 , 478, 215-221	28
1165	Proton implantation for the isolation of AlGaAs/GaAs quantum cascade lasers. 2016 , 31, 075010	5
1164	Defect studies of zirconia implanted by high energy Xe ions. 2016 , 674, 012016	

1163	Novel BF+ Implantation for High Performance Ge pMOSFETs. 2016 , 37, 954-957	5
1162	In Situ Monitoring of Cu(In1¼,Gax)Se2 Composition and Target Poisoning by Real Time Optical Emission Spectroscopy During Deposition From a Hybrid Sputtering/Evaporation Process. 2016 , 13, 997-1007	6
1161	Structure and properties of poly(4-methylpentene-1) track-etched membranes. 2016 , 56, 294-302	1
1160	Effect of cobalt implantation on structural and optical properties of rutile TiO2(110). 2016 , 122, 1	7
1159	From photoluminescence emissions to plasmonic properties in platinum nanoparticles embedded in silica by ion implantation. 2016 , 179, 8-15	7
1158	Tilted pillar array fabrication by the combination of proton beam writing and soft lithography for microfluidic cell capture: Part 1 Design and feasibility. 2016 , 37, 498-503	10
1157	Ni ion damage structures and hardness changes in austenitic stainless steels and their model alloys. 2016 , 674, 012009	
1156	Activation of Si implants into InAs characterized by Raman scattering. 2016 , 119, 095705	2
1155	Irradiation of nitrogen-rich ices by swift heavy ions. 2016 , 592, A99	17
1154	High density nitrogen-vacancy sensing surface created via He+ ion implantation of 12C diamond. 2016 , 108, 202401	47
1153	FIP effect for minor heavy solar wind ions as seen with SOHO/CELIAS/MTOF. 2016,	
1152	Formation of the single-phase ferromagnetic semiconductor (Ga,Mn)As by pulsed laser annealing. 2016 , 58, 2218-2222	4
1151	Hyperfine-enhanced gyromagnetic ratio of a nuclear spin in diamond. 2016 , 18, 083016	5
1150	Response of timepix detector with GaAs:Cr and Si sensor to heavy ions. 2016 , 13, 363-369	3
1149	Measurement and simulation of the momentum transferred to a surface by deposition of sputtered atoms*. 2016 , 70, 1	8
1148	NbO Nanostructure Evolution on Nb Surfaces via Low-Energy He Ion Irradiation. 2016 , 8, 34896-34903	8
1147	Additional control of bombardment by deep oscillation magnetron sputtering: Effect on the microstructure and topography of Cr thin films. 2016 , 619, 250-260	14
1146	Simulations on time-of-flight ERDA spectrometer performance. 2016 , 87, 083309	3

1145	Helium ion beam enhanced local etching of silicon nitride. 2016 ,	2
1144	Ballistic effects on the copper precipitation and re-dissolution kinetics in an ion irradiated and thermally annealed Fe-Cu alloy. 2016 , 145, 104704	14
1143	Production yield of rare-earth ions implanted into an optical crystal. 2016 , 108, 053108	16
1142	Different effects of laser contrast on proton emission from normal large foils and transverse-size-reduced targets. 2016 , 58, 075010	10
1141	Zn precipitation and Li depletion in Zn implanted ZnO. 2016 , 109, 022102	2
1140	Experimental probe for the production of Ru97 from the Li7+Nb93 reaction: A study of precompound emissions. 2016 , 94,	16
1139	Neutron imaging with the short-pulse laser driven neutron source at the Trident laser facility. 2016 , 120, 154901	22
1138	Defect-engineered optical bandgap in self-assembled TiO2 nanorods on Si pyramids. 2016 , 108, 011907	20
1137	Depth dependent modification of optical constants arising from H+ implantation in n-type 4H-SiC measured using coherent acoustic phonons. 2016 , 1, 036102	9
1136	A Novel Method for Simultaneous on Wafer Level Monitoring of Ion Implantation Energy and Dose. 2016 ,	
1135	Deterministic Atom Placement by Ion Implantation: Few and Single Atom Devices for Quantum Computer Technology. 2016 ,	3
1134	Diffusion Suppression of Delta Doped Phosphorus in Germanium by Implantation of Nitrogen. 2016	
1133	Thermoacoustic range verification using a clinical ultrasound array provides perfectly co-registered overlay of the Bragg peak onto an ultrasound image. 2016 , 61, 5621-38	24
1132	3 MeV Proton Irradiation of Commercial State of the Art Photonic Mixer Devices. 2016 ,	
1131	O17+Ni58 scattering and reaction dynamics around the Coulomb barrier. 2016 , 94,	7
1130	Boron abundances and isotopic ratios of olivine grains on Itokawa returned by the Hayabusa spacecraft. 2016 , 51, 1721-1729	3
1129	Characterisation of irradiation-induced defects in ZnO single crystals. 2016 , 674, 012014	1
1128	Formation and annihilation of E4 centers in ZnO: Influence of hydrogen. 2016 , 119, 181506	13

Synthesis of graphene and graphene nanostructures by ion implantation and pulsed laser annealing. 2016 , 120, 025105	3
Observation of oversaturation-induced defect formation in tungsten irradiated by low energy deuterium ion. 2016 , 69, 518-524	2
Gate dielectric ion implantation to modulate the threshold voltage of In2O3 nanowire field effections. 2016 , 109, 193505	ect 7
1124 Formation of swift heavy ion tracks on a rutile TiO (001) surface. 2016 , 49, 1704-1712	13
Compact Dual Ion Composition Experiment for space plasmas@oDICE. 2016 , 121, 6632-6638	3
1122 Carbon foils for space plasma instrumentation. 2016 , 121, 3931-3950	24
Optical far-field super-resolution microscopy using nitrogen vacancy center ensemble in bulk diamond. 2016 , 109, 111107	9
Dynamic properties of the energy loss of multi-MeV charged particles traveling in two-components warm dense plasmas. 2016 , 94, 063203	ent 6
Stopping dynamics of ions passing through correlated honeycomb clusters. 2016 , 94,	29
Effect of medium range order on pulsed laser crystallization of amorphous germanium thin film 2016 , 108, 221906	ns. 9
Experimental study of the astrophysically important Na23(ﷺ) Mg26 and Na23(ੴ)Al26 reactions. 2016 , 94,	12
Mechanical properties and plasticity size effect of Fe-6%Cr irradiated by Fe ions and by neutror 2016 , 482, 236-247	10
Modelling the thermomechanical behaviour of the tungsten first wall in HiPER laser fusion scenarios. 2016 , 56, 126014	15
Measurement of radiative proton capture on F18 and implications for oxygen-neon novae reexamined. 2016 , 94,	2
1113 Investigation of proton damage in III-V semiconductors by optical spectroscopy. 2016 , 119, 235	702 2
1112 Measurement of the6Li(n,∄neutron standard cross-section at the GELINA facility. 2016 , 122, 080	006 1
1111 The effect of structural disorder on the secondary electron emission of graphite. 2016 , 6, 09517	17 3
Structural and compositional dependence of the CdTexSe1-x alloy layer photoactivity in CdTe-based solar cells. 2016 , 7, 12537	82

1109	Independent control of electrical and heat conduction by nanostructure designing for Si-based thermoelectric materials. 2016 , 6, 22838	3	38
1108	Evolution kinetics of elementary point defects in ZnO implanted with low fluences of helium at cryogenic temperature. 2016 , 94,	1	13
1107	Development toward a double focusing isotopic separator for noble gas isotope enrichment. 2016 , 51, 908-913	5	5
1106	Efficient creation of dipolar coupled nitrogen-vacancy spin qubits in diamond. 2016 , 752, 012001	1	10
1105	Effect of the implantation dose and annealing time on the luminescence properties of (113) defects in silicon implanted by oxygen ions. 2016 , 58, 2499-2502	4	1
1104	The effects of annealing a 2-dimensional array of ion-irradiated Josephson junctions. 2016 , 29, 094004	3	;
1103	Annealing bounds to prevent further Charge Transfer Inefficiency increase of the Chandra X-ray CCDs. <i>Nuclear Instruments & Methods in Physics Research B</i> , 2016 , 389-390, 23-27	2 1	[
1102	Thermal spike effect in sputtering of porous germanium to form surface pattern by high energy heavy ions irradiation. 2016 , 108, 201603	4	1
1101	The modification of the structure of multilayer Co/Pt films by the irradiation with a focused helium ion beam. 2016 ,	3	3
1100	Depletion region surface effects in electron beam induced current measurements. 2016 , 120,	1	17
1099	High energy electron irradiation of interstellar carbonaceous dust analogs: Cosmic ray effects on the carriers of the 3.4 μ m absorption band. 2016 , 831,	1	[1
1098	Picosecond metrology of laser-driven proton bursts. 2016, 7, 10642	5	5 6
1097	A two-dimensional angular-resolved proton spectrometer. 2016 , 87, 103301	2	2
1096	Increase in elastic anisotropy of single crystal tungsten upon He-ion implantation measured with laser-generated surface acoustic waves. 2016 , 109, 151906	1	16
1095	Engineered magnetic domain textures in exchange bias bilayer systems. 2016 , 120, 033902	1	15
1094	Probing electron density across Ar+ irradiation-induced self-organized TiO2⊠ nanochannels for memory application. 2016 , 108, 244104	1	[1
1093	Lattice site specific diffusion properties for substitutional and interstitial impurity atoms in ZnO crystals. 2016 , 120, 115102		
1092	Platinum nanoclusters in silica: Photoluminescent properties and their application for enhancing the emission of silicon nanocrystals in an integrated configuration. 2016 , 120, 123106	3	3

1091	Experimental validation of gallium production and isotope-dependent positron range correction in PET. 2016 , 814, 110-116		5
1090	Target nanomaterials at CERN-ISOLDE: synthesis and release data. <i>Nuclear Instruments & Methods in Physics Research B</i> , 2016 , 376, 81-85	1.2	18
1089	Origin of microplasma instabilities during DC operation of silicon based microhollow cathode devices. 2016 , 25, 025021		5
1088	Rate of F center formation in sapphire under low-energy low-fluence Ar+ irradiation. <i>Nuclear Instruments & Methods in Physics Research B</i> , 2016 , 371, 303-306	1.2	6
1087	Investigation of the magnetic properties of proton irradiated type Ib HPHT diamond. 2016 , 64, 197-201		О
1086	Variable helium diffusion characteristics in fluorite. 2016 , 188, 21-34		7
1085	Using the Doppler broadened □line of the 10B(n,⊞)7Li reaction for thermal neutron detection. 2016 , 810, 140-143		2
1084	Hydrogen ion-implantation induced low resistive layer in KNbO 3 bulk single crystal: Evaluation by elastic recoil detection analysis. <i>Nuclear Instruments & Methods in Physics Research B</i> , 2016 , 371, 283-285	5 ^{1.2}	2
1083	Buried Boron Doped Layer for CVD Diamond Photo-Thermionic Cathodes. 2016 , 15, 862-866		6
1082	Revisiting alpha decay-based near-light-speed particle propulsion. 2016 , 114, 14-8		1
1081	Accelerator-based production of the (99m)Tc-(186)Re diagnostic-therapeutic pair using metal disulfide targets (MoS2, WS2, OsS2). 2016 , 114, 159-66		12
1080	Ionoluminescence study of Znland Olimplanted ZnO crystals: An additional perspective. 2016 , 371, 28-34		30
1079	Swift-heavy ion irradiation-induced latent tracks in few- and mono-layer MoS2. 2016 , 122, 1		9
1078	Resistance to He2+ irradiation damage in metallic glass Ta38Ni62. 2016 , 383, 106-112		6
1077	Comparative analysis of CR-39 sensitivity for different sets of measurable track parameters. 2016 , 91, 44-49		7
1076	Morphology and magnetic properties of the ethylene-co-vinyl acetate/iron nanocomposite films prepared by implantation with Fe6+ ions. 2016 , 378, 362-367		2
1075	Directing Matter: Toward Atomic-Scale 3D Nanofabrication. 2016 , 10, 5600-18		76
1074	Tungsten contamination in ion implantation. <i>Nuclear Instruments & Methods in Physics Research B</i> , 2016 , 377, 99-104	1.2	2

Composition dependent thermal annealing behaviour of ion tracks in apatite. <i>Nuclear Instruments & Methods in Physics Research B</i> , 2016 , 379, 211-214	1.2	2
Methodology for determining void swelling at very high damage under ion irradiation. 2016 , 477, 273-27	79	15
Assessment of experimental d-PIGE I-ray production cross sections for 12C, 14N and 16O and comparison with absolute thick target yields. <i>Nuclear Instruments & Methods in Physics Research B</i> , 2016 , 380, 1-10	1.2	2
Enhancement in luminescence properties of ZrO2:Dy3+ under 100 MeV swift Ni7+ ion irradiation. 2016 , 6, 55240-55247		12
Dose dependence of helium bubble formation in nano-engineered SiC at 700IIC. 2016 , 472, 153-160		17
Molecular dynamics simulation of bipartite bimetallic clusters under low-energy argon ion bombardment. 2016 , 58, 387-393		5
Porosity estimation of alumina samples based on resonant backscattering spectrometry. <i>Nuclear Instruments & Methods in Physics Research B</i> , 2016 , 373, 80-84	1.2	1
Engineered Pinning Landscapes for Enhanced 2G Coil Wire. 2016 , 26, 1-4		33
Effects of excess oxygen on the 4.58.3 eV absorption spectra of oxygen-rich high purity silica. <i>Nuclear Instruments & Methods in Physics Research B</i> , 2016 , 375, 40-48	1.2	
Energetic and kinetic dataset on interaction of the vacancy and self-interstitial atom with the grain boundary in \exists ron. 2016 , 7, 798-813		4
Time dependent modeling of single particle displacement damage in silicon devices. 2016 , 60, 25-32		3
Ion beam induced cubic to monoclinic phase transformation of nanocrystalline yttria. <i>Nuclear Instruments & Methods in Physics Research B</i> , 2016 , 379, 73-77	1.2	9
Measurement of deuteron induced gamma-ray emission differential cross sections on natCl from 1.0 to 2.0 MeV. <i>Nuclear Instruments & Methods in Physics Research B</i> , 2016 , 377, 37-42	1.2	3
	1.2	3 45
1.0 to 2.0 MeV. <i>Nuclear Instruments & Methods in Physics Research B</i> , 2016 , 377, 37-42 Low energy ion scattering (LEIS). A practical introduction to its theory, instrumentation, and applications. 2016 , 8, 3419-3439 Optimization of sedimentation of tungsten on copper substrate for production of 186g Re via 186	1.2	
1.0 to 2.0 MeV. <i>Nuclear Instruments & Methods in Physics Research B</i> , 2016 , 377, 37-42 Low energy ion scattering (LEIS). A practical introduction to its theory, instrumentation, and applications. 2016 , 8, 3419-3439 Optimization of sedimentation of tungsten on copper substrate for production of 186g Re via 186 W(p,n) nuclear reaction: Feasibility of using high current, long irradiation. <i>Nuclear Instruments &</i>		45
1.0 to 2.0 MeV. <i>Nuclear Instruments & Methods in Physics Research B</i> , 2016 , 377, 37-42 Low energy ion scattering (LEIS). A practical introduction to its theory, instrumentation, and applications. 2016 , 8, 3419-3439 Optimization of sedimentation of tungsten on copper substrate for production of 186g Re via 186 W(p,n) nuclear reaction: Feasibility of using high current, long irradiation. <i>Nuclear Instruments & Methods in Physics Research B</i> , 2016 , 366, 224-226 Radioactive by-products of a self-shielded cyclotron and the liquid target system for F-18 routine		45
	Assessment of experimental d-PIGE [Fray production cross sections for 12C, 14N and 16O and comparison with absolute thick target yields. <i>Nuclear Instruments & Methods in Physics Research B</i> , 2016, 380, 1-10 Enhancement in luminescence properties of ZrO2:Dy3+ under 100 MeV swift Ni7+ ion irradiation. 2016, 6, 55240-55247 Dose dependence of helium bubble formation in nano-engineered SiC at 700 [IC. 2016, 472, 153-160] Molecular dynamics simulation of bipartite bimetallic clusters under low-energy argon ion bombardment. 2016, 58, 387-393 Porosity estimation of alumina samples based on resonant backscattering spectrometry. <i>Nuclear Instruments & Methods in Physics Research B</i> , 2016, 373, 80-84 Engineered Pinning Landscapes for Enhanced 2G Coil Wire. 2016, 26, 1-4 Effects of excess oxygen on the 4.58.3 eV absorption spectra of oxygen-rich high purity silica. <i>Nuclear Instruments & Methods in Physics Research B</i> , 2016, 375, 40-48 Energetic and kinetic dataset on interaction of the vacancy and self-interstitial atom with the grain boundary in Bron. 2016, 7, 798-813 Time dependent modeling of single particle displacement damage in silicon devices. 2016, 60, 25-32 Ion beam induced cubic to monoclinic phase transformation of nanocrystalline yttria. <i>Nuclear</i>	comparison with absolute thick target yields. Nuclear Instruments & Methods in Physics Research B, 2016, 380, 1-10 Enhancement in luminescence properties of ZrO2:Dy3+ under 100 MeV swift Ni7+ ion irradiation. 2016, 6, 55240-55247 Dose dependence of helium bubble formation in nano-engineered SiC at 700 IEC. 2016, 472, 153-160 Molecular dynamics simulation of bipartite bimetallic clusters under low-energy argon ion bombardment. 2016, 58, 387-393 Porosity estimation of alumina samples based on resonant backscattering spectrometry. Nuclear Instruments & Methods in Physics Research B, 2016, 373, 80-84 Engineered Pinning Landscapes for Enhanced 2G Coil Wire. 2016, 26, 1-4 Effects of excess oxygen on the 4.58.3 eV absorption spectra of oxygen-rich high purity silica. Nuclear Instruments & Methods in Physics Research B, 2016, 375, 40-48 Energetic and kinetic dataset on interaction of the vacancy and self-interstitial atom with the grain boundary in Bron. 2016, 7, 798-813 Time dependent modeling of single particle displacement damage in silicon devices. 2016, 60, 25-32 lon beam induced cubic to monoclinic phase transformation of nanocrystalline yttria. Nuclear

1055	SHI induced effects on the electrical and optical properties of HfO2 thin films deposited by RF sputtering. <i>Nuclear Instruments & Methods in Physics Research B</i> , 2016 , 379, 230-234	16
1054	A direct comparison between in-situ transmission electron microscopy observations and Dislocation Dynamics simulations of interaction between dislocation and irradiation induced loop in a zirconium alloy. 2016 , 119, 71-75	23
1053	Nuclear Reaction Analysis. 2016 , 315-336	3
1052	Effects of 3.5 MeV proton irradiation on pure zirconium. 2016 , 22, 443-450	2
1051	Flower color mutants induced by carbon ion beam irradiation of geranium (Pelargonium II hortorum, Bailey). 2016 , 27, 1	8
1050	Corrosion of the alloys Magnox AL80, Magnox ZR55 and pure magnesium in air containing water vapour. 2016 , 112, 347-363	9
1049	Formation of He-Rich Layers Observed by Neutron Reflectometry in the He-Ion-Irradiated Cr/W Multilayers: Effects of Cr/W Interfaces on the He-Trapping Behavior. 2016 , 8, 24300-5	8
1048	Thin film depth profiling by ion beam analysis. 2016 , 141, 5944-5985	65
1047	Radon induced hyperplasia: effective adaptation reducing the local doses in the bronchial epithelium. 2016 , 36, 653-666	4
1046	Transport of spin qubits with donor chains under realistic experimental conditions. 2016, 94,	14
1045	Design of the prototype of a beam transport line for handling and selection of low energy laser-driven beams. 2016 , 837, 80-87	3
1044	Photocarrier radiometry for predicting the degradation of electrical parameters of monocrystalline silicon (c-Si) solar cell irradiated by 100 KeV proton beams. <i>Nuclear Instruments & Methods in Physics</i> 1.2 <i>Research B</i> , 2016 , 383, 171-176	8
1043	An O2+ probe energy study for boron quantification in Si1 (O (L) (1) using secondary ion mass spectrometry. 2016 , 390, 778-783	1
1042	Radiation response of alloy T91 at damage levels up to 1000 peak dpa. 2016 , 482, 257-265	45
1041	Gallium ion irradiation induced compaction and hardening of sputter deposited amorphous carbon thin films. 2016 , 112, 512-518	
1040	High-rate axial-field ionization chamber for particle identification of radioactive beams. 2016 , 837, 28-33	2
1039	The influence of carbon on the resistivity recovery of proton irradiated Fell 1 at.% Cr alloys. 2016 , 9, 465-470	5
1038	Nature of gallium focused ion beam induced phase transformation in 316L austenitic stainless steel. 2016 , 120, 391-402	37

1037	In situ Transmission Electron Microscopy He+ implantation and thermal aging of nanocrystalline iron. 2016 , 482, 139-146		5
1036	Electron backscatter diffraction studies of focused ion beam induced phase transformation in cobalt. 2016 , 120, 210-219		9
1035	L-shell X-ray production cross sections of Ce, Nd, Sm, Eu, Gd, and Dy by impact of 14 N 2+ ions with energies between 7.0 MeV and 10.5 MeV. <i>Nuclear Instruments & Methods in Physics Research B</i> , 2016 , 383, 89-92	1.2	6
1034	Persistent photoconductivity in oxygen-ion implanted KNbO 3 bulk single crystal. 2016 , 248, 120-122		
1033	Mesoscale model for fission-induced recrystallization in U-7Mo alloy. 2016 , 124, 228-237		24
1032	A table-top ion and electron beam facility for ionization quenching measurement and gas detector calibration. 2016 , 832, 214-218		4
1031	Hydrogen Emission and Macromolecular Radiation-Induced Defects in Polyethylene Irradiated under an Inert Atmosphere: The Role of Energy Transfers toward trans-Vinylene Unsaturations. 2016 , 120, 10367-10380		8
1030	. 2016 , 63, 2183-2192		11
1029	Quantitative autoradiography of alpha particle emission in geo-materials using the Beaver system. 2016 , 833, 15-22		24
1028	Deuteron induced Tb-155 production, a theranostic isotope for SPECT imaging and auger therapy. 2016 , 118, 281-289		13
1027	Electronic band structure effects in the stopping of protons in copper. 2016 , 94,		35
1026	Theoretical model analysis of (d,xn) reactions on Be9 and C12 at incident energies up to 50 MeV. 2016 , 94,		25
1025	Ionoluminescence. 2016 , 325-351		4
1024	Structural response of titanate pyrochlores to swift heavy ion irradiation. 2016 , 117, 207-215		46
1023	Electronic stopping power in liquid water for protons and particles from first principles. 2016 , 94,		27
1022	A new study of 10B(p,(alpha))7Be reaction at low energies. 2016 , 52, 1		10
1021	Production of bulk NV centre arrays by shallow implantation and diamond CVD overgrowth. 2016 , 213, 2594-2600		18
1020	Microstructure of Au-ion irradiated 316L and FeNiCr austenitic stainless steels. 2016 , 480, 436-446		15

1019	New excitation functions for proton induced reactions on natural titanium, nickel and copper up to 70 MeV. <i>Nuclear Instruments & Methods in Physics Research B</i> , 2016 , 383, 191-212	1.2	22
1018	Interactions of Ionizing Radiation with Matter and Direct Energy Conversion. 2016, 81-175		
1017	A computer program TRACK_P for studying proton tracks in PADC detectors. 2016 , 5, 74-79		8
1016	Creation and characterization of He-related color centers in diamond. 2016 , 179, 59-63		10
1015	Photoluminescence of gallium ion irradiated hexagonal and cubic GaN quantum dots. <i>Nuclear Instruments & Methods in Physics Research B</i> , 2016 , 383, 1-5	1.2	3
1014	Nonstoichiometry, Structure, and Properties of BiFeO3 Films. 2016 , 28, 5952-5961		42
1013	Fast neutron spectroscopy with tensioned metastable fluid detectors. 2016 , 830, 355-365		6
1012	Displacement rate and temperature equivalence in stochastic cluster dynamics simulations of irradiated pure Fe. 2016 , 480, 129-137		6
1011	Anti-biofilm activity of Fe heavy ion irradiated polycarbonate. <i>Nuclear Instruments & Methods in Physics Research B</i> , 2016 , 384, 6-13	1.2	11
1010	Role of composition, bond covalency, and short-range order in the disordering of stannate pyrochlores by swift heavy ion irradiation. 2016 , 94,		37
1009	Electronic sputtering of vitreous SiO2: Experimental and modeling results. <i>Nuclear Instruments & Methods in Physics Research B</i> , 2016 , 379, 2-8	1.2	16
1008	Intercalation of graphene on SiC(0001) via ion implantation. 2016 , 94,		17
1007	Precipitation kinetics of dilute Cu-W alloys during low-temperature ion irradiation. 2016 , 120, 46-55		24
1006	Introduction to Nuclear Batteries and Radioisotopes. 2016 , 1-37		2
1005	Power Density Dilution Due to the Interface of the Isotope with the Transducer. 2016 , 177-220		
1004	Void swelling and microstructure evolution at very high damage level in self-ion irradiated ferritic-martensitic steels. 2016 , 480, 159-176		65
1003	Influence of ion beam irradiation induced defects on the structural, optical and electrical properties of tellurium nanowires. 2016 , 183, 165-172		5
1002	Atomistic Simulations of Ceramic Materials Relevant for Nuclear Waste Management: Cases of Monazlte and Pyrochlore. 2016 , 165-175		10

1001	Mutagenic effects of carbon ion beam irradiations on dry Lotus japonicus seeds. <i>Nuclear Instruments & Methods in Physics Research B</i> , 2016 , 383, 123-128	13
1000	On the efficiency of combined ion implantation for the creation of near-surface nitrogen-vacancy centers in diamond. 2016 , 213, 2044-2050	10
999	Optical studies of cobalt implanted rutile TiO2 (110) surfaces. 2016 , 387, 938-943	8
998	Multinucleon transfer in O16,18,F19+Pb208 reactions at energies near the fusion barrier. 2016 , 94,	26
997	Efficiency Limitations for Various Nuclear Battery Configurations. 2016, 221-284	
996	Formation of donors in germanium lilicon alloys implanted with hydrogen ions with different energies. 2016 , 50, 1122-1124	
995	Pixel pitch and particle energy influence on the dark current distribution of neutron irradiated CMOS image sensors. 2016 , 24, 4299-315	14
994	Radiation Hardness and Self-Healing of Perovskite Solar Cells. 2016 , 28, 8726-8731	128
993	Dating kimberlite emplacement with zircon and perovskite (U-Th)/He geochronology. 2016 , 17, 4517-4533	13
992	Threshold concentration for ion implantation-induced Co nanocluster formation in TiO2:Co thin films. <i>Nuclear Instruments & Methods in Physics Research B</i> , 2016 , 389-390, 13-16	3
991	Atomic layer deposition ultrathin film origami using focused ion beams. 2016 , 27, 49LT02	9
990	Direct measurement of low-energy Ne22(p,□)Na23 resonances. 2016 , 94,	26
989	Tailoring Spin Textures in Complex Oxide Micromagnets. 2016 , 10, 8545-51	10
988	How to produce high specific activity tin-117m using alpha particle beam. 2016 , 115, 113-124	6
987	Experimental validation of simulations of radiation shielding effectiveness of materials by MULASSIS. 2016 , 58, 2376-2384	4
986	Measurement of proton inelastic scattering cross sections on fluorine. <i>Nuclear Instruments & Methods in Physics Research B</i> , 2016 , 384, 37-41	
985	Mechanical behavior of copper containing a gas-bubble superlattice. 2016 , 121, 78-84	38
984	Radiation track, DNA damage and response-a review. 2016 , 79, 116601	170

983	Scattering of hydrogen, nitrogen and water ions from micro pore optic plates for application in spaceborne plasma instrumentation. <i>Nuclear Instruments & Methods in Physics Research B</i> , 2016 , 385, 9-14	2
982	□Ray spectroscopy using a binned likelihood approach. 2016 , 830, 427-437	7
981	Narrow-Linewidth Homogeneous Optical Emitters in Diamond Nanostructures via Silicon Ion Implantation. 2016 , 5,	90
980	Adiabatic perturbation theory of electronic stopping in insulators. 2016 , 93,	9
979	Low-temperature conducting state in two candidate topological Kondo insulators: SmB6 and Ce3Bi4Pt3. 2016 , 94,	27
978	Low-lying isovector 2+ valence-shell excitations of Po212. 2016 , 93,	12
977	Measurement of the Tm169(n,3n)Tm167 cross section and the associated branching ratios in the decay of Tm167. 2016 , 93,	11
976	Proton capture cross sections on neutron-magic Sm144 at astrophysically relevant energies. 2016 , 93,	4
975	Partial cross sections of the Mo92(p,[]) reaction and the 🛭 strength in Tc93. 2016 , 93,	15
974	First direct measurement of the C11(p)N14 stellar reaction by an extended thick-target method. 2016 , 93,	5
973	Electron Elevator: Excitations across the Band Gap via a Dynamical Gap State. 2016 , 116, 043201	46
972	Characterization of the ELIMED Permanent Magnets Quadrupole system prototype with laser-driven proton beams. 2016 , 11, T07005-T07005	15
971	Radiation damage-controlled localization of alteration haloes in albite: implications for alteration types and patterns vis-Bvis mineralization and element mobilization. 2016 , 110, 823-843	9
970	On the Use of Scalable NanoISFET Arrays of Silicon with Highly Reproducible Sensor Performance for Biosensor Applications. 2016 , 1, 84-92	26
969	Production of 3He in rocks by reactions induced by particles of the nuclear-active and muon components of cosmic rays: Geological and petrological implications. 2016 , 24, 21-34	7
968	Highly Selective Ionic Transport through Subnanometer Pores in Polymer Films. 2016 , 26, 5796-5803	106
967	Evidence for Magnetic Order in Graphite from Magnetization and Transport Measurements. 2016 , 45-76	3
966	Differential cross sections measurement of 31 P(p,p \square 1) 31 P reaction for PIGE applications. Nuclear Instruments & Methods in Physics Research B, 2016 , 383, 152-155	3

965	Nanoscale Engineering of Closely-Spaced Electronic Spins in Diamond. 2016 , 16, 4982-90		34
964	Traceable stopping cross sections of Al and Mo elemental targets for 0.9B.6-MeV protons. 2016 , 93,		5
963	Ion-beam nanopatterning of silicon surfaces under codeposition of non-silicide-forming impurities. 2016 , 93,		12
962	Combined high-resolution laser spectroscopy and nuclear decay spectroscopy for the study of the low-lying states in Fr206, At202, and Bi198. 2016 , 93,		11
961	Second 0+ state of unbound O12: Scaling of mirror asymmetry. 2016 , 93,		8
960	Absolute hydrogen depth profiling using the resonant 1H(15N,. <i>Nuclear Instruments & Methods in Physics Research B</i> , 2016 , 381, 58-66	1.2	9
959	Magneto-transport properties of As-implanted highly oriented pyrolytic graphite. 2016 , 500, 118-125		1
958	Relatively low temperature deposition of graphene like films with ethane GCIB irradiation. 2016 , 306, 218-221		
957	Effect of noble gas ion pre-irradiation on deuterium retention in tungsten. 2016 , T167, 014001		3
956	All-carbon multi-electrode array for real-time in vitro measurements of oxidizable neurotransmitters. 2016 , 6, 20682		25
955	Layer-by-layer composition and structure of silicon subjected to combined gallium and nitrogen ion implantation for the ion synthesis of gallium nitride. 2016 , 50, 271-275		6
954	Reconstruction of Ge spatial distribution in ICF target using PIXE-T. 2016 , 113, 43-50		6
953	Recent developments in the Thomson Parabola Spectrometer diagnostic for laser-driven multi-species ion sources. 2016 , 11, C10005-C10005		9
952	Overview of the NASA space radiation laboratory. 2016 , 11, 18-23		69
951	A new method of making ohmic contacts to p-GaN. <i>Nuclear Instruments & Methods in Physics Research B</i> , 2016 , 388, 35-40	1.2	6
950	Ion-beam synthesis and thermal behaviour of luminescent Zn2SiO4 nanoparticles in silica glasses and films. 2016 , 253, 2180-2184		1
949	Precipitation behavior of AlxCoCrFeNi high entropy alloys under ion irradiation. 2016 , 6, 32146		54
948	Highly Efficient Power Conversion from Salinity Gradients with Ion-Selective Polymeric Nanopores. 2016 , 33, 096103		5

947	Uncovering Special Nuclear Materials by Low-energy Nuclear Reaction Imaging. 2016 , 6, 24388	26
946	Monte Carlo Simulations of Focused Ion Beam Induced Processing. 2016 , 89-118	1
945	DirectWrite Milling and Deposition with Noble Gases. 2016 , 355-393	14
944	Laser-Assisted Focused He Ion Beam Induced Etching with and without XeF Gas Assist. 2016 , 8, 29155-29162	23
943	Non-monotonic temperature dependence of radiation defect dynamics in silicon carbide. 2016 , 6, 30931	15
942	Deep proton writing with 12IMeV protons for rapid prototyping of microstructures in polymethylmethacrylate. 2016 , 15, 044501	2
941	Observation of a helium ion energy threshold for retention in tungsten exposed to hydrogen/helium mixture plasma. 2016 , 56, 104002	15
940	ION-INDUCED PROCESSING OF COSMIC SILICATES: A POSSIBLE FORMATION PATHWAY TO GEMS. 2016 , 831, 66	5
939	Ion Micro Beam, promising methods for interdisciplinary research. 2016, 11, C05001-C05001	4
938	Development of a pepper-pot emittance meter for diagnostics of low-energy multiply charged heavy ion beams extracted from an ECR ion source. 2016 , 87, 02B920	7
937	In vacuo growth studies of Ru thin films on Si, SiN, and SiO2 by high-sensitivity low energy ion scattering. 2016 , 120, 065303	9
936	Growth of Graphene on SiC(111) Surfaces via Ion-Beam Irradiation. 2016 , 14, 121-124	O
935	Interdiffusion and stress development in single-crystalline Pd/Ag bilayers. 2016, 119, 145308	6
934	Estimating the magnetic moment of microscopic magnetic sources from their magnetic field distribution in a layer of nitrogen-vacancy (NV) centres in diamond. 2016 , 73, 20701	5
933	Hard X-ray irradiation of cosmic silicate analogs: structural evolution and astrophysical implications. 2016 , 587, A144	7
932	Highly spatially resolved structural and optical investigation of Bi nanoparticles in Y-Er disilicate thin films. 2016 , 109, 061902	3
931	TEM with in situ Ion Irradiation of Nuclear Materials under In-Service Conditions. 2016 , 22, 1460-1461	1
930	A simple and compact method for measuring the hydrogen ion fraction of hybrid ion beams. 2016 , 6, 125046	

929	ANTS2 package: simulation and experimental data processing for Anger camera type detectors. 2016 , 11, P04022-P04022	26
928	Irradiation Effects on the Retention of Hydrogen in Al 2 O 3. 2016 , 33, 066102	1
927	Evidence of secondary electron emission during PIII pulses as measured by calorimetric probe. 2016 , 70, 1	5
926	Effects of cesium ion-implantation on mechanical and electrical properties of organosilicate low-k films. 2016 , 108, 202901	1
925	In Situ Electrochemical Behavior of Titanium Alloys (T40, T64) Under 4He2+ Irradiation. 2016 , 1845-1848	
924	Surface-Directed Nanoepitaxy on a Surface with an Irregular Lattice. 2016 , 3, 1500598	2
923	Estimation of atmospheric neutrinos background in Borexino. 2016 , 675, 012014	2
922	Shaping and compositional modification of zinc oxide nanowires under energetic manganese ion irradiation. 2016 , 27, 175301	9
921	Sensitivity of 57Fe emission M\(\text{S}\)sbauer spectroscopy to Ar and C induced defects in ZnO. 2016 , 237, 1	1
920	Effect of ion beam parameters on engineering of nanoscale voids and their stability under post-growth annealing. 2016 , 122, 1	8
919	Graphene: the ultimately thin sputtering shield. 2016 , 3, 025032	18
918	Enhanced surface and interface diffusion in Ni B i bilayers by swift heavy ion irradiation. 2016 , 6, 58950-58956	6
917	Evaluation of hardening behaviors in ion-irradiated FeBCr and FeBOCr alloys by nanoindentation technique. 2016 , 478, 50-55	24
916	Resonant Raman spectroscopy study of swift heavy ion irradiated MoS2. <i>Nuclear Instruments & Methods in Physics Research B</i> , 2016 , 381, 1-5	5
915	4H-SiC Neutron Sensors Based on Ion Implanted 10B Neutron Converter Layer. 2016 , 63, 1976-1980	7
914	ION IRRADIATION OF ETHANE AND WATER MIXTURE ICE AT 15 K: IMPLICATIONS FOR THE SOLAR SYSTEM AND THE ISM. 2016 , 824, 81	12
913	Curved gratings as an integrated photon fluence monitor in x-ray transmission scattering experiments. 2016 , 24, 13091-100	6
912	Altering the luminescence properties of self-assembled quantum dots in GaAs by focused ion beam implantation. 2016 , 122, 1	4

911	Lattice sites, charge states and spinlattice relaxation of Fe ions in 57 Mn + implanted GaN and AlN. 2016 , 401, 1130-1138		5
910	Response functions of semiconducting lithium indium diselenide. 2016 , 822, 9-14		5
909	MultiSIMNRA: A computational tool for self-consistent ion beam analysis using SIMNRA. <i>Nuclear Instruments & Methods in Physics Research B</i> , 2016 , 371, 86-89	1.2	56
908	Status of the low-energy super-heavy element facility at RIKEN. <i>Nuclear Instruments & Methods in Physics Research B</i> , 2016 , 376, 425-428	1.2	9
907	Nanoscale nonlinear effects in Erbium-implanted Yttrium Orthosilicate. 2016 , 177, 266-274		2
906	The diffusion of cesium, strontium, and europium in silicon carbide. 2016 , 476, 155-167		10
905	In situ TEM annealing of ion-amorphized Hi Nicalon S and Tyranno SA3 SiC fibers. <i>Nuclear Instruments & Methods in Physics Research B</i> , 2016 , 374, 76-81	1.2	4
904	Mono and sequential ion irradiation induced damage formation and damage recovery in oxide glasses: Stopping power dependence of the mechanical properties. 2016 , 469, 244-250		45
903	Experimental results of the laserwire emittance scanner for LINAC4 at CERN. 2016 , 830, 526-531		2
902	A comparison of lower and higher LET heavy ion irradiation effects on silicon NPN rf power transistors. 2016 , 822, 34-42		3
901	Time dependence of silica optical properties during the implantation of fast hydrogen ions: Experiment. <i>Nuclear Instruments & Methods in Physics Research B</i> , 2016 , 366, 90-95	1.2	3
900	Optical properties and surface damage studies of crystalline silicon caused by swift iron ions. <i>Nuclear Instruments & Methods in Physics Research B</i> , 2016 , 375, 67-70	1.2	
899	SHI induced modification in structural, optical, dielectric and thermal properties of poly ethylene oxide films. <i>Nuclear Instruments & Methods in Physics Research B</i> , 2016 , 379, 156-161	1.2	5
898	Access of energetic particles to Titan?s exobase: A study of Cassini?s T9 flyby. 2016 , 130, 40-53		18
897	Direct investigation of (sub-) surface preparation artifacts in GaAs based materials by FIB sectioning. 2016 , 163, 19-30		9
896	GEANT 4 simulation of (99)Mo photonuclear production in nanoparticles. 2016 , 114, 7-13		O
895	Growth of simplified buffer template on flexible metallic substrates for YBa2Cu3O coated conductors. 2016 , 673, 47-53		12
894	Relating the 3D electrode morphology to Li-ion battery performance; a case for LiFePO 4. 2016 , 324, 358-367		29

(2016-2016)

893	Design and performance of an ionisation chamber for the measurement of low alpha-activities. 2016 , 814, 12-18	14
892	Efficiency and spatial resolution of the CASCADE thermal neutron detector. 2016 , 828, 242-249	26
891	Misconceptions impairing the validity of the stopping power tables in the SRIM library and suggestions for doing better in the future. <i>Nuclear Instruments & Methods in Physics Research B</i> , 1.2 2016 , 380, 57-70	22
890	Induced Electronic and Thermal Effects of 86 MeV Nickel Ions in Bisphenol-A Polycarbonate. 2016 , 55, 765-773	
889	Capture-gated Spectroscopic Measurements of Monoenergetic Neutrons with a Composite Scintillation Detector. 2016 , 63, 1227-1235	9
888	Biaxial Texture Evolution in MgO Films Fabricated Using Ion Beam-Assisted Deposition. 2016 , 45, 3546-3553	2
887	Energy loss of slow Ne ions in Pt and Ag from TOF-MEIS and Monte-Carlo simulations. <i>Nuclear Instruments & Methods in Physics Research B</i> , 2016 , 371, 76-80	7
886	Structural Transitions Induced by Ion Irradiation in V2AlC and Cr2AlC. 2016 , 99, 1769-1777	27
885	The effect of alloying nickel with iron on the supersonic ballistic stage of high energy displacement cascades. 2016 , 116, 136-142	27
884	Evaluation of the relative TL efficiency of the thermoluminescent detectors to heavy charged particles. 2016 , 168, 27-32	7
883	Energy Dependence of Fission Product Yields from 235U, 238U and 239Pu for Incident Neutron Energies Between 0.5 and 14.8 MeV. 2016 , 131, 319-356	41
882	Fabrication of free-standing lithium niobate nanowaveguides down to 50 nm in width. 2016 , 27, 065301	8
881	Monte Carlo Simulations of 17.902.3 MeV Energetic Proton Irradiation Effects on bcc-Zirconium Fusionic Materials. 2016 , 35, 591-596	16
880	Neutron background signal in superheated droplet detectors of the Phase II SIMPLE dark matter search. 2016 , 76, 48-60	8
879	Influence of Particle radiation on the structural and electronic properties of thin film GaAs solar cells: A simulation study. 2016 , 127, 3844-3847	5
878	Helium Scanning Transmission Ion Microscopy and Electrical Characterization of Glass Nanocapillaries with Reproducible Tip Geometries. 2016 , 10, 1918-25	11
877	Characterization of nitrogen species incorporated into graphite using low energy nitrogen ion sputtering. 2016 , 18, 458-65	18
876	A coupled effect of nuclear and electronic energy loss on ion irradiation damage in lithium niobate. 2016 , 105, 429-437	34

875	Low energy and low fluence helium implantations in tungsten: Molecular dynamics simulations and experiments. 2016 , 470, 44-54	41
874	Investigation of electrically-active deep levels in single-crystalline diamond by particle-induced charge transient spectroscopy. <i>Nuclear Instruments & Methods in Physics Research B</i> , 2016 , 372, 151-155 1.2	1
873	Lithium fluoride colour centres-based imaging detectors for proton beam characterization at high doses. 2016 , 90, 188-191	2
872	The effect of Ni pre-implantation on surface morphology and optical absorption properties of Ag nanoparticles embedded in SiO2. 2016 , 363, 310-317	4
871	Characterization of gold leaves on Greek terracotta figurines: A PIXE-RBS study. 2016 , 126, 446-453	14
870	Study of hydrogen isotopes behavior in tungsten by a multi trapping macroscopic rate equation model. 2016 , T167, 014011	20
869	Synthesis and characterization of Y-doped TiH 2 films prepared by magnetron sputtering. 2016 , 41, 2820-282	86
868	Effects of D and He implantation depth on D retention in tungsten under simultaneous D⊞e ion irradiation. 2016 , T167, 014042	7
867	Nanopores formation and shape evolution in Ge during intense ionizing irradiation. 2016 , 225, 323-330	6
866	Radiation Interaction with Matter. 2016 , 63-100	
866	Radiation Interaction with Matter. 2016 , 63-100 Decomposition mechanism of indium oxide nanoparticles sandwiched between zinc oxide layers by energetic ions. 2016 , 42, 2846-2853	3
	Decomposition mechanism of indium oxide nanoparticles sandwiched between zinc oxide layers by	3 26
865	Decomposition mechanism of indium oxide nanoparticles sandwiched between zinc oxide layers by energetic ions. 2016 , 42, 2846-2853 Nanoscale doping profiles within CdTe grain boundaries and at the CdS/CdTe interface revealed by	
86 ₅	Decomposition mechanism of indium oxide nanoparticles sandwiched between zinc oxide layers by energetic ions. 2016, 42, 2846-2853 Nanoscale doping profiles within CdTe grain boundaries and at the CdS/CdTe interface revealed by atom probe tomography and STEM EBIC. 2016, 150, 95-101 Cavity Evolution at Grain Boundaries as a Function of Radiation Damage and Thermal Conditions in	26
865 864 863	Decomposition mechanism of indium oxide nanoparticles sandwiched between zinc oxide layers by energetic ions. 2016, 42, 2846-2853 Nanoscale doping profiles within CdTe grain boundaries and at the CdS/CdTe interface revealed by atom probe tomography and STEM EBIC. 2016, 150, 95-101 Cavity Evolution at Grain Boundaries as a Function of Radiation Damage and Thermal Conditions in Nanocrystalline Nickel. 2016, 4, 96-103	26
865 864 863	Decomposition mechanism of indium oxide nanoparticles sandwiched between zinc oxide layers by energetic ions. 2016, 42, 2846-2853 Nanoscale doping profiles within CdTe grain boundaries and at the CdS/CdTe interface revealed by atom probe tomography and STEM EBIC. 2016, 150, 95-101 Cavity Evolution at Grain Boundaries as a Function of Radiation Damage and Thermal Conditions in Nanocrystalline Nickel. 2016, 4, 96-103 The effect of magnetic and non-magnetic ion damage on the surface state in SmB6. 2016, 400, 62-65 Measurement of the equilibrium charge state distributions of Ni, Co, and Cu beams in Mo at 2 MeV/u: Review and evaluation of the relevant semi-empirical models. <i>Nuclear Instruments</i> & 1.2	26 10 2
865 864 863 862	Decomposition mechanism of indium oxide nanoparticles sandwiched between zinc oxide layers by energetic ions. 2016, 42, 2846-2853 Nanoscale doping profiles within CdTe grain boundaries and at the CdS/CdTe interface revealed by atom probe tomography and STEM EBIC. 2016, 150, 95-101 Cavity Evolution at Grain Boundaries as a Function of Radiation Damage and Thermal Conditions in Nanocrystalline Nickel. 2016, 4, 96-103 The effect of magnetic and non-magnetic ion damage on the surface state in SmB6. 2016, 400, 62-65 Measurement of the equilibrium charge state distributions of Ni, Co, and Cu beams in Mo at 2 MeV/u: Review and evaluation of the relevant semi-empirical models. Nuclear Instruments & Methods in Physics Research B, 2016, 373, 117-125 The spectrum of Jupiter's Great Red Spot: The case for ammonium hydrosulfide (NH4SH). 2016,	26 10 2

857	Web-based description of the space radiation environment using the Bethe B loch model. 2016 , 37, 015605	O
856	Interdiffusion in epitaxial, single-crystalline Au/Ag thin films studied by Auger electron spectroscopy sputter-depth profiling and positron annihilation. 2016 , 107, 133-143	10
855	Modeling injected interstitial effects on void swelling in self-ion irradiation experiments. 2016 , 471, 200-207	46
854	Raman investigation of lattice defects and stress induced in InP and GaN films by swift heavy ion irradiation. <i>Nuclear Instruments & Methods in Physics Research B</i> , 2016 , 372, 29-37	11
853	Experimental and Monte Carlo study relevant to the cyclotron production of 51Cr through 51V(p,n) reaction. 2016 , 309, 1321-1326	
852	Influence of hydrogen fluence on surface blistering of H and He co-implanted Ge. <i>Nuclear Instruments & Methods in Physics Research B</i> , 2016 , 368, 86-89	1
851	Low-Resistance Titanium Contacts and Thermally Unstable Nickel Germanide Contacts on p-Type Germanium. 2016 , 37, 482-485	26
850	Investigation of defect clusters in ion-irradiated Ni and NiCo using diffuse X-ray scattering and electron microscopy. 2016 , 469, 153-161	20
849	Ion-beam-assisted spatial modulation of inhomogeneous broadening of a quantum well resonance: excitonic diffraction grating. 2016 , 41, 104-6	8
848	A three-dimensional imaging detector based on nano-scale silver-related defects in X- and gamma-ray-irradiated glasses. 2016 , 55, 02BC01	10
847	Effective atomic number, energy loss and radiation damage studies in some materials commonly used in nuclear applications for heavy charged particles such as H, C, Mg, Fe, Te, Pb and U. 2016 , 122, 15-23	16
846	Retention and damage in 3C-IsiC irradiated with He and H ions. 2016 , 469, 187-193	13
845	Atomic simulations of Fe/Ni multilayer nanocomposites on the radiation damage resistance. 2016 , 468, 164-170	10
844	Stopping power measurements with the Time-of-Flight (ToF) technique. <i>Nuclear Instruments & Methods in Physics Research B</i> , 2016 , 366, 104-116	4
843	Nuclear excitation functions from 40 to 200 MeV proton irradiation of terbium. <i>Nuclear Instruments & Methods in Physics Research B</i> , 2016 , 366, 206-216	2
842	700 keV Ni +2 ions induced modification in structural, surface, magneto-optic and optical properties of ZnO thin films. <i>Nuclear Instruments & Methods in Physics Research B</i> , 2016 , 368, 45-49	13
841	Vacuum Chromatography of Tl on SiO2 at the Single-Atom Level. 2016 , 120, 7122-7132	19
840	Measurement of LET (linear energy transfer) spectra using CR-39 at different depths of water irradiated by 171 MeV protons: A comparison with Monte Carlo simulation. 2016 , 818, 14-19	3

839	A novel track imaging system as a range counter. 2016 , 817, 57-62	1
838	Swift heavy ion irradiation induced phase transformation in undoped and niobium doped titanium dioxide composite thin films. <i>Nuclear Instruments & Methods in Physics Research B</i> , 2016 , 379, 224-229	9
837	Probing disorder in isometric pyrochlore and related complex oxides. 2016 , 15, 507-11	133
836	Toward Optimized Surface Profiles of Nitrogen-Vacancy Centers Activated by Helium Irradiation in Diamond. 2016 , 16, 2228-33	27
835	Radiation resistance of nano-crystalline iron: Coupling of the fundamental segregation process and the annihilation of interstitials and vacancies near the grain boundaries. 2016 , 109, 115-127	46
834	Towards the understanding of non-thermal air plasma action: effects on bacteria and fibroblasts. 2016 , 6, 25286-25292	12
833	Differential cross sections measurement of 28 Si(p,p / \square) 28 Si and 29 Si(p,p / \square) 29 Si reactions for PIGE applications. <i>Nuclear Instruments & Methods in Physics Research B</i> , 2016 , 371, 37-40	8
832	Effects of trap-assisted tunneling on gate-induced drain leakage in silicongermanium channel p-type FET for scaled supply voltages. 2016 , 55, 04ED03	1
831	NPTool: a simulation and analysis framework for low-energy nuclear physics experiments. 2016 , 43, 045113	19
830	Shape manipulation of ion irradiated Ag nanoparticles embedded in lithium niobate. 2016 , 27, 145202	23
829	In-situ luminescence monitoring of ion-induced damage evolution in SiO2 and Al2O3. 2016 , 172, 208-218	48
828	Accelerated radiation damage test facility using a 5 MV tandem ion accelerator. 2016 , 806, 109-116	22
827	Characterization of the recovery of mechanical properties of ion-implanted diamond after thermal annealing. 2016 , 63, 75-79	6
826	Optical, electrical and microstructural properties of nanocomposite Ag/diamond by Ag ion implantation and subsequent annealing. 2016 , 123, 160-166	4
825	Comparative study of irradiation effects in graphite and graphene induced by swift heavy ions and highly charged ions. 2016 , 100, 16-26	34
824	Laser-driven x-ray and neutron source development for industrial applications of plasma accelerators. 2016 , 58, 014039	65
823	The interplay between biological and physical scenarios of bacterial death induced by non-thermal plasma. 2016 , 82, 71-83	92
822	Hierarchical reinforcement of randomly-oriented carbon nanotube mats by ion irradiation. 2016 , 99, 491-501	4

(2016-2016)

821	Electronic structure modification and Fermi level shifting in niobium-doped anatase titanium dioxide thin films: a comparative study of NEXAFS, work function and stiffening of phonons. 2016 , 18, 3618-27		22
820	Surface, structural and tensile properties of proton beam irradiated zirconium. <i>Nuclear Instruments</i> & <i>Methods in Physics Research B</i> , 2016 , 368, 120-128	1.2	20
819	Rate capability of a cryogenic stopping cell for uranium projectile fragments produced at 1000 MeV/u. <i>Nuclear Instruments & Methods in Physics Research B</i> , 2016 , 376, 240-245	1.2	8
818	Regrowth of Ge with different degrees of damage under thermal and athermal treatment. 2016 , 6, 4570	5-4580	5 5
817	Effects of high-power laser irradiation on sub-superficial graphitic layers in single-crystal diamond. 2016 , 103, 665-671		10
816	Hydrogen analysis depth calibration by CORTEO Monte-Carlo simulation. <i>Nuclear Instruments & Methods in Physics Research B</i> , 2016 , 371, 161-166	1.2	4
815	Radiation chemical behavior of aqueous butanal oxime solutions irradiated with helium ion beams. 2016 , 119, 186-193		4
814	Enhanced architectures for soft error detection and correction in combinational and sequential circuits. 2016 , 56, 212-220		6
813	Production and separation of carrier-free B e. 2016 , 107, 199-202		2
812	Measurement of proton induced thick target 🛭 ray yields on B, N, Na, Al and Si from 2.5 to 4.1 MeV. <i>Nuclear Instruments & Methods in Physics Research B</i> , 2016 , 366, 77-82	1.2	12
811	Tailoring the properties of copper nanowires by ion beam irradiation. 2016 , 119, 44-50		7
810	Channeling energy loss and dechanneling of He along axial and planar directions of Si. <i>Nuclear Instruments & Methods in Physics Research B</i> , 2016 , 366, 57-62	1.2	2
809	Ab initio prediction of threshold displacement energies in ZrC. 2016 , 471, 214-219		11
808	Anisotropic expansion and amorphization of Ga2O3 irradiated with 946 MeV Au ions. <i>Nuclear Instruments & Methods in Physics Research B</i> , 2016 , 374, 40-44	1.2	8
807	Near-surface hydrogen depletion of diamond-like carbon films produced by direct ion deposition. <i>Nuclear Instruments & Methods in Physics Research B</i> , 2016 , 371, 230-234	1.2	6
806	A figure of meritifor susceptibility of irradiated amorphous metal alloys to thermal spike-induced plasticity. 2016 , 102, 251-262		2
805	Ion beam induced luminescence studies of sol gel derived Y2O3:Dy3+ nanophosphors. 2016 , 169, 627-63	34	14
804	Determination of the density of siliconflitride thin films by ion-beam analytical techniques (RBS, PIXE, STIM). 2016 , 307, 341-346		17

803	Production of 186gRe using low-energy protons. 2016 , 307, 253-258	3
802	Characterization of a single electrode focusing lens for ion beam deceleration. 2017 , 45, 12-21	3
801	Dark matter directional detection: comparison of the track direction determination. 2017 , 2017, 027-027	8
800	Defect engineering of single- and few-layer MoS 2 by swift heavy ion irradiation. 2017 , 4, 015034	41
799	Observation of Edelayed two-proton emission in the decay of 22Si. 2017 , 766, 312-316	21
798	Effects of sequential helium and hydrogen ion irradiation on the nucleation and evolution of bubbles in tungsten. 2017 , 115, 80-84	13
797	Characterization of M2X formed during 5 MeV Fe2+ irradiation. 2017 , 485, 154-158	8
796	The effects of ion irradiation on the micromechanical fracture strength and hardness of a self-passivating tungsten alloy. 2017 , 486, 34-43	6
795	Monte Carlo studies of the interaction of relativistic ions with nuclear emulsion. 2017, 841, 72-86	2
794	Collision cascades enhanced hydrogen redistribution in cobalt implanted hydrogenated diamond-like carbon films. <i>Nuclear Instruments & Methods in Physics Research B</i> , 2017 , 394, 6-11	5
793	Initial results of tests of depth markers as a surface diagnostic for fusion devices. 2017 , 12, 1277-1281	6
792	Study of surface exfoliation on 6H-SiC induced by H2+ implantation. 2017 , 508, 104-111	14
791	Lithography-free positioned GaAs nanowire growth with focused ion beam implantation of Ga. 2017 , 35, 011803	6
79 ⁰	Direct Trace Element Analysis of Liquid Blood Samples by In-Air Ion Beam Analytical Techniques (PIXE-PIGE). 2017 , 89, 1558-1564	9
789	Single- and Double-Strand Breaks of Dry DNA Exposed to Protons at Bragg-Peak Energies. 2017 , 121, 497-507	14
788	Spectroellipsometric detection of silicon substrate damage caused by radiofrequency sputtering of niobium oxide. 2017 , 421, 636-642	
787	Comparison of blistering of W bulk and film deposited by magnetron sputtering under helium irradiation. 2017 , 12, 588-592	10
786	Study of the formation mechanism of hierarchical silicon structures produced by sequential ion beam irradiation and anodic etching. 2017 , 138, 238-243	2

7 ⁸ 5	Quasi-atomic layer etching of silicon nitride. 2017 , 35, 01A102	45
7 ⁸ 4	A review on single photon sources in silicon carbide. 2017 , 80, 034502	115
783	Monte Carlo simulation to calculate the rate of 137Cs gamma rays dispersion in gallium arsenide compound. 2017 ,	
782	A 3D lateral electrode structure for diamond based microdosimetry. 2017 , 110, 013503	12
781	Surface functionalization of epitaxial graphene on SiC by ion irradiation for gas sensing application. 2017 , 403, 707-716	19
780	Modification of the saturation magnetization of exchange bias thin film systems upon light-ion bombardment. 2017 , 29, 125801	10
779	Characterization of a pixelated CdTe Timepix detector operated in ToT mode. 2017, 12, P01018-P01018	8
778	Spectroscopic study of prompt-gamma emission for range verification in proton therapy. 2017 , 34, 7-17	28
777	Ion-irradiation-induced structural evolution in Ti4AlN3. 2017 , 133, 19-23	5
776	Effects of Thickness on the Metal-Insulator Transition in Free-Standing Vanadium Dioxide Nanocrystals. 2017 , 17, 1762-1767	22
775	Resistance State Locking in CBRAM Cells Due to Displacement Damage Effects. 2017, 1-1	4
774	Interdiffusion in amorphous AlxZr1-x alloys. 2017 , 121, 015302	
773	Research on a Neutron Detector With a Boron-Lined Honeycomb Neutron Converter. 2017 , 64, 1048-1055	9
772	Void and cavity determination in micro-PIXE analysis of composed material using binocular detectors: A computational study. <i>Nuclear Instruments & Methods in Physics Research B</i> , 2017 , 404, 189-192	
771	Proton focusing driven by laser triggered Coulomb explosion. 2017 , 24, 030703	1
770	Radiolytic Events in Nanostructured Aluminum Hydroxides. 2017 , 121, 6365-6373	23
769	Synthesis of sponge-like hydrophobic NiBi3 surface by 200 keV Ar ion implantation. 2017 , 410, 519-524	3
768	Deuterium retention in recrystallized tungsten irradiated with simultaneous deuteriumBeon ion beams. 2017 , 12, 1288-1293	7

767	Tuning of mechanical and structural properties of 20IMC 5 steel using N ion implantation and subsequent annealing. 2017 , 710, 253-259		6
766	High velocity proton collision with liquid lithium: a time dependent density functional theory study. 2017 , 19, 9053-9058		10
765	Tungsten Diselenide Patterning and Nanoribbon Formation by Gas-Assisted Focused-Helium-Ion-Beam-Induced Etching. 2017 , 1, 1600060		28
764	Dynamic energy spectrum and energy deposition in solid target by intense pulsed ion beams. 2017 , 28, 1		4
763	The influence of the dose assessment method on the LET dependence of the relative luminescence efficiency of LiF:Mg,Ti and LiF:Mg,Cu,P. 2017 , 98, 34-40		16
762	Indentation behaviour of ion-irradiated X-750 Ni-based superalloy. 2017 , 97, 101-109		7
761	Potassium self-diffusion in a K-rich single-crystal alkali feldspar. 2017 , 44, 345-351		9
760	Rn/At and At production with intense mass separated Fr ion beams for preclinical At-based Etherapy research. 2017 , 122, 222-228		14
759	Modifications in physico-chemical properties of 100 MeV oxygen ions irradiated polyimide Kapton-H polymer. <i>Nuclear Instruments & Methods in Physics Research B</i> , 2017 , 406, 188-192	1.2	16
758	Lattice Location of Mg in GaN: A Fresh Look at Doping Limitations. 2017 , 118, 095501		29
757	Reactive Ar ion beam sputter deposition of TiO2 films: Influence of process parameters on film properties. <i>Nuclear Instruments & Methods in Physics Research B</i> , 2017 , 395, 17-23	1.2	13
756	The role of Frenkel defect diffusion in dynamic annealing in ion-irradiated Si. 2017, 7, 39754		11
755	Single particle irradiation permits real-time visualization of RNF8 accumulation at DNA damaged sites. 2017 , 7, 41764		5
754	The surface morphology, structural properties and chemical composition of Cd 1½ Zn x Te polycrystalline thick films deposited by close spaced vacuum sublimation. 2017 , 63, 64-71		10
753	Electrical characterization of a graphite-diamond-graphite junction fabricated by MeV carbon implantation. 2017 , 74, 125-131		7
75 ²	High resolution imaging of 2D distribution of lithium in thin samples measured with multipixel detectors in sandwich geometry. 2017 , 88, 023706		4
75 ¹	Ion beam modification of two-dimensional materials: Characterization, properties, and applications. 2017 , 4, 011103		114
750	Enhanced superconductivity, Kondo behavior, and negative-curvature resistivity of oxygen-irradiated thin films of aluminium. 2017 , 95,		2

749	Large electronic sputtering yield of nanodimensional Au thin films: Dominant role of thermal conductivity and electron phonon coupling factor. 2017 , 121, 095308	18
748	Novel concept for neutron detection: proportional counter filled with B nanoparticle aerosol. 2017 , 7, 41699	9
747	Monte Carlo track chemistry simulations of the radiolysis of water induced by the recoil ions of the 10B(n, 知Li nuclear reaction. 1. Calculation of the yields of primary species up to 350 ℃. 2017 , 7, 10782-10790	5
746	On the threshold for ion track formation in CaF2. 2017 , 19, 023023	14
745	L shell x ray production in high-Z elements using 4B MeV/u fluorine ions. <i>Nuclear Instruments & Methods in Physics Research B</i> , 2017 , 395, 39-51	9
744	Sulfur-Doped Silicon Photodiode by Ion Implantation and Femtosecond Laser Annealing. 2017 , 17, 2367-2371	7
743	3D map distribution of metallic nanoparticles in whole cells using MeV ion microscopy. 2017 , 267, 227-236	6
742	Structural characteristics and optical properties of methylcellulose/polyaniline films modified by low energy oxygen irradiation. 2022 , 141, 109502	4
741	Electronic excitation-induced tunneling and charge-trapping explored by in situ electrical characterization in Ni/HfO2/EGa2O3 metal®xideBemiconductor capacitors. 2022 , 281, 115716	1
740	Thick target neutron spectral yield and dose measurements with natC (p, n) system at intermediate proton energies between 8½0 MeV. 2022 , 1034, 166767	0
739	Measurements of linear energy transfer (LET) distributions by CR-39 for a therapeutic carbon ion beam with a new 2D ripple filter. 2022 , 197, 110193	
738	The effect of some modifier oxides on the radiation shielding properties of zirconia doped sodium borosilicate glasses. 2022 , 197, 110164	0
737	Effects of swift heavy ions at different fluencies on WC-6Co hard metal alloy. 2022, 106, 105865	2
736	H2 production from the radiolysis of aqueous suspensions of ZnO nanoparticles by 5.5IMeV He2+ ions. 2022 , 197, 110189	
735	Investigations of thermoluminescence characteristics of CaSiO:Yb phosphor irradiated with gamma rays and carbon ion beam 2022 , 186, 110253	
734	Study on damage mechanisms of silicon carbide Schottky barrier diode caused by heavy ion irradiation. 2022 ,	
733	Modeling Fission Spikes in Nuclear Fuel using a Multigroup Model of Electronic Energy Transport. 2022 , 153797	
732	Triple ion beam irradiation of glass-ceramic materials for nuclear fusion technology. 2022 , 153783	0

731	Preparation, microstructure and ion-irradiation damage behavior of Al4SiC4-added SiC ceramics. 2022 ,	0
73°	Pulsed laser deposition and structural evolution of BaF2 nanolayers in Eu-doped BaF2/Al2O3 layered optical nanocomposite thin films. 2022 , 139298	
729	Transport of an intense proton beam from a cone-structured target through plastic foam with unique proton source modeling. 2022 , 105,	1
728	Impact of Nd3+ladditive on the radiation shielding competence of borosilicate glasses fabricated from agro-waste materials. 2022 , 590, 121691	O
727	Friction Stir Welding and Self-Ion Irradiation Effects on Microstructure and Mechanical Properties Changes within Oxide Dispersion Strengthened Steel MA956. 2022 , 153795	
726	Electrochemical co-deposition of Nited2O3 for composite thin targets preparation: Production of 155Tb as a case study. 2022 , 110287	O
725	Xe-ion-irradiation-induced structural transitions and elemental diffusion in high-entropy alloy and nitride thin-film multilayers. 2022 , 110749	O
724	Evidence of structural changes in ion-irradiated graphene independent of the incident ions mass. 2022 , 153701	1
723	Measurement of alpha-induced reaction cross-sections on \$\$^{nat}\$\$Mo with detailed covariance analysis. 2022 , 58,	O
722	Creation of multiple NV centers by phthalocyanine ion implantation.	
721	Dosimetric characterization of an irradiation set-up for electronic components testing at the TOP-IMPLART proton linear accelerator. 2019 ,	1
720	Effect of Proton Irradiation Energy on AlGaN/GaN HEMTs fabricated by Ion-implanted Isolation. 2019 ,	
719	Vertical Line Fault Mechanism Induced by Heavy Ions in an SLC NAND Flash. 2019,	
718	EVALUATION OF THE PHASE STABILITY, MICROSTRUCTURE AND DEFECTS IN HIGH-ENTROPY CERAMICS AFTER HIGH-ENERGY ION IMPLANTATION. 2022 ,	O
717	The Effect of Deposition Conditions and Irradiation on the Structure, Substructure, Stress-Strain State, and Mechanical Properties of TiN Coatings. 2022 , 475-484	
716	Characterization and Modeling of a 1.3 kV Vertical GaN Diode. 2022 ,	
715	Experimental Demonstration of the Thin-Film Liquid-Metal Jet as a Charge Stripper. 2022, 128,	1
714	High efficiency laser-driven proton sources using 3D-printed micro-structure. 2022 , 5,	1

713	Perturbed Angular Correlation Technique at ISOLDE/CERN Applied for Studies of Hydrogenated Titanium Dioxide (TiO2): Observation of Cd-H Pairs. 2022 , 12, 756	
712	The Enhanced Swelling Resistance of W/Cu Nanocomposites by Vacancy-Type Defects Self-Recovery. 2022 , 12, 759	О
711	Thermal conductivity reduction in (Zr0.25Ta0.25Nb0.25Ti0.25)C high entropy carbide from extrinsic lattice defects. 2022 , 10, 611-617	Ο
710	Surface Modification of 304L Stainless Steel and Interface Engineering by HiPIMS Pre-Treatment. 2022 , 12, 727	1
709	Effect of Post-irradiation Annealing on Microstructure Evolution and Hardening in GH3535 Alloy Irradiated by Au Ions.	
708	Multifunctional Irradiation-Induced Defects for Enhancing Thermoelectric Properties of Scandium Nitride Thin Films.	Ο
707	Rapid, uniform, and efficient heat transfer into dense matter using energetic proton beams with finite energy spreads. 2022 , 135, 106070	0
706	Structural study of W2B obtained via mechanical alloying of W, B4C, TiC and graphite before and after He ions irradiation. 2022 , 31, 101201	1
705	Characterization of microstructure and hardening of SLM nickel-based alloy irradiated by He ions. 2022 , 566, 153794	0
704	Influence of nitrogen interstitials in E itanium and nitrogen vacancies in Eitanium nitride on lattice parameters and bulk modulus - computational study. 2022 , 211, 111509	O
703	Investigating the effect of helium ion irradiation on deformation behaviour of Ni-Mo-Cr alloy via in-situ micro-tensile testing. 2022 , 567, 153812	1
702	Improved Limit on Tensor Currents in the Weak Interaction from Li8 Decay. 2022, 128,	1
701	Intermetallic cobaltgallium targets for production of germanium radioisotopes. 2022, 110307	
700	Hybrid alpha power source. 2022 ,	
699	Thermal activation of low-density Ga implanted in Ge. 2022 , 120, 201902	1
698	Charged-particle emission in neutron reactions on B10. 2022 , 105,	
697	Development of low gain avalanche detectors (LGAD) in frame of the acceptor removal phenomenon.	
696	Modeling Radiation Damage in Materials Relevant for Exploration and Settlement on the Moon.	

695	Absolute calibration of Fujifilm BAS-TR image plate response to laser driven protons up to 40 MeV. 2022 , 93, 053303	
694	High-precision modeling of dynamic etching in high-power magnetron sputtering. 2022 , 55, 325203	O
693	Irradiation-induced microstructural transformations in UO2 accelerated upon electronic energy deposition. 2022 ,	O
692	Direct evidence of Be as an amphoteric dopant in GaN. 2022 , 105,	
691	Measurement of the Ne18(争)Na21 reaction with the ANASEN active-target detector system at . 2022 , 105,	0
690	Effect of Ultra-High-Pressure Annealing on Defect Reactions in Ion-Implanted GaN Studied by Positron Annihilation. 2200183	1
689	Role of precursor nuclei in heavy-ion induced reactions at low energies. 2022, 105,	
688	Superior radiation tolerance via reversible disorderingBrdering transition of coherent superlattices.	1
687	Ion Implantation Enhanced Exfoliation Efficiency of V2AlC Single Crystals: Implications for Large V2CTz Nanosheet Production.	
686	SHI irradiation of water ice at different temperatures: H2O2 and O3 synthesis and sputtering yield.	0
685	Radiological source terms estimation for the Divertor Tokamak Test (DTT) facility. 2022, 180, 113198	
684	Investigations of N+-ion implanted polymethylmethacrylate for flexible electronics. 2022 , 129, 112521	Ο
683	Improvements and validation of particle channeling model in GEANT4. <i>Nuclear Instruments & Methods in Physics Research B</i> , 2022 , 525, 1-12	
682	Modeling ionization quenching in organic scintillators.	O
681	Effects of Metal Hydride Coatings at the Electrodes on Neutron Production Rate in a Discharge-Type Fusion Neutron Source. 2022 , 1-6	1
680	Emerging Device Architectures for Space Electronics. 2023 , 181-208	
679	Deformation behaviour of ion-irradiated FeCr: A nanoindentation study.	
678	The reliabilities of HfO2-based ferroelectric devices under swift heavy ion irradiation.	O

677	Evaluation of neutron irradiation-induced displacement damage in heat pipe reactor. 2022, 101216	
676	A method to predict texture effect on ion beam channeling analysis of polycrystals and the application to study the mosaic spreading effect in highly oriented pyrolytic graphite. 2022 , 131, 225305	
675	DLTS study of the influence of annealing on deep level defects induced in xenon ions implanted n-type 4H-SiC.	O
674	Charge State Effects in Swift-Heavy-Ion-Irradiated Nanomaterials. 2022 , 12, 865	2
673	Enhanced ferroelectric and piezoelectricity in 100 MeV Ag7+ ion-irradiated <011>-oriented TGS single crystals. 2022 , 128,	
672	Modulating properties by light ion irradiation: From novel functional materials to semiconductor power devices. 2022 , 43, 063101	O
671	Fusion and back-angle quasielastic measurements in Si30+Gd156 near the Coulomb barrier. 2022 , 105,	
670	A broad analysis of directly and indirectly ionizing radiation interaction parameters of PbF2-CaF2-Bi2O3-B2O3-Cr2O3 glass system. 2022 , 97, 075306	O
669	P2O5Pb3O4InOIli2CO3IIuO glasses and their radiation attenuation properties for shielding applications.	1
668	Effects of Simulated Solar Wind on Polymethyl Methacrylate Thin Film. 2022 , 12, 1992	
667	Computational approach of alpha and proton interaction of gadolinium bismuth borate glass system using SRIM program. 2022 ,	1
666	Charon∃ refractory factory. 2022 , 8,	
665	Stopping-power calculations and the Levine-Mermin dielectric function for inner shells. 2022, 105,	1
664	Optical, structural, and electrical properties of modified indium-tin-oxide (ITO) films on glass surface by low energy ion implantation. 2022 , 128,	O
663	Radiation Effect in Ti-Cr Multilayer-Coated Silicon Carbide under Silicon Ion Irradiation up to 3 dpa. 2022 , 12, 832	
662	Effect of self-ion with high-energy irradiation on the surface morphology, microstructure and mechanical properties of nanocrystalline TiAlN coating. 2022 , 112041	
661	Formation of cesium carbonate in ion-implanted graphite, examined with dual-source x-ray photoelectron spectroscopy, density functional theory calculations and thermodynamic modelling. 2022 ,	
660	A photonic integrated circuitBased erbium-doped amplifier. 2022 , 376, 1309-1313	7

659	Dislocation structure of tungsten irradiated by medium to high-mass ions.	Ο
658	INFLUENCE OF THE IRRADIATION OF IONS OF DIFFERENT MASS ON THE FORMATION OF SURFACE DEFECTS OF LITHIUM FLUORIDE THIN FILMS.	O
657	Compositional Effects of Additively Manufactured Refractory High-Entropy Alloys under High-Energy Helium Irradiation. 2022 , 12, 2014	1
656	Hierarchical 2D to 3D micro/nano-histology of human dental caries lesions using light, X-ray and electron microscopy. 2022 , 220, 110829	1
655	Charge collection efficiency of scCVD diamond detectors at low temperatures. 2022, 127, 109184	
654	Linear Energy Transfer (LET) dependence of graphene oxide dosimeter for different ionizing radiations. 2022 , 203, 111240	
653	The total and the partial charge-changing cross sections of 40Ar fragmentation on elemental targets at 500 A MeV. 2022 , 1025, 122493	
652	Effects of preliminary ion beam treatment of carbon nanotubes on structures of interfaces in #multi-walled carbon nanotube (M =Ti,Sn) composites: Experimental and theoretical study. 2022 , 169, 110831	O
651	Geometrical aspects of alpha dose rates from UO2 based fuels. 2022 , 199, 110336	0
650	RDM: An R interface for high-throughput simulation of ion-material interactions using TRIM. 2022 , 279, 108451	
649	In-situ microstructure observation of oxidized SiC layer in surrogate TRISO fuel particles under krypton ion irradiation. 2022 , 920, 165833	
648	Enhanced hole transport in Ni/Y2O3/n-4H-SiC MOS for self-biased radiation detection. 2022 , 1-1	1
647	A Combined Theoretical-Experimental Investigation of Thermal Transport in Low-Dose Irradiated Thorium Dioxide.	
646	Concentric Core-Shell Tracks and Spectroscopic Properties of Srtio3 Under Intense Electronic Excitation.	
645	Spherical nanoindentation stressEtrain responses of SIMP steel to synergistic effects of irradiation by H and He ions. 2022 , 33,	0
644	Tuning Plasmonic Resonance Damping through Interfacial Defects. 2022 , 126, 11372-11379	
643	Modeling and Experimental Study of Hysteresis during the Reactive Sputter Deposition of Titanium Oxides and Nitrides Using a Pulsed DC Magnetron. 1065, 215-229	
642	Impact of Helium Ion Implantation Dose and Annealing on Dense Near-Surface Layers of NV Centers. 2022 , 12, 2234	O

641 Cu ion and adatom interaction with stainless steel and silicon. **2022**,

640	Gamma photon and charged particle shielding features of praseodymium based glass matrix. 2022 , 169629	
639	Synthesis of Nano-Oxide Precipitates by Implantation of Ti, Y and O Ions in Fe-10%Cr: Towards an Understanding of Precipitation in Oxide Dispersion-Strengthened (ODS) Steels. 2022 , 15, 4857	
638	Crystallization of A3Ln(BO3)2 (A = Na, K; Ln = Lanthanide) from a Boric Acid Containing Hydroxide Melt: Synthesis and Investigation of Lanthanide Borates as Potential Nuclear Waste Forms.	O
637	Photoluminescent Bragg curves in lithium fluoride thin films on silicon substrates irradiated with a 35 MeV proton beam. 2022 , 132, 014501	О
636	History of heavy r-process elements in galactic cosmic rays from nuclei tracks in meteorite olivine. 2022 ,	O
635	Foundations of physical vapor deposition with plasma assistance.	2
634	Superficial Si nanostructure synthesis by low-energy ion-beam- induced phase separation. 2022 , 154190	
633	Recovery and recrystallization of warm-rolled tungsten during helium thermal desorption spectroscopy annealing. 2022 , 153914	
632	A Model for Radiolysis in a Flowing-Water Target during High-Intensity Proton Irradiation.	
631	A multi-component nanocrystalline FeCrV alloy with improved mechanical properties and excellent irradiation resistance. 2022 ,	1
630	Effect of cold work deformation on irradiation hardening of vanadium alloys.	O
629	Anisotropy of the Electric Field Gradient in Two-Dimensional HMoO3 Investigated by 57Mn(57Fe) Emission MBsbauer Spectroscopy. 2022 , 12, 942	О
628	Establishment of multi-beam irradiation facility at Wuhan University. 2022 , 167202	1
627	In-depth investigation of low-energy proton irradiation effect on the structural and photoresponse properties of []-Ga2O3 thin films. 2022 , 110944	1
626	Characterization of ion-induced microstructural changes in oxygen irradiated TiBAlBV. 1-20	
625	Contribution of f -electron excitation to electronic stopping power of platinum for protons. 2022 , 106,	
624	Short-Range Charge Density Wave and Bandgap Modulation by Au-Implanted Defects in TiSe2.	

623	Microdosimetry performance of the first multi-arrays of 3D-cylindrical microdetectors. 2022, 12,	O
622	Effect of grain size on the irradiation response of grade 91 steel subjected to Fe ion irradiation at 300 IC.	O
621	Thermal Spike Responses and Structure Evolutions in Lithium Niobate on Insulator (LNOI) under Swift Ion Irradiation. 2022 , 12, 943	0
620	Changes in electric field noise due to thermal transformation of a surface ion trap. 2022 , 106,	
619	The mechanism of heavy ion incident angle on the reliability of MOS device. 2022, 135, 114604	
618	High quality low thermal budget low cost SiO2 film fabricated by O2 plasma immersion ion implantation. 2022 , 756, 139385	1
617	Simulation of radiation damage via alpha decay in BFS:PC grouts using 4He2+ ion acceleration. 2022 , 159, 106895	
616	Optical borophosphate glass system with excellent properties for radiation shielding applications. 2022 , 266, 169568	1
615	A new model for predicting proton SEE cross sections based on heavy ion data. <i>Nuclear Instruments & Methods in Physics Research B</i> , 2022 , 526, 62-67	
614	Understanding effects of chemical complexity on helium bubble formation in Ni-based concentrated solid solution alloys based on elemental segregation measurements. 2022 , 569, 153902	
613	A novel method to assess the incident angle and the LET of protons using a compact single-layer Timepix detector. 2022 , 199, 110349	O
612	Effect of Cu ion implantation on charge transport of the PbZr0.52Ti0.48O3/FAPbI3 interface. 2022 , 643, 414169	
611	Atomistically-informed modeling of point defect clustering and evolution in irradiated ThO2. 2022 , 562, 111645	О
610	A Monte Carlo simulation for studying grid inefficiency of Frisch grid ionization chamber. 2022 , 188, 110365	
609	Mechanistic insights into ion-beam induced reduction of graphene oxide: An experimental and theoretical study. 2022 , 199, 110355	
608	Effects of Au2+ irradiation induced damage in a high-entropy pyrochlore oxide single crystal. 2022 , 220, 114916	1
607	MODELING OF TIME BEHAVIOR OF H, H2 NEUTRAL DENSITIES, AND HELINE INTENSITY IN THE RF PLASMA OF THE URAGAN-3M TORSATRON. 2019 , 13-16	0
606	Exploring current conduction mechanisms in 6 MeV \$text{Si}^{3+}\$ ion irradiated Au/SiO2/beta-Ga2O3 metal-oxide-semiconductor devices. 2020 ,	O

605	Simulations of recoil trajectories in Dubna Gas-Filled Recoil Separator 2 by GEANT4 toolkit. 2022 , 17, P07033	O
604	Depth-Adjustable Magnetostructural Phase Transition in Fe60V40 Thin Films.	O
603	Microstructural changes of proton irradiated Hastelloy-N and in situ micropillar compression testing of one single grain at different local damage levels. 2022 , 153939	
602	Empirical formula and computer code for the range of charged particles with $\$Z = 2{-}103\$$ and $\$E = 2.5{-}500\$$ AMeV in aluminum.	
601	Multifunctional Metal Matrix Composites by Friction Stir Additive Manufacturing.	1
600	Measurement of mass and total kinetic energy distributions for the C12+Lu175 system. 2022 , 106,	O
599	3D Nanoscale Analysis of Implanted Deuterium in Tungsten using Atom Probe Tomography. 2022 , 28, 2102-2104	
598	Nanoindentation applied to ion-irradiated and neutron-irradiated Fe-9Cr and Fe-9Cr-NiSiP model alloys. 2022 , 132, 045101	
597	Delithiation dynamics of the LICGC electrolyte out of the voltage limits. 2022, 102207	
596	Heavy Ion Irradiation Hardening Study on 4kb arrays HfO2-based OxRAM. 2020 ,	1
595	Impact of High Particle Flux in Radiation Ground Tests with Protons. 2020,	
594	Influence Of Formation Conditions, Subsequent Annealing and Ion Irradiation on the Properties of Nanostructured Coatings Based on Amorphous Carbon with Gold, Silver and Nitrogen Additives. 2021 , 124-133	
593	Confirming the Unusual Temperature Dependence of the Electric-Field Gradient in Zn. 2022, 12, 1064	
592	68Ga-DOTATATE Prepared from Cyclotron Produced Gallium-68:An Integrated Solution from Cyclotron Vault to Safety Assessment and Diagnostic Efficacy in Neuroendocrine Cancer Patients. jnumed.121.	.263768
591	Depth Profiling of Multilayer Thin Films Using Ion Beam Techniques.	
590	Heterophase Interface and Surface Functionalization of TiO x /TiSi x Metastable Nanofilms. 2022 , 9, 2200799	O
589	Ion induced effects and defects on surface, structural and mechanical properties of Ni ion irradiated titanium. 2022 ,	
588	Nuclear magnetic resonance of Li8 ions implanted in ZnO. 2022 , 106,	O

Influence of swift heavy ions on aluminum thin films. 2022, 1855 Cuprous Oxide Thin Films Implanted with Chromium IonsDptical and Physical Properties Studies. 2022, 23, 8358 184 Directionality and head-tail recognition in the keV-range with the MIMAC detector by deconvolution of the Ionic signal. 2022, 2022, 057 185 Outgassing of implanted He via short circuit transport along phase and grain boundaries in vapor co-deposited Cu-W nanocomposites. 2022, 118306 185 Transparent Conductive Oxide Sputtering Damage on Contact Passivation in Silicon Heterojunction Solar Cells with Hydrogenated Nanocrystalline Silicon. 2200651 186 Unmasking the ResolutionIllhroughput Tradespace of Focused-Ion-Beam Machining. 2111840 187 Direct measurement of the low-energy resonances in Ne22(H)Mg26 reaction. 2022, 106, One Negative muons reveal the economic chaos of RomeBAD 68/9 Civil Wars. 2022, 14, Input Mechanism of improved crystallinity by defect-modification in proton-irradiated GaAsPN photovoltaics: Experimental and first-principle calculations approach. 2022, 132, 065701 187 Mechanism of improved crystallinity by defect-modification in proton-irradiated GaAsPN photovoltaics: Experimental and first-principle calculations approach. 2022, 132, 065701 187 Structural and chemical changes in He+ bombarded polymers and related performance properties. 2022, 132, 074701 187 Characterisation of Channel Waveguides Fabricated in an Er3+-Doped Tellurite Glass Using Two Ion Beam Techniques. 2022, 10, 337 187 SPACEDOS: AN OPEN-SOURCE PIN DIODE DOSEMETER FOR APPLICATIONS IN SPACE. 2022, 198, 611-616 On Implantation effects on the characteristics of E5a2O3 epilayers grown on sapphire by MOCVD. 2022. 187 Levitonic performance and ultrafast dynamics in defective WSe2. 2022, 121, 1083102.	587	Interfacial Cation Mixing and Microstructural Changes in Bilayer GTO/GZO Thin Films After Irradiation.	
Directionality and head-tail recognition in the keV-range with the MIMAC detector by deconvolution of the ionic signal. 2022, 2022, 057 Directionality and head-tail recognition in the keV-range with the MIMAC detector by deconvolution of the ionic signal. 2022, 2022, 057 Direct measurement Conductive Oxide Sputtering Damage on Contact Passivation in Silicon Heterojunction Solar Cells with Hydrogenated Nanocrystalline Silicon. 2200651 Unmasking the Resolution/Ilhroughput Tradespace of Focused-Ion-Beam Machining. 2111840 Direct measurement of the low-energy resonances in Ne22(AJMg26 reaction. 2022, 106, o Negative muons reveal the economic chaos of Romell AD 68/9 Civil Wars. 2022, 14, 1 Mechanism of improved crystallinity by defect-modification in proton-irradiated GaASPN photovoltaics: Experimental and first-principle calculations approach. 2022, 132, 065701 Structural and chemical changes in He+ bombarded polymers and related performance properties. 2022, 132, 074701 Characterisation of Channel Waveguides Fabricated in an Er3+-Doped Tellurite Class Using Two Ion Beam Techniques. 2022, 10, 337 SPACEDOS: AN OPEN-SOURCE PIN DIODE DOSEMETER FOR APPLICATIONS IN SPACE. 2022, 198, 611-616 o Ion implantation effects on the characteristics of EGa2O3 epilayers grown on sapphire by MOCVD. 2022, Heavy Ion irradiation induced phase transitions and their impact on the switching behavior of ferroelectric hafnia. 2022, 132, 064102 Understanding irradiation amage in high-temperature superconductors for fusion reactors using high resolution X-ray absorption spectroscopy. 2022, 3,	586	Influence of swift heavy ions on aluminum thin films. 2022,	
deconvolution of the ionic signal. 2022, 2022, 057 Outgassing of implanted He via short circuit transport along phase and grain boundaries in vapor co-deposited Cu-W nanocomposites. 2022, 118306 Transparent Conductive Oxide Sputtering Damage on Contact Passivation in Silicon Heterojunction Solar Cells with Hydrogenated Nanocrystalline Silicon. 2200651 1 Unmasking the ResolutionIllhroughput Tradespace of Focused-Ion-Beam Machining. 2111840 Direct measurement of the low-energy resonances in Ne22(III)Mg26 reaction. 2022, 106, Negative muons reveal the economic chaos of Romell AD 68/9 Civil Wars. 2022, 14, Mechanism of improved crystallinity by defect-modification in proton-irradiated GaAsPN photovoltaics: Experimental and first-principle calculations approach. 2022, 132, 065701 Structural and chemical changes in He+ bombarded polymers and related performance properties. 2022, 132, 074701 Characterisation of Channel Waveguides Fabricated in an Er3+-Doped Tellurite Glass Using Two Ion Beam Techniques. 2022, 10, 337 OBJACEDOS: AN OPEN-SOURCE PIN DIODE DOSEMETER FOR APPLICATIONS IN SPACE. 2022, 198, 611-616 Ion implantation effects on the characteristics of EG2O3 epilayers grown on sapphire by MOCVD. 2022. Heavy ion irradiation induced phase transitions and their impact on the switching behavior of Ferroelectric hafnia. 2022, 132, 064102 Understanding irradiation damage in high-temperature superconductors for fusion reactors using high resolution X-ray absorption spectroscopy. 2022, 3,	585		
co-deposited Cu-W nanocomposites. 2022, 118306 Transparent Conductive Oxide Sputtering Damage on Contact Passivation in Silicon Heterojunction Solar Cells with Hydrogenated Nanocrystalline Silicon. 2200651 Unmasking the ResolutionIII broughput Tradespace of Focused-Ion-Beam Machining. 2111840 Direct measurement of the low-energy resonances in Ne22(II) Mg26 reaction. 2022, 106, Negative muons reveal the economic chaos of RomeBAD 68/9 Civil Wars. 2022, 14, Mechanism of improved crystallinity by defect-modification in proton-irradiated GaAsPN photovoltaics: Experimental and first-principle calculations approach. 2022, 132, 065701 Structural and chemical changes in He+ bombarded polymers and related performance properties. 2022, 132, 074701 Characterisation of Channel Waveguides Fabricated in an Er3+-Doped Tellurite Glass Using Two Ion Beam Techniques. 2022, 10, 337 SPACEDOS: AN OPEN-SOURCE PIN DIODE DOSEMETER FOR APPLICATIONS IN SPACE. 2022, 198, 611-616 Jon implantation effects on the characteristics of IGa2O3 epilayers grown on sapphire by MOCVD. 2022, Heavy ion irradiation induced phase transitions and their impact on the switching behavior of ferroelectric hafnia. 2022, 132, 064102 Understanding irradiation damage in high-temperature superconductors for fusion reactors using high resolution X-ray absorption spectroscopy. 2022, 3,	584		
Solar Cells with Hydrogenated Nanocrystalline Silicon. 2200651 1 581 Unmasking the Resolution Throughput Tradespace of Focused-Ion-Beam Machining. 2111840 580 Direct measurement of the low-energy resonances in Ne22 (#L) Mg26 reaction. 2022, 106, 579 Negative muons reveal the economic chaos of Rome BAD 68/9 Civil Wars. 2022, 14, 578 Mechanism of improved crystallinity by defect-modification in proton-irradiated GaAsPN photovoltaics: Experimental and first-principle calculations approach. 2022, 132, 065701 577 Structural and chemical changes in He+ bombarded polymers and related performance properties. 2022, 132, 074701 576 Characterisation of Channel Waveguides Fabricated in an Er3+-Doped Tellurite Glass Using Two Ion Beam Techniques. 2022, 10, 337 575 SPACEDOS: AN OPEN-SOURCE PIN DIODE DOSEMETER FOR APPLICATIONS IN SPACE. 2022, 198, 611-616 574 Ion implantation effects on the characteristics of #Ga2O3 epilayers grown on sapphire by MOCVD. 2022, 575 Heavy Ion irradiation induced phase transitions and their impact on the switching behavior of ferroelectric hafnia. 2022, 132, 064102 572 Understanding irradiation damage in high-temperature superconductors for fusion reactors using high resolution X-ray absorption spectroscopy. 2022, 3,	583		
Direct measurement of the low-energy resonances in Ne22(II)Mg26 reaction. 2022, 106, Negative muons reveal the economic chaos of Rome® AD 68/9 Civil Wars. 2022, 14, Mechanism of improved crystallinity by defect-modification in proton-irradiated GaAsPN photovoltaics: Experimental and first-principle calculations approach. 2022, 132, 065701 Structural and chemical changes in He+ bombarded polymers and related performance properties. 2022, 132, 074701 Characterisation of Channel Waveguides Fabricated in an Er3+-Doped Tellurite Glass Using Two Ion Beam Techniques. 2022, 10, 337 SPACEDOS: AN OPEN-SOURCE PIN DIODE DOSEMETER FOR APPLICATIONS IN SPACE. 2022, 198, 611-616 Jon implantation effects on the characteristics of IGa2O3 epilayers grown on sapphire by MOCVD. 2022, Heavy ion irradiation induced phase transitions and their impact on the switching behavior of ferroelectric hafnia. 2022, 132, 064102 Understanding irradiation damage in high-temperature superconductors for fusion reactors using high resolution X-ray absorption spectroscopy. 2022, 3,	582		1
Negative muons reveal the economic chaos of RomeB AD 68/9 Civil Wars. 2022, 14, Mechanism of improved crystallinity by defect-modification in proton-irradiated GaAsPN photovoltaics: Experimental and first-principle calculations approach. 2022, 132, 065701 Structural and chemical changes in He+ bombarded polymers and related performance properties. 2022, 132, 074701 Characterisation of Channel Waveguides Fabricated in an Er3+-Doped Tellurite Glass Using Two Ion Beam Techniques. 2022, 10, 337 SPACEDOS: AN OPEN-SOURCE PIN DIODE DOSEMETER FOR APPLICATIONS IN SPACE. 2022, 198, 611-616 Ion implantation effects on the characteristics of EGa2O3 epilayers grown on sapphire by MOCVD. Heavy ion irradiation induced phase transitions and their impact on the switching behavior of ferroelectric hafnia. 2022, 132, 064102 Understanding irradiation damage in high-temperature superconductors for fusion reactors using high resolution X-ray absorption spectroscopy. 2022, 3,	581	Unmasking the Resolution⊞hroughput Tradespace of Focused-Ion-Beam Machining. 2111840	
Mechanism of improved crystallinity by defect-modification in proton-irradiated GaAsPN photovoltaics: Experimental and first-principle calculations approach. 2022, 132, 065701 Structural and chemical changes in He+ bombarded polymers and related performance properties. 2022, 132, 074701 Characterisation of Channel Waveguides Fabricated in an Er3+-Doped Tellurite Glass Using Two Ion Beam Techniques. 2022, 10, 337 SPACEDOS: AN OPEN-SOURCE PIN DIODE DOSEMETER FOR APPLICATIONS IN SPACE. 2022, 198, 611-616 Ion implantation effects on the characteristics of Ea2O3 epilayers grown on sapphire by MOCVD. 2022, Heavy ion irradiation induced phase transitions and their impact on the switching behavior of ferroelectric hafnia. 2022, 132, 064102 Understanding irradiation damage in high-temperature superconductors for fusion reactors using high resolution X-ray absorption spectroscopy. 2022, 3,	580	Direct measurement of the low-energy resonances in Ne22(田)Mg26 reaction. 2022 , 106,	O
photovoltaics: Experimental and first-principle calculations approach. 2022, 132, 065701 Structural and chemical changes in He+ bombarded polymers and related performance properties. 2022, 132, 074701 Characterisation of Channel Waveguides Fabricated in an Er3+-Doped Tellurite Glass Using Two Ion Beam Techniques. 2022, 10, 337 SPACEDOS: AN OPEN-SOURCE PIN DIODE DOSEMETER FOR APPLICATIONS IN SPACE. 2022, 198, 611-616 Ion implantation effects on the characteristics of EGa2O3 epilayers grown on sapphire by MOCVD. 2022, Heavy ion irradiation induced phase transitions and their impact on the switching behavior of ferroelectric hafnia. 2022, 132, 064102 Understanding irradiation damage in high-temperature superconductors for fusion reactors using high resolution X-ray absorption spectroscopy. 2022, 3,	579	Negative muons reveal the economic chaos of Rome AD 68/9 Civil Wars. 2022, 14,	1
2022, 132, 074701 Characterisation of Channel Waveguides Fabricated in an Er3+-Doped Tellurite Glass Using Two Ion Beam Techniques. 2022, 10, 337 SPACEDOS: AN OPEN-SOURCE PIN DIODE DOSEMETER FOR APPLICATIONS IN SPACE. 2022, 198, 611-616 Ion implantation effects on the characteristics of EGa2O3 epilayers grown on sapphire by MOCVD. 2022, Heavy ion irradiation induced phase transitions and their impact on the switching behavior of ferroelectric hafnia. 2022, 132, 064102 Understanding irradiation damage in high-temperature superconductors for fusion reactors using high resolution X-ray absorption spectroscopy. 2022, 3,	578		
Beam Techniques. 2022, 10, 337 SPACEDOS: AN OPEN-SOURCE PIN DIODE DOSEMETER FOR APPLICATIONS IN SPACE. 2022, 198, 611-616 Ion implantation effects on the characteristics of EGa2O3 epilayers grown on sapphire by MOCVD. 2022, Heavy ion irradiation induced phase transitions and their impact on the switching behavior of ferroelectric hafnia. 2022, 132, 064102 Understanding irradiation damage in high-temperature superconductors for fusion reactors using high resolution X-ray absorption spectroscopy. 2022, 3,	577		
Ion implantation effects on the characteristics of EGa2O3 epilayers grown on sapphire by MOCVD. 2022, Heavy ion irradiation induced phase transitions and their impact on the switching behavior of ferroelectric hafnia. 2022, 132, 064102 Understanding irradiation damage in high-temperature superconductors for fusion reactors using high resolution X-ray absorption spectroscopy. 2022, 3,	576		O
Heavy ion irradiation induced phase transitions and their impact on the switching behavior of ferroelectric hafnia. 2022, 132, 064102 Understanding irradiation damage in high-temperature superconductors for fusion reactors using high resolution X-ray absorption spectroscopy. 2022, 3,	575	SPACEDOS: AN OPEN-SOURCE PIN DIODE DOSEMETER FOR APPLICATIONS IN SPACE. 2022 , 198, 611-616	O
ferroelectric hafnia. 2022 , 132, 064102 Understanding irradiation damage in high-temperature superconductors for fusion reactors using high resolution X-ray absorption spectroscopy. 2022 , 3,	574		O
high resolution X-ray absorption spectroscopy. 2022 , 3,	573		О
Excitonic performance and ultrafast dynamics in defective WSe2. 2022 . 121. 083102	572		0
	571	Excitonic performance and ultrafast dynamics in defective WSe2. 2022 , 121, 083102	1
LaserBolid interaction studies enabled by the new capabilities of the iP2 BELLA PW beamline. 2022 57°, 29, 083102	570		0

569	Unveiling the interaction of nanopatterned void superlattices with irradiation cascades. 2022 , 118282	О
568	Thermal conductivity evaluation of ion irradiated Si3N4 and ZrN ceramics using spatial domain thermoreflectance. 2022 , 132, 075105	1
567	Monte Carlo Simulations of Superconducting Tunnel Junction Quantum Sensors for the BeEST Experiment.	
566	Mechanism of reverse gate leakage current reduction in AlGaN/GaN high-electron-mobility-transistor after 3-MeV proton irradiation. 2022 , 121, 072109	
565	Uncovering the morphological effects of high-energy Ga+ focused ion beam milling on hBN single-photon emitter fabrication. 2022 , 157, 074703	2
564	On the randomness and correlation in the trajectories of alpha particle emitted from 241Am: statistical inference based on information entropy. 2022 , 12,	
563	Visible radiophotoluminescence of colour centres in lithium fluoride: from lasers to versatile radiation sensors. 2022 , 2298, 012001	
562	Low-energy ion channeling in nanocubes.	1
561	Influence of Generated Defects by Ar Implantation on the Thermoelectric Properties of ScN.	O
560	Measurements of the Zr96(h)Mo99 cross section[for astrophysics and applications. 2022 , 106,	O
559	Comprehensive characterization of irradiation induced defects in ceria: Impact of point defects on vibrational and optical properties. 2022 , 132, 085105	O
558	Hydrogen targetry in laser-plasma physics. 2022 , 48, 645-650	
557	New data on Ho(脉) reactions and the aspects of 167Tm and 165Er production for medical use.	
556	Driving Third-Order Optical Nonlinearities in Photoluminescent Si Nanoparticles by Nitrogen Co-Implantation in a Silica Matrix. 2022 , 15, 5670	
555	1 MeV Au+ ion modification of Fe3O4-based epitaxial films. 2022 , 13, 035009	
554	Monte-Carlo-based simulation study of ion-implantation in gallium oxide devices.	
553	Role of Fermi-level depinning in quenching of V4+ related photoluminescence in semi-insulating 4H-SiC. 2022 , 37, 095024	
552	Defect engineered blue photoluminescence in ZnO:Al/TiO2 heterostructures. 2022 , 132, 065302	

551	Measuring sub-surface spatially varying thermal conductivity of silicon implanted with krypton. 2022 , 132, 075112	2
550	Microstructure Evolution of Reactor Pressure Vessel A508-3 Steel under High-Dose Heavy Ion Irradiation. 2022 , 12, 1091	O
549	Endotaxial Fe Nanoparticles in the High-Fluence Iron-Implanted Single-Crystal MgO. 2022 , 12, 1095	
548	Stopping Force Analysis of 235U Elemental Fission Product Yields for E = 0.1182.4 MeV. 2022, 184, 1-28	O
547	Structural, thermal and nuclear shielding properties of lithium lead phosphate glasses: Influence of lithium oxide additive. 2022 , 151, 104340	
546	Structural stability of REE-PO4 (REE\(\text{ISm,Tb} \) under swift heavy ion irradiation. 2022 , 527, 34-39	O
545	Processes controlling helium bubble dynamics at varying temperatures in simulated radioactive materials. 2022 , 25, 101529	
544	In-situ TEM analysis on early-stage evolution of dislocation loops in 30lkeV H2+ irradiated W. 2022 , 852, 143730	O
543	A Simple Edge Termination Design for Vertical GaN P-N Diodes. 2022 , 69, 5096-5103	2
542	Band gap engineering of the top layer of mica by organized defect formation. 2022 , 33, 102283	
542 541	Band gap engineering of the top layer of mica by organized defect formation. 2022 , 33, 102283 Conductive tracks in graphene oxide foils induced by micro beams of MeV helium ions. 2022 , 128, 109281	
		O
541	Conductive tracks in graphene oxide foils induced by micro beams of MeV helium ions. 2022 , 128, 109281 Interactions between irradiation defects and nitrogen in Fe: an integrated experimental and	0 2
54 ¹ 54 ⁰	Conductive tracks in graphene oxide foils induced by micro beams of MeV helium ions. 2022 , 128, 109281 Interactions between irradiation defects and nitrogen in Fe: an integrated experimental and theoretical study. 2022 , 239, 118227 ZnO/CdO translocation in P2O5-TeO2-ZnO ternary glass systems: A reformative enhancement tool	
541 540 539	Conductive tracks in graphene oxide foils induced by micro beams of MeV helium ions. 2022, 128, 109281 Interactions between irradiation defects and nitrogen in Fe: an integrated experimental and theoretical study. 2022, 239, 118227 ZnO/CdO translocation in P2O5-TeO2-ZnO ternary glass systems: A reformative enhancement tool for physical, optical, and heavy-charged particles attenuation properties. 2022, 268, 169807 Characterization and quenching correction for a 2D real time radioluminescent system in	2
541 540 539 538	Conductive tracks in graphene oxide foils induced by micro beams of MeV helium ions. 2022, 128, 109281 Interactions between irradiation defects and nitrogen in Fe: an integrated experimental and theoretical study. 2022, 239, 118227 ZnO/CdO translocation in P2O5-TeO2-ZnO ternary glass systems: A reformative enhancement tool for physical, optical, and heavy-charged particles attenuation properties. 2022, 268, 169807 Characterization and quenching correction for a 2D real time radioluminescent system in therapeutic proton and carbon charged beams. 2022, 345, 113781	2
541 540 539 538	Conductive tracks in graphene oxide foils induced by micro beams of MeV helium ions. 2022, 128, 109281 Interactions between irradiation defects and nitrogen in Fe: an integrated experimental and theoretical study. 2022, 239, 118227 ZnO/CdO translocation in P2O5-TeO2-ZnO ternary glass systems: A reformative enhancement tool for physical, optical, and heavy-charged particles attenuation properties. 2022, 268, 169807 Characterization and quenching correction for a 2D real time radioluminescent system in therapeutic proton and carbon charged beams. 2022, 345, 113781 Ion irradiation of supported graphene: Defect formation and atmospheric doping. 2022, 284, 115918 Simultaneous experimental verification of indirect thrust measurement method based on	2 O

532	Damage in Xe-implanted 4H-SiC under severe conditions. 2022 , 570, 153941	
531	Composition-dependent changes in mechanical property of borosilicate glass induced by electron-ion sequential irradiation. 2022 , 596, 121880	О
530	High-Fluence Multi-Energy Ion Irradiation for Testing of Materials. 2022, 15, 6443	1
529	Swift Heavy Ion-Induced Reactivity and Surface Modifications in Indium Thin Films. 2022 , 7, 31869-31876	O
528	Photon extraction enhancement of praseodymium ions in gallium nitride nanopillars.	О
527	Molecular Dynamics Simulation of Solar Wind Implantation in the Permanently Shadowed Regions on the Lunar Surface. 2022 , 49,	O
526	Concentric core-shell tracks and spectroscopic properties of SrTiO3 under intense electronic excitation. 2022 , 46, 101612	1
525	50 MeV lithium ion irradiation studies on silicon-germanium heterojunction bipolar transistors at low temperature. 2022 , 137, 114754	О
524	Investigation of radiation response for III-V binary compound semiconductors due to protons using Geant4. 2022 , 529, 38-48	О
523	In situ work function measurements of W, WO3 nanostructured surfaces. 2022 , 447, 128870	O
522	Characterising the pigment on a Mesolithic cranium from Corsica using ion beam analysis. 2022 , 529, 24-28	O
521	Physical design of the APEP beam line at CSNS. 2022 , 1042, 167431	0
520	Backgrounds and blanks in Iodine-129 measurements at the Australian National University. 2022 , 530, 8-12	О
519	An ion beam spot size monitor based on a nano-machined Si photodiode probed by means of the ion beam induced charge technique. 2022 , 205, 111392	О
518	Structure and fracture behavior of ion-beam-modified SiC-Al2O3-ZrO2 ceramic composites. 2022 , 193, 112328	1
517	Study on the reusability of fluorescent nuclear track detectors using optical bleaching. 2022, 158, 106863	0
516	TEM based applications in solid state nanopores: From fabrication to liquid in-situ bio-imaging. 2022 , 162, 103347	1

515	Effects of different silicon content on irradiation defects and hardening in 9Cr ferritic/martensitic steel. 2022 , 571, 154026	O
514	Disorder and cavity evolution in single-crystalline Ge during implantation of Sb ions monitored in-situ by spectroscopic ellipsometry. 2022 , 152, 107062	О
513	Control of the irradiation-resistant structure inside MOST films by heat effect. 2022 , 605, 154622	О
512	Hardening and ductility loss of RAFM steel CLF-1 irradiated with high-energy heavy ions. 2022 , 572, 154024	О
511	Atomistic simulation of helium diffusion and clustering in plutonium dioxide. 2022, 24, 20709-20720	1
510	The electronic stopping power of heavy targets. 2022 , 157-175	О
509	3D Thermal Spike Simulation: Swift Heavy Ion Irradiation of Embedded a-SiC Nano-Zone Inside 4H-SiC. 2022 , 25-30	О
508	Improved uranium particle analysis by SIMS using O3[primary ions.	О
507	Fragmented high-energy heavy ion beams for electronics testing. 2022, 1-1	О
506	Radiation Hardness, a New Characterization Technique and Bistability Regarding Methylammonium Containing Perovskite Solar Cells. 2022 , 135-147	О
505	Diamond surface engineering for molecular sensing with nitrogen∏acancy centers. 2022 , 10, 13533-13569	2
504	Atomic-Scale Study of He Ion Irradiation-Induced Clustering in Ezirconium.	О
503	Low-E Glass Improvement by the Understanding and Control of the Ag Growth.	О
502	Taming the Pseudoelastic Response of Nitinol Using Ion Implantation.	О
501	Latent track formation and recrystallization in swift heavy ion irradiation.	О
500	Drastic evolution of point defects in vertically grown ZnO nanorods induced by lithium ion implantation. 2022 , 24, 23858-23869	O
499	Recording of Superenergetic Electrons and Ions in the High-Current Pulsed Relativistic Electron Beam Generator. 2022 , 48, 599-605	О
498	Simulation of the Particle Transport Behaviors in Nanoporous Matter. 2022 , 14, 3563	О

497	Ion distribution and damage profile of Au irradiated GaN. 2022,	О
496	New insights on Ni-Si system for microelectronics applications. 2022 , 264, 111871	O
495	Deep Underground Laboratory Measurement of C13(舟)O. 2022 , 129,	1
494	TCAD Simulation of Single Event Effects on Electronic Devices. 2022 , 2340, 012047	O
493	Structural, morphological, and phase transformation studies of 1.4 [MeV Kr ion beam irradiated zirconia thin films.	О
492	Tailoring critical material properties of some ternary glasses through ZnO/CdO alteration: a focusing study on multiple behavioral changes. 2022 , 128,	1
491	Shockwave and spallation in silver and other materials by sub-ns laser pulse at 10 16 W/cm 2 intensity.	1
490	Versatile Approach of Silicon Nanofabrication without Resists: Helium Ion-Bombardment Enhanced Etching. 2022 , 12, 3269	O
489	Interplay of the disorder and strain in gallium oxide. 2022 , 12,	1
488	First-principles simulation of light-ion microscopy of graphene. 2022 , 9, 045023	O
488 487	First-principles simulation of light-ion microscopy of graphene. 2022 , 9, 045023 Single-Nitrogen Wacancy NMR of Amine-Functionalized Diamond Surfaces. 2022 , 22, 7294-7303	0
, i		
487	Single-Nitrogen Vacancy NMR of Amine-Functionalized Diamond Surfaces. 2022, 22, 7294-7303 Temperature evolution of dense gold and diamond heated by energetic laser-driven aluminum	1
487 486	Single-Nitrogen Wacancy NMR of Amine-Functionalized Diamond Surfaces. 2022, 22, 7294-7303 Temperature evolution of dense gold and diamond heated by energetic laser-driven aluminum ions. 2022, 12, Distribution of radial dose in water at nanometer scale for ions of the same linear energy transfer:	1 O
487 486 485	Single-Nitrogen Vacancy NMR of Amine-Functionalized Diamond Surfaces. 2022, 22, 7294-7303 Temperature evolution of dense gold and diamond heated by energetic laser-driven aluminum ions. 2022, 12, Distribution of radial dose in water at nanometer scale for ions of the same linear energy transfer: benefits of the concept of annular dose. 2022, 97, 105003	1 O
487 486 485 484	Single-Nitrogen Vacancy NMR of Amine-Functionalized Diamond Surfaces. 2022, 22, 7294-7303 Temperature evolution of dense gold and diamond heated by energetic laser-driven aluminum ions. 2022, 12, Distribution of radial dose in water at nanometer scale for ions of the same linear energy transfer: benefits of the concept of annular dose. 2022, 97, 105003 Production and characterisation of 20,22Ne targets. 2022, 96,	1 0 0
487 486 485 484 483	Single-Nitrogen Macancy NMR of Amine-Functionalized Diamond Surfaces. 2022, 22, 7294-7303 Temperature evolution of dense gold and diamond heated by energetic laser-driven aluminum ions. 2022, 12, Distribution of radial dose in water at nanometer scale for ions of the same linear energy transfer: benefits of the concept of annular dose. 2022, 97, 105003 Production and characterisation of 20,22Ne targets. 2022, 96, First experimental measurements of 2D microdosimetry maps in proton therapy. Direct measurement of the ionization quenching factor of nuclear recoils in germanium in the keV	1 0 0

479	Materials Genomics Search for Possible Helium-Absorbing Nano-Phases in Fusion Structural Materials. 2203555	О
478	Rethinking radiation effects in materials science using the plasma-focused ion beam. 2022 , 57, 16795-16808	О
477	A knock-on deuteron imager for measurements of fuel and hotspot asymmetry in direct-drive inertial confinement fusion implosions (invited). 2022 , 93, 093507	1
476	Cratering Induced by Slow Highly Charged Ions on Ultrathin PMMA Films. 2022 , 10, 96	O
475	Near-Surface Te+125 Spins with Millisecond Coherence Lifetime. 2022 , 129,	0
474	Near-Surface Electrical Characterization of Silicon Electronic Devices Using Focused keV-Range Ions. 2022 , 18,	O
473	Double-GEM based thermal neutron detector prototype. 2022 , 17, P09018	Ο
472	Effects of Sn-ion irradiation on local structure and flux pinning properties of MgB2 thin films. 2022 ,	Ο
471	Alpha-Particle Generation from H-11B Fusion Initiated by Laser-Accelerated Boron Ions. 2022 , 2022, 1-8	О
470	Diffusing alpha-emitters radiation therapy in combination with temozolomide or bevacizumab in human glioblastoma multiforme xenografts. 12,	O
469	The elasto-plastic nano- and microscale compressive behaviour of rehydrated mineralised collagen fibres.	0
468	Effects of self-irradiation on deuterium retention and reflectivity of molybdenum, fusion plasma-facing material: Combined experimental and modeling study. 2022 , 132, 125902	Ο
467	Experimental characterisation of diamond-based neutron spectrometer. 2022 , 17, T09001	О
466	Combinatorial sputter deposition of ultrathick Au-Bi alloy films.	O
465	Structural and Electrical Response of Emerging Memories Exposed to Heavy Ion Radiation. 2022 , 16, 14463-14478	0
464	Epitaxial Lateral Overgrowth of Tin Spheres Driven and Directly Observed by Helium Ion Microscopy. 2022 , 126, 16332-16340	O
463	Possible modifications of parchment during ion beam analysis. 2022 , 10,	1
462	Nuclear batteries: Current context and near-term expectations.	O

461	Room temperature fabrication of poly-crystalline Si thin films via Al-induced crystallization under 500 keV Xe+ ion irradiation. 2022 , 132, 095303	1
460	Observable consequences of self-irradiation damage in a MIMAS-type MOX nuclear fuel as analyzed by x-ray diffraction, electron microprobe analysis, and Raman imaging. A possible methodological approach. 2022 , 132, 115106	O
459	Role of Metal Selection in the Radiation Stability of Isostructural M-UiO-66 Metal Drganic Frameworks. 2022 , 34, 8403-8417	2
458	A unified model for TCAD simulation of the charge generated in semiconductors by low-energy alpha particles and protons. 2022 , 114725	O
457	Self-aligned patterning technique for fabricating high-performance diamond sensor arrays with nanoscale precision. 2022 , 8,	O
456	Model on degradation of thick solid molecular targets by energetic ion and electron beams. 2022 , 2340, 012044	O
455	Microstructural evolution, swelling and hardening of CVD-SiC induced by He ions irradiation at 650 IIC. 2022 ,	O
454	Experimental Study of Nano-Structural Coatings Formed by Microwave Plasma. 2022 , 50, 2845-2849	O
453	Tetragonal distortion modified magnetism and anomalous Hall effect of Mn2CoAl Heusler alloys through Ar ion irradiation. 2022 , 55, 475001	O
452	Ion beam stopping power effects on nuclear fusion reactions. 2022 , 29, 103103	O
451	First direct limit on the 334 keV resonance strength in $22 \$Ne($$$ alpha $$$,\$\$gamma $$$ 5)\$\$^{26}\$Mg reaction. 2022 , 58,	O
450	Measurements of the 27Al(舟) Thick Target Yield near Threshold. 1-7	O
449	Unusual charge states and lattice sites of Fe in Al x Ga1⊠ N:Mn. 2022 , 24, 103007	0
448	Recycling potential of mobile phone waste glasses for radiation shielding applications. 2022 , 110565	O
447	A peridynamic elasto-plastic damage model for ion-irradiated materials. 2022, 107806	0
446	Density changes in amorphous silicon induced by swift heavy ions. 2022 , 106,	1
445	Radiation damage on SiPMs for space applications. 2022 , 167488	0
444	Gamma-ray and charged particles shielding potency of hard/soft spinel ferrite composites.	O

443	Investigation of Ni/Y2O3/n-4H-SiC metal-oxide-semiconductor structure for high-resolution radiation detection. 2022 ,	О
442	The rapid growth of He nanobubbles in vicinity of the axis of W nanofibers under fusion-relevant He ion irradiations. 2022 , 154062	O
441	Inner-shell ionisation of Xeq+Au and Pb collision systems: MO picture. 2022 , 531, 9-23	0
440	Laser Doppler vibrometry for piezoelectric coefficient (d33) measurements in irradiated aluminum nitride. 2022 , 347, 113886	O
439	A hybrid numerical approach to the propagation of charged particle beams through matter for hadron therapy beamline simulations. 2022 , 531, 56-64	O
438	Ion implantation of 109Ag stable isotope as a tracer in SS316L biomedical implant for failure detection. 2022 , 33, 104563	O
437	A combined theoretical-experimental investigation of thermal transport in low-dose irradiated thorium dioxide. 2022 , 241, 118379	0
436	Study of HTS Nanobridge Josephson Junctions Made by FIB. 2022 , 32, 1-6	2
435	Tunable magnetic field source for magnetic field imaging microscopy. 2022 , 242, 113624	0
434	Structural, optical, and magnetic properties of Ag+, Mn+ and Ar+ ions implanted ZnO thin films: effect of implantation dose and stopping energy. 2022 , 12, 29666-29676	O
433	Damage in InGaN/GaN bilayers upon Xe and Pb swift heavy ion irradiation. 2022, 24, 25773-25787	0
432	The liquid-lithium target at the soreq applied research accelerator facility. 2022, 58,	O
431	□Nuclear-Recoil Correlation from He6 Decay in a Laser Trap. 2022 , 129,	1
430	Control of magnetoelastic coupling in Ni/Fe multilayers using He+ ion irradiation. 2022, 121, 182401	0
429	Diamond surface electric-field noise detection using shallow nitrogen-vacancy centers. 2022, 106,	0
428	Creating two-dimensional solid helium via diamond lattice confinement. 2022 , 13,	O
427	Swelling and He-Embrittlement of Austenitic Stainless Steels and Ni-Alloys in Nuclear Reactors. 2022 , 12, 1692	0
426	EBSD coupled indentation: Nanoscale mechanics of lithium metal. 2022 , 101183	Ο

425	YBa2Cu3Oy Superconducting Ceramics Incorporated with Different Types of Oxide Materials as Promising Radiation Shielding Materials: Investigation of The Structure, Morphology, and Ionizing Radiations Shielding Performances. 2022 , 12, 3490	О
424	Temperature Spectra of Interstellar Dust Grains Heated by Cosmic Rays. III. Mixed-composition Grains. 2022 , 263, 5	O
423	First inverse kinematics measurement of resonances in Be7 (田)C11. 2022 , 106,	О
422	Kilotesla plasmoid formation by a trapped relativistic laser beam. 2022 , 106,	O
421	Exploring Femtosecond Laser Ablation by Snapshot Ultrafast Imaging and Molecular Dynamics Simulation. 2022 , 2022, 1-11	1
420	Tailoring functional properties of graphene oxide by defect-assisted surface and interface modifications.	O
419	Formation of defects on the surface of LiF crystals under irradiation with different ions mass. 1-14	О
418	Computation of Gamma Buildup Factors and Heavy Ions Penetrating Depths in Clay Composite Materials Using Phy-X/PSD, EXABCal and SRIM Codes. 2022 , 12, 1512	O
417	Structural stability of EGa2O3 under ion irradiation. 2022 , 121, 171903	1
416	Supersonic Motion of Atoms in an Octahedral Channel of fcc Copper. 2022 , 15, 7260	O
415	Radiation effects on the structure and alteration behavior of an SiO 2 Δ l 2 O 3 Δ l 3 Δ l 2 O 3 Δ l 3 Δ l 2 O 3 Δ l 2 O 3 Δ l 3	0
414	K X-ray Emission for Slow Oxygen Ions Approaching a Copper Metal Surface. 2022 , 10, 124	O
413	Micropillar Compression of Additively Manufactured 316L Stainless Steels after 2 MeV Proton Irradiation: A Comparison Study between Planar and Cross-Sectional Micropillars. 2022 , 12, 1843	1
412	Multi-arrays of 3D cylindrical microdetectors for beam characterization and microdosimetry in proton therapy. 10,	O
411	Development of a simple non-destructive method to quantify low Z elements in ore samples using tantalum as an external current normalizer in external (in-air) PIGE method for Nuclear Forensic applications. 2022 , 331, 4369-4376	O
410	The Effect of Ne+ Ion Implantation on the Crystal, Magnetic, and Domain Structures of Yttrium Iron Garnet Films. 2022 , 12, 1485	O
409	New aspects of the low-energy structure of At211. 2022 , 106,	O
408	The Effects of Total Ionizing Dose on the SEU Cross-Section of SOI SRAMs. 2022 , 11, 3188	O

407	Process design for the manufacturing of soft X-ray gratings in single-crystal diamond by high-energy heavy-ion irradiation. 2022 , 137,	0
406	Methodologies for Detecting Quantal Exocytosis in Adrenal Chromaffin Cells Through Diamond-Based MEAs. 2023 , 213-221	Ο
405	Optimizing ion implantation to create shallow NV centre ensembles in high-quality CVD diamond.	О
404	Charge carrier motion and effect of fixed oxide charge in a microstructured silicon radiation detector. 2022 , 132, 164501	Ο
403	High Sensitivity Spin Defects in hBN Created by High-Energy He Beam Irradiation. 2201941	1
402	Tuning optical bandgap of crystalline MgO by MeV Co ion beam induced defects. 2022 , 128,	Ο
401	The Solar Probe ANalyzerIbns on the Parker Solar Probe. 2022 , 938, 138	1
400	Graphene oxide and manganese thiophosphate modifications induced by lasers, ion beams and intercalation process. 1-17	Ο
399	Gamma-ray cross-sections of the 27Al(p,p'I)27Al reaction in the proton energy range 1490B000[keV. 2022 , 58,	0
398	Total and Differential Sputtering Yields Explored by SRIM Simulations. 2022 , 12, 1541	O
397	Advances of LINAC-based boron neutron capture therapy in Korea. 2022, 32,	0
396	Effects of substrate rotation during AlSi-HiPIMS/Ti-DCMS co-sputtering growth of TiAlSiN coatings on phase content, microstructure, and mechanical properties. 2022 , 128986	0
395	Impact of intragranular misorientation on void swelling and inter-granular cavities after ion irradiation in standard and additive manufacturing 316 L austenitic steels. 2022 , 154102	0
394	Effects of different He+ irradiating ion energies on the evolution behavior of helium bubbles in dispersion-strengthened NiMoM2O3NP alloys. 2022 , 132, 155901	O
393	Use of combined linear and nonlinear formalisms applied to the transport of protons and secondary electrons in a Monte Carlo code: Applications for space missions. 2022 , 132, 145103	0
392	Modeling tungsten response under helium plasma irradiation: a review.	O
391	Combined Au/Ag nanoparticle creation in ZnO nanopillars by ion implantation for optical response modulation and photocatalysis. 2022 , 155556	0
390	Clinical dose assessment for scanned carbon-ion radiotherapy using linear energy transfer measurements and Monte Carlo simulations.	Ο

389	Preparation of Actinide Targets at Oregon State University.	Ο
388	Morphology and chemical state of platinum ions implanted into glassy carbon substrates. 2022 , 132, 175303	O
387	Nanostructures evolution assessment and spectroscopic properties modification induced by electronic energy loss in KTaO3 crystal. 2022 , 223, 111248	1
386	GaAs a model system to study the role of electronphonon coupling on ionization stimulated damage recovery. 2022 , 55, 505301	O
385	hPIC2: a hardware-accelerated, hybrid particle-in-cell code for dynamic plasma-material interactions. 2022 , 108569	0
384	Diamond-based sensors for in vitro cellular radiobiology: Simultaneous detection of cell exocytic activity and ionizing radiation. 2022 , 114876	O
383	Deducing Lunar Regolith Porosity From Energetic Neutral Atom Emission. 2022 , 49,	1
382	The 40Ar(d,p)41Ar cross section between 3🛭 MeV. 2022 , 190, 110509	Ο
381	Tailoring surface electronic properties of GO-TiO2 hybrid nanostructures through interface modifications. 2023 , 609, 155398	O
380	High-quality single-crystalline epitaxial regrowth on pulsed laser melting of Ti implanted GaAs. 2023 , 153, 107191	O
379	Experimental and theoretical investigation on physical, structure and protection features of TeO2B2O3 glass doped with PbO in terms of gamma, neutron, proton and alpha particles. 2023 , 202, 110586	0
378	A comprehensive study on structural properties, photon and particle attenuation competence of CoNiFeCr-Ti/Al high entropy alloys (HEAs). 2023 , 931, 167561	0
377	Structural and thermodynamic evolution of an amorphous SiOC ceramic after swift heavy ion irradiation. 2023 , 242, 118475	0
376	EFFECTIVE ATOMIC NUMBERS AND ELECTRON DENSITIES OF GEL DOSIMETERS FOR He, B, C, AND O HIGHLY CHARGED PARTICLES INTERACTION IN THE ENERGY RANGE 10 keV1100 MeV. 2021 , 16, 61-71	0
375	Feasibility study of Samarium-153 production by secondary fast neutron bombardment. 2022,	О
374	Single Event Upsets Under Proton, Thermal, and Fast Neutron Irradiation in Emerging Nonvolatile Memories. 2022 , 10, 114566-114585	Ο
373	An optimization study for targeted alpha therapy: Ion behaviours and dose calculations within ICRU-compact bone tissue. 2023 , 191, 110552	O
372	Helium and strontium co-implantation into SiC at room temperature and isochronal annealing: Structural evolution of SiC and migration behaviour of strontium. 2023 , 294, 126998	О

371	Role of ion beams and their energies in the properties of zinc tin phosphide thin films. 2023, 534, 1-10	0
370	A quantitative method to determine the region not influenced by injected interstitial and surface effects during void swelling in ion-irradiated metals. 2023 , 573, 154140	О
369	Swift heavy ion irradiation of thymine at cryogenic temperature. 2023 , 534, 11-15	0
368	A combined rate theory-population balance model of the evolution of irradiation-induced helium bubbles in metals during annealing. 2023 , 573, 154136	О
367	Measurement of X-ray production cross sections for lower-energy (0.7-3 MeV) proton induced Cu_K, Ag_L and Au_M X-rays from thick samples. 2022 , 2326, 012003	0
366	Plasma atomic layer etching of GaN/AlGaN materials and application: An overview. 2022 , 43, 113101	1
365	Enhanced irradiation-resistance of polymer-derived SiC by incorporation of multiwalled carbon nanotubes. 2022 ,	0
364	CMOS Manufacturing Processes. 2023 , 3-36	O
363	Environment-Dependent Radiation Tolerance of Graphene Transistors under Proton Irradiation. 10722-10727	0
362	Effects of swift heavy ion irradiation and annealing on the microstructure and recrystallizationof SiC pre-implanted with Sr ions. 1,	O
361	Detection of high energy ionizing radiation using deeply depleted graphene®xide®emiconductor junctions. 2022 , 132, 184503	0
360	Chemically vapor deposited oxide-based thick film scintillators.	0
359	Differential Recruitment of DNA Repair Proteins KU70/80 and RAD51 upon Microbeam Irradiation with Particles. 2022 , 11, 1652	0
358	Installation of a solid state neutral particle analyzer array on mega ampere spherical tokamak upgrade. 2022 , 93, 113517	О
357	In-situ TEM investigations on the microstructural evolution of SiC fibers under ion irradiation: Amorphization and grain growth. 2022 ,	0
356	Neon-concentration dependent retarding effect on the recrystallization of irradiated tungsten: experimental analysis and molecular dynamics simulation. 2022 ,	О
355	Spectroscopic performance of Ni/4H-SiC and Ti/4H-SiC Schottky barrier diode alpha particle detectors. 2022 , 17, P11014	О
354	Calculating the maximum possible yield for a typical pyroelectric neutron generator. 2022 , 17, P11015	O

353	Ion Lithography of Single Ions Irradiation for Spatially Regular Arrays of Pores in Membranes of Polyethylene Terephthalate. 2022 , 12, 3927	2
352	Computational simulation of the bombardment of molecular clump by realistic cosmic ray field employing GEANT4 code.	O
351	Absolute response of a proton detector composed of a microchannel plate assembly and a charge-coupled device to laser-accelerated multi-MeV protons. 2022 , 93, 113311	0
350	Structure Formation and Regulation of Au Nanoparticles in LiTaO3 by Ion Beam and Thermal Annealing Techniques. 2022 , 12, 4028	Ο
349	Electronic effects on the radiation damage in high-entropy alloys. 2022, 118511	Ο
348	ATHENA: An active target detector for the measurement of total cross sections. 2022, 167777	O
347	Ionoluminescence and optical transmission investigation of ZnO(In) fast ceramic scintillator irradiated with swift heavy ions. 2022 , 132, 195901	О
346	The Cosmic-Ray Induced Sputtering Process On Icy Grains.	O
345	Proton radiation effects on high-speed silicon Mach-Zehnder modulators for space application. 2022 , 65,	0
344	Low-E glass improvement by the understanding and control of the Ag growth. 2022, 155600	O
343	Characterisation of a monolithic E -E diamond telescope detector using low energy ion microbeams. 2022 , 159, 106875	0
342	Directional detection of dark matter using solid-state quantum sensing. 2022 , 4, 044701	O
341	Mechanical property and irradiation resistance of high entropy pyrochlore (Sm0.2Eu0.2Gd0.2Y0.2Lu0.2)2Ti2O7. 2022 , 533, 17-22	О
340	Enhanced helium ion irradiation tolerance in a Fe-Co-Ni-Cr-Al-Ti high-entropy alloy with L12 nanoparticles. 2022 ,	Ο
339	Deuterium erosion and retention properties on MoAlB ceramics by ion irradiation. 2022, 111691	О
338	Simultaneous enhancement in hardness and He-irradiation tolerance of TiVCr/W medium entropy nanolaminates. 2022 , 168114	O
337	Highly stable electrical performances of HfO2-based ferroelectric devices under proton irradiation. 2023 , 534, 45-47	Ο
336	Spatially Resolved Dynamics of Cobalt Color Centers in ZnO Nanowires. 2205304	O

335	Optimization of Reactive Ion Beam Sputtered Ta2O5 for IIIIV Compounds. 2022 , 139601	0
334	236U analyses with the ETH Zurich MILEA prototype system. 2023 , 534, 61-71	O
333	Transuranium isotopes at ISAC/TRIUMF. 2023 , 534, 90-96	O
332	Novel ultraviolet and ionizing radiation detectors made from TiO2 wide bandgap semiconductor. 2022 , 1-1	O
331	Domain State Exchange Bias in a Single Layer FeRh Thin Film Formed via Low Energy Ion Implantation.	1
330	A new multidisciplinary non-destructive protocol for the analysis of stony meteorites: gamma spectroscopy, neutron and muon techniques supported by Raman microscopy and SEM-EDS.	O
329	Total and partial charge changing cross-sections of 300 A MeV Fe26+ ion beam in different target media. 2023 , 534, 54-60	0
328	Dynamic equilibrium of displacement damage defects in heavy-ion irradiated tungsten. 2023 , 244, 118578	O
327	Ruthenium ion modification of glassy carbon: Implication on the structural evolution and migration behaviour of implanted Ru atoms. 2023 , 534, 72-80	O
326	Improved 26Al and 10Be cathode performance and data analysis at KIST. 2023 , 535, 21-28	O
325	Heavy ion irradiation effects on CrFeMnNi and AlCrFeMnNi high entropy alloys. 2023, 574, 154163	O
324	Atomic-scale study of He ion irradiation-induced clustering in ⊠irconium. 2023 , 244, 118584	O
323	Radiation transmittance of the optical SiO2-based glass system. 2023 , 273, 170385	0
322	DIGE differential cross-section data for 6Li and 19F analysis. 2023 , 535, 96-101	O
321	Energy loss of MeV protons in diamond: Stopping power and mean ionization energy. 2023 , 132, 109621	O
320	Activation cross sections of proton-induced reactions on natural platinum up to 30 MeV. 2023, 192, 110621	O
319	Excitation functions of alpha particle induced nuclear reactions on natBa up to 60 MeV. 2023 , 535, 47-54	1
318	Illustrating the atomic structure and formation mechanism of ion tracks in polyethylene terephthalate with molecular dynamics simulations. 2023 , 535, 102-111	O

317	Surface modification of low-background polymers by applying nitrogen ion implantation for electronic substrates of rare event detection. 2023 , 204, 110700	0
316	Fabrication of GaN-air channels for embedded photonic structures. 2023 , 155, 107234	O
315	Sensitivity of ion implantation to low-energy electronic stopping cross-sections. 2023, 204, 110681	0
314	Analysis of stress in sputter-deposited films using a kinetic model for Cu, Ni, Co, Cr, Mo, W. 2023 , 613, 156000	Ο
313	Structural responses of heterogeneous nanocrystalline/amorphous laminated alloy under irradiation. 2023 , 27, 101653	0
312	Shielding effectiveness of different polymers and low-density hydrides in a combined radiation shield for crewed interplanetary space missions. 2023 , 205, 110706	0
311	Structural, magnetic and gamma-ray shielding features of cerium doped Mg2FeTiO6 double perovskite. 2023 , 1276, 134762	0
310	Helium radiation blistering mechanisms in tungsten: Ion channeling effects. 2023 , 27, 101664	Ο
309	Mono-energetic Proton Induced Damages in SiC Power MOSFETs. 2022 , 1-1	0
308	Heavy-Ion-Induced Avalanche Multiplication in Low-Voltage Power VDMosfet. 2021,	O
307	Oxide Damage Induced Leakage Current Degradation in SiC MOSFETs during Heavy-ion Irradiation. 2021 ,	0
306	Measurement of the Yield of Protactinium Radioisotopes 230,232,233Pa on Irradiation of ThO2 Targets by 1,2H AND 3,4He Nuclei. 2022 , 132, 34-36	Ο
305	Strain Engineering on Lithium Niobate Crystal Based SAW Resonators Through Ion Implantation. 2022 ,	0
304	Method for Determining the Etching Rate in Phosphate Glass Detectors. 2022 , 49, 350-355	Ο
303	Study on the Lateral Scattering of High Energy Heavy Ions Penetrating through Solids.	0
302	Mixed 3DID Perovskite Flexible Films for the Direct Detection of 5 MeV Protons. 2204815	Ο
301	Study of fusionfission dynamics in 12C + 197Au system. 2022 , 137,	Ο
300	Thermomechanical responses of the drift tube to beam loss at the China spallation neutron source. 2022 , 93, 115113	O

299	Positron annihilation analysis of nanosized metal coatings Zr/Nb after He+ ion irradiation.	O
298	Repair Kinetics of DSB-Foci Induced by Proton and Particle Microbeams of Different Energies. 2022 , 12, 2040	O
297	Application of the LPE-Grown LuAG: Ce Film/YAG Crystal Composite Thermoluminescence Detector for Distinguishing the Components of the Mixed Radiation Field. 2022 , 15, 8708	0
296	Rocks, water, and noble liquids: Unfolding the flavor contents of supernova neutrinos. 2022 , 106,	1
295	Measurements of the ionization efficiency of protons in methane. 2022 , 82,	O
294	Classification of different post-hyperdoping treatments for enhanced crystallinity of IR-sensitive femtosecond-laser processed silicon.	O
293	Sputter Gas Damage in Nanolayered Pt/Co/Ir-based Synthetic Antiferromagnets for Top-Pinned Magnetic Tunnel Junctions.	0
292	Applying the Inelastic Thermal Spike Model to the Investigation of Damage Induced by High-Energy Ions in Polymers. 2200339	O
291	On the study of Cu-64 production from 18 MeV proton-induced secondary fast neutron bombardment.	0
290	Lead-free inorganic metal perovskites beyond photovoltaics: Photon, charged particles and neutron shielding applications. 2022 ,	O
289	Anisotropic superconductivity of niobium based on its response to nonmagnetic disorder. 2022 , 106,	0
288	Dislocation structure of tungsten irradiated by light ions. 2023 , 63, 026005	O
287	Organic Scintillator-Fibre Sensors for Proton Therapy Dosimetry: SCSF-3HF and EJ-260. 2023 , 12, 11	0
286	Hydrogen Diffusion in Clinopyroxene at Low Temperatures (195˚C400˚C) and Consequences for Subsurface Processes. 2022 , 23,	O
285	Reconstruction of thermoacoustic emission sources induced by proton irradiation using numerical time reversal.	O
284	Wafer-scale nanofabrication of telecom single-photon emitters in silicon. 2022 , 13,	2
283	Three-dimensional strain imaging of irradiated chromium using multi-reflection Bragg coherent diffraction. 2022 , 6,	0
282	Simulation of the Deposition of Thin-Film Materials Used in the Manufacturing of Devices with Miniaturized Circuits. 2022 , 16, 1221-1230	O

281	Effective self-healing behavior of nanocrystalline-amorphous laminated alloy under irradiation. 2022 , 132, 225105	О
280	Convolutional neural network analysis of X-ray diffraction data: strain profile retrieval in ion beam modified crystals.	O
279	A novel method for investigation of the impact of sterilization by gamma radiation on polycaprolactone scaffold. 10,	O
278	Microstructure and hardness evolution induced by annealing of ion irradiated LiTaO3. 2022, 156222	O
277	Using Metal®rganic Frameworks to Confine Liquid Samples for Nanoscale NV-NMR.	О
276	Sulfur Ion Implantations Into Condensed CO 2 : Implications for Europa. 2022 , 49,	O
275	Measurements of the Cumulative Yield of the 103Ru Radioisotope through the 100Mo(4He, n + p)103Ru Reaction and a Technique for Gas Thermal Separation of 103Ru from a 100MoO3 Target. 2022 , 65, 891-895	О
274	Heavily Doped Zinc Oxide with Plasma Frequencies in the Telecommunication Wavelength Range. 2200181	O
273	Probing the Critical Nucleus Size in the Metal-Insulator Phase Transition of VO2. 2022 , 129,	О
272	CoreBhell Nanostructures of Tungsten Oxide and Hydrogen Titanate for H2 Gas Adsorption.	2
271	Charged and uncharged radiation shielding performance of CaO+ZnO+Na2B2O7 glass system. 2022 , 110673	О
270	Energy-loss enhancement and charge-equilibration time for highly charged xenon ions at near-Bohr velocity in solids. 2022 , 106,	O
269	ESPNN: A novel electronic stopping power neural-network code built on the IAEA stopping power database. I. Atomic targets. 2022 , 132, 245103	O
268	Photon extraction enhancement of praseodymium ions in gallium nitride nanopillars. 2022 , 12,	O
267	On neutron detection with silicon carbide and its resistance to large accumulated fluence. 2022 , 137,	О
266	Lifetime measurements in the yrast band of Po212 with a shell-model investigation. 2022, 106,	O
265	On the interpretation of confocal spectral depth profiling of color center and carrier concentration by photoluminescence and Raman of implanted 4HBiC. 2022 ,	О
264	Production of monochromatic \$\${^{228}text{Ra}}\$\$ \$\$alpha \$\$-sources for detector characterization. 2022 , 137,	O

263	New Monte-Carlo based simulation program suitable for low-energy ions irradiation in pure materials. 2022 ,	O
262	Alpha backgrounds in the AMoRE-Pilot experiment. 2022 , 82,	О
261	Effect of different pre-existing dislocation densities on the microstructure evolution of W-0.5ZrC alloy during in-situ He+ irradiation. 2022 , 154206	0
260	Influence of defect dynamics on the nanoindentation hardness in NiCoCrFePd high entropy alloy under high dose Xe+3 irradiation. 2022 , 144523	o
259	Absence of ferromagnetic behaviour in Mn implanted ZnO. 2022 , 243,	0
258	Structural Damage and Recrystallization Response of Garnet Crystals to Intense Electronic Excitation. 2212853	o
257	Determining the bubble nucleation efficiency of low-energy nuclear recoils in superheated C3F8 dark matter detectors. 2022 , 106,	O
256	Tuning defect-related optical bands by channeling implants in semiconductors. 2022 , 56, 035103	О
255	Temperature dependence of germanium vacancy centers in high-quality diamond after 300 keV ion implantation. 2022 , 132, 225703	O
254	Parasitic side channel formation due to ion implantation isolation of GaN HEMT.	О
253	Radiation-induced D-to-H Exchange in Ices Containing Ethane or Benzene: Reactions and Rate Constants. 2022 , 941, 94	0
252	Impact of MeV Ni Ion-Implanted Defects in Band Modification of MgO.	О
251	Halide Perovskite Excitonic Diffraction Grating. 2202152	0
250	Helium-induced damage behaviour in hot-rolled Ni-201/Inconel 617 alloy at elevated temperature. 2022 , 101355	О
249	Timing properties of radioluminescence in nanoparticle ZnS:Ag scintillators. 2022, 100226	O
248	Facets of reaction mechanism in 6Li+181Ta system.	О
247	Probing reaction mechanisms through residual cross section measurement for 7Li+Zn system.	O
246	Damage Effects of Heavy Ion Irradiation on MOST/C Multilayer Films. 2023 , 13, 176	О

245	Surface morphology and carbon structure effects on sputtering: Bridging scales between molecular dynamics simulations and experiments. 2023 ,	O
244	In-Situ Measurement of 1.8MeV Proton Radiation Effects on Comb-Drive MEMS Resonators. 2023 , 1-1	O
243	Probing Defects and Spin-Phonon Coupling in CrSBr via Resonant Raman Scattering. 2211366	1
242	Fast neutron background characterization of the future Ricochet experiment at the ILL research nuclear reactor. 2023 , 83,	O
241	Revisiting methods for the assessment of naturally-occurring radioactivity in drinking water. 2023, 110667	O
240	Modelling simultaneous transport of natural and anthropogenic radionuclides in fractured media Diffusion into the heterogeneous layered rock matrix for an arbitrary length decay chain. 2023 , 104138	O
239	Positron annihilation studies of Eurofer97/ODS steels after helium ion implantation. 2023, 101369	0
238	Modulation of the Work Function of TiO2 Nanotubes by Nitrogen Doping: Implications for the Photocatalytic Degradation of Dyes. 2023 , 6, 50-60	O
237	Atomic-displacement threshold energies and defect generation in irradiated EGa2O3: A first-principles investigation. 2023 , 133, 015703	O
236	Optical characterization of the impact of 100 keV protons on the optical properties of ZrO2 films prepared by ALD on fused silica substrates.	O
235	Bonding, retention and thermal stability of shallow nitrogen in diamond (100) by low energy nitrogen implantation. 2023 , 102649	O
234	The Structure, Property, and Ion Irradiation Effects of Pyrochlores: A Comprehensive Review. 2023 , 13, 143	O
233	Meteorite Parent Body Aqueous Alteration Simulations of Interstellar Residue Analogs.	O
232	Fabrication and Evaluation of YBa2Cu3O7-IProbe for Scanning Probe Microscopy. 2023 , 1-4	O
231	Ionisation of inner T Tauri star discs: effects of in-situ energetic particles produced by strong magnetic reconnection events.	0
230	Spectral tracking of proton beams by the Timepix3 detector with GaAs, CdTe and Si sensors. 2023 , 18, C01022	O
229	Entrapment and thermal stability of low energy Argon implanted into diamond studied by in-situ X-ray photoelectron spectroscopy and thermal programmed desorption. 2023 , 156358	0
228	Studies on irradiated photovoltaic cells by proton beam in a plasma focus device. 2023 , 110663	O

227	Predicting and Accessing Metastable Phases.	О
226	Scanning Transmission Ion Microscopy Time-of-Flight Spectroscopy Using 20 keV Helium Ions.	Ο
225	The Microstructure of Zr/Nb Nanoscale Multilayer Coatings Irradiated with Helium Ions. 2023, 13, 193	0
224	Gas gain measurement for charged particle spectroscopy using glass GEM in low-pressure P-10 gas. 2023 , 18, P01001	O
223	Microstructural and mechanical property evolution of Ar9+ ion irradiated Zr-based alloys leffect of initial microstructure and alloying addition. 1-22	O
222	Estimating the dimensional change behavior of nuclear graphite with heavy-ion irradiation-induced bending. 2023 , 204, 357-366	O
221	Front-side and back-side secondary ion mass spectrometry analyses on advanced doping processes for ultra-large scale integrated circuit: A case study. 2023 , 766, 139654	О
220	Irradiation hardening and deuterium retention behaviour of tungsten under synergistic irradiations of 3.5 MeV Fe13+ ions and deuterium plasma. 2023 , 34, 101358	O
219	Correlation between radiation resistance and structural factors of ABO3-type perovskites. 2023 , 536, 88-96	0
218	Microstructural evolution in tungsten binary alloys under proton and self-ion irradiations at 800 IC. 2023 , 575, 154239	O
217	Development towards 53Mn Accelerator Mass Spectrometry capabilities at the University of Notre Dame. 2023 , 536, 1-6	0
216	The suppression of He bubble growth in Ni-Mo-Cr alloy by yttrium doping: Irradiation experiment combined with the first-principles calculation. 2023 , 226, 115270	O
215	Taming the Pseudoelastic Response of Nitinol Using Ion Implantation. 2023, 226, 115261	0
214	He bubble growth in nickel simulated by object kinetic Monte Carlo. 2023 , 576, 154231	O
213	GPU-accelerated artificial neural network potential for molecular dynamics simulation. 2023, 285, 108655	Ο
212	Annular energy and radial dose distributions study for a wide range of ions of different equal LET groups in water. 2023 , 206, 110771	Ο
211	Cavity evolution and void swelling in dual ion irradiated tempered martensitic steels. 2022, 154201	0
210	High conductivity EGa2O3 formed by hot Si ion implantation. 2022 , 121, 262101	O

209	Radiation-Tolerant Proton Detector Based on the MAPbBr3 Single Crystal.	0
208	Detection of ferric iron in an exsolved lunar pyroxene using electron energy loss spectroscopy (EELS): Implications for space weathering and redox conditions on the Moon.	O
207	Tuning heterogeneous ion-radiation damage by composition in NixFe1-x binary single crystals.	О
206	Cluster structure of C11 investigated with a breakup reaction. 2023 , 107,	О
205	Helium-driven element depletion and phase transformation in irradiated Ti3SiC2 at high temperature. 2023 ,	0
204	Deuteron and particle-induced nuclear reactions on 45Sc: activation cross section measurement and thick target yield evaluation.	O
203	Photovoltaics and nuclear energy conversion for space power. 2023 , 157-171	1
202	Electronic stopping power of magnesium including inner-electron excitation. 2023, 107,	O
201	Investigation of the IV characteristics of $n+/n$ homojunctions introduced by heavy ion irradiation in CdZnTe crystals.	О
200	Metal oxide barrier layers for terrestrial and space perovskite photovoltaics.	O
199	Analysis of Single Event Transients in Arbitrary Waveforms using Statistical Window Analysis. 2023, 1-1	O
198	Overview of Polyethylene Terephthalate Foils Patterned Using 10 MeV Carbon Ions for Realization of Micromembranes. 2023 , 14, 284	1
197	Natural and enriched Cr target development for production of Manganese-52. 2023, 13,	0
196	Perovskite solar cells on the horizon for space power systems. 2023 , 175-195	O
195	Development of the Dual-Beam Ion Irradiation Facility for Fusion Materials (DiFU). 2023, 16, 1144	O
194	(Na, Zr) and (Ca, Zr) Phosphate-Molybdates and Phosphate-Tungstates: II R adiation Test and Hydrolytic Stability. 2023 , 16, 965	O
193	Low-Energy Ion-Induced Single-Event Burnout in Gallium Oxide Schottky Diodes. 2023, 1-1	O
192	Proton and Electron Irradiations of CH4:H2O Mixed Ices. 2023 , 11, 19	O

191	Determination of uranium and thorium contents in various material samples of Morocco using a new Monte Carlo code for evaluating the mean critical angle of etching of the CR-39 and LR-115 type II SSNTDs. 2023 , 261, 107117	О
190	Tunable Dimensionality of Pinning Centers From Silver-Ion Irradiation of REBCO Coated Conductors. 2023 , 33, 1-5	O
189	Prospects of Searches for Unstable States in Relativistic Fragmentation of Nuclei. 2022, 85, 528-539	O
188	An Investigation on Production Routes of \$\${}^{mathbf{230}}\$\$U Radioisotope Used in Targeted Alpha Therapy by Different Level Density Models. 2022 , 77, 878-885	O
187	A novel Ni/Y2O3/4H-SiC heteroepitaxial metal@xideBemiconductor (MOS) betavoltaic cell. 2023 , 34,	O
186	Evaluation of the Minority-Carrier Lifetime of IMM3J Solar Cells under Proton Irradiation Based on Electroluminescence. 2023 , 13, 297	O
185	Compact high repetition rate Thomson parabola ion spectrometer. 2023 , 94, 023505	0
184	Oblique nanomachining of gallium arsenide explained using AFM experiments and MD simulations. 2023 , 90, 125-138	Ο
183	Surface characterization of CaF2 crystals irradiated with MeV ions below charge state equilibrium. 2023 , 536, 132-137	0
182	MACHINA, the Movable Accelerator for Cultural Heritage In-situ Non-destructive Analysis: project overview.	Ο
181	Modelling the strain build-up in nitrogen implanted tungsten films on silicon substrates. 2023 , 537, 81-87	0
180	Role of magnetic field and bias configuration on HiPIMS deposition of W films. 2023 , 458, 129343	Ο
179	Reduced He ion irradiation damage in ZrC-based high-entropy ceramics. 2023, 1-14	0
178	In situ investigation of ion irradiation-induced amorphization of (Ge2Sb2Te5)1\(\textbf{LC} \text{ (0 \textbf{Lk \textbf{D}}.12 \textbf{]}.} \) 2023 , 133, 135302	O
177	Production and characterization of a 222Rn-emanating stainless steel source. 2023 , 194, 110666	0
176	Enhancing the photocatalytic properties of doped TiO2 nanowires grown by seed-assisted thermal oxidation. 2023 , 771, 139783	O
175	High hole mobility and non-localized states in amorphous germanium. 2023, 11, 041115	0
174	Results from single event effect tests with MIMOSIS-1. 2023 , 18, C04002	Ο

173	Measurement of total and partial cross sections of the $\90 \$Zr(p, $\$$ gamma $\$$)\$ 91 \$Nb reaction with in-beam $\$$ gamma $\$$ -ray spectroscopy. 2023 , 59,	О
172	Charge stabilization of shallow nitrogen-vacancy centers using graphene/diamond junctions. 2023 , 122, 141601	О
171	Predicting electronic stopping powers using stacking ensemble machine learning method. 2023 , 538, 8-16	О
170	Performance of low-energy AMS measurement of 10Be at Tianjin University. 2023 , 538, 192-197	O
169	Formation of crystalline Si1-xGex top layers by ion implantation in crystalline silicon. 2023 , 538, 17-23	0
168	The elasto-plastic nano- and microscale compressive behaviour of rehydrated mineralised collagen fibres. 2023 ,	O
167	The effect of pre-damage distribution on deuterium-induced blistering and retention in Tungsten. 2023 , 189, 113494	1
166	Application of ion implantation as a tool to study neutron induced morphological changes in HOPG and RBMK-1500 reactor graphite. 2023 , 538, 218-226	О
165	Mechanical behavior of cold-worked, precipitation-hardened Inconel X-750 before and after helium-implantation. 2023 , 199, 112810	O
164	Deuterium and helium retention in W and W-Ta coatings irradiated with energetic ion beams. 2023 , 538, 41-46	O
163	High-energy heavy ion irradiation of HOPG. 2023 , 578, 154370	О
162	A multiscale and multiphysics framework to simulate radiation damage in nano-crystalline materials. 2023 , 578, 154347	О
161	Multilength scale characterization of point defects in thermally oxidized, proton irradiated iron oxides. 2023 , 28, 101762	О
160	A 30 MeV-cyclotron-based quasi-monoenergetic neutron source. 2023 , 55, 1559-1566	О
159	Recycling of waste cathode-ray tube glasses as building materials for shielding structures in medical and nuclear facilities. 2023 , 376, 131029	О
158	A gas-filled recoil separator, SHANS2, at the China Accelerator Facility for Superheavy Elements. 2023 , 1050, 168113	О
157	Monte Carlo simulations of ion channeling in the presence of dislocation loops: New development in the McChasy code. 2023 , 538, 198-204	О
156	Comparison of PMMA shrinkage in ion beam lithography: PMMA on glass substrate vs free-standing PMMA film. 2023 , 538, 123-130	O

155	Coulomb explosion of BeO[molecular ions [Revisited. 2023, 538, 205-211	O
154	Helium focused ion beam induced subsurface damage on Si and SiC substrates: experiments and generative deep neural network modeling via position-dependent input. 2023 , 24, 3363-3382	O
153	Surface morphologies, chemical compositions and luminescent properties of ZnO thin films flattened by ion milling procedure. 2023 , 11, 100105	0
152	Evaluation of a therapeutic carbon beam using a G2000 glass scintillator. 2023 , 196, 110753	O
151	LIME 🖪 gas TPC prototype for directional Dark Matter search for the CYGNO experiment. 2023 , 1051, 168207	0
150	Conducting surface layers formed by hydrogenation of O-implanted EGa2O3. 2023, 945, 169258	O
149	Thermal diffusivity variation assessment on Radio-Frequency Quadrupole Cu-OF copper due to proton irradiation. 2023 , 539, 179-189	0
148	The preparation of LiF target for reactions involving 7Li target. 2023 , 212, 112055	O
147	In situ studies on the evolution of damage microstructures in tungsten under heavy ion irradiation and post annealing. 2023 , 160, 104677	0
146	Microstructures, mechanical properties, and irradiation tolerance of the TiZrNbVMo refractory high-entropy alloys. 2023 , 157, 107873	O
145	Ho and Nd ion beam modifications of ZnO thin films. 2023 , 301, 127669	0
144	Simulations and analysis tools for charge-exchange (d, 2He) reactions in inverse kinematics with the AT-TPC. 2023 , 1051, 168213	O
143	Characterization and applications of highly optical transparency tellurite glasses doped with Er3+, Tm3+, and Nd3+. 2023 , 281, 170825	0
142	Measurement, evaluation and benchmarking of differential cross sections for proton elastic scattering on natO in the energy range E⊫⊈B™eV, suitable for EBS. 2023 , 539, 15-21	O
141	Effects of simultaneous proton irradiation on the corrosion of commercial alloys in molten fluoride salt. 2023 , 217, 111154	O
140	An extensive survey on radiation protection features of novel hafnium iron-borophosphate glasses: Experimental and theoretical study. 2023 , 160, 104690	O
139	Monitoring of alpha-decay radiation damage in a 241Am-doped glass-ceramic material. 2023 , 580, 154397	0
138	Mechanical design of target holder for irradiation damage experiment at high power. 2023 , 1052, 168246	Ο

137	Extraordinary radiation tolerance of a Ni nanocrystal-decorated carbon nanotube network encapsulated in amorphous carbon. 2023 , 155, 253-261	О
136	Helium bubbles in Gd2Ti2O7 borosilicate glass-ceramic composites. 2023 , 581, 154424	О
135	Prompt-gamma fall-off estimation with C-ion irradiation at clinical energies, using a knife-edge slit camera: A Monte Carlo study. 2023 , 107, 102554	O
134	Tritium-titanium target degradation due to deuterium irradiation for DT neutron production.	Ο
133	The effects of radiation-induced grain subdivision and dislocations on the fracture properties of uranium dioxide. 2023 , 577, 154297	О
132	Irradiation-induced strain localization and strain burst suppression investigated by microcompression and concurrent acoustic emission experiments. 2023 , 199, 112780	О
131	Helium ions irradiation of lantalum-zirconium carbide thin films: The effect of acetylene gas contents. 2023 , 208, 110927	О
130	Morphology and chemical composition of Si-ion-irradiated zirconolite glass-ceramic. 2023, 43, 3610-3620	O
129	Delivery of proton FLASH at the TRIUMF Proton Therapy Research Centre. 2023, 1052, 168243	О
128	Investigating changes in the diffuse reflectance spectra of BaSO4 powders modified with SiO2 nanoparticles exposed to proton irradiation. 2023 , 539, 62-67	О
127	Combining MD-LAMMPS and MC-McChasy2 codes for dislocation simulations of Ni single crystal structure. 2023 , 540, 38-44	О
126	On quantitative off-axis Scanning Transmission Ion Microscopy (STIM). 2023 , 540, 51-61	О
125	120 MeV swift Au9+ ion induced phase transition in ZrO2: monoclinic to tetragonal and cubic to tetragonal structure. 2023 , 35, 135401	О
124	Atomic displacement damage energy model up to high recoil energy. 2023 , 536, 104-112	O
123	Novel effects of grain size and ion implantation on grain boundary segregation in ion irradiated austenitic steel. 2023 , 246, 118714	O
122	Analysis of Ti nanolayers irradiated with Xeq+ ions using synchrotron radiation based X-ray reflectometry. 2023 , 536, 126-131	О
121	Deterioration of irradiation resistance of ODS-F/M steel under high concentration of helium. 2023 , 577, 154293	О
120	Radiation shielding properties of low-density Ti-based bulk metallic glass composites: a computational study. 2023 , 98, 035003	O

119	Proton radiation effects on electronic defect states in MOCVD-grown (010) EGa2O3. 2023, 133, 045702	0
118	Early-stage aqueous corrosion-related defects in heavy ion irradiated P92 ferritic/martensitic alloy. 2023 , 536, 138-143	О
117	Effect of surface modification by Ar+ ion irradiation on thermal hysteresis of VO2. 2023 , 133, 045305	0
116	Thermal versus radiation-assisted defect annealing in EGa2O3. 2023 , 41, 023101	О
115	Fabrication of single color centers in sub-50[hm nanodiamonds using ion implantation. 2023 , 12, 485-494	1
114	Effect of irradiation temperature on radiation hardening of CLF-1 steel. 2023, 189, 113488	О
113	Cosmic-ray sputtering of interstellar ices in the electronic regime. 2023 , 671, A156	0
112	Two-dimensional spin systems in PECVD-grown diamond with tunable density and long coherence for enhanced quantum sensing and simulation. 2023 , 11, 021101	О
111	Molecular dynamics simulation of surface phenomena due to high electronic excitation ion irradiation in amorphous silica. 2023 , 77,	O
110	4H-SiC Schottky diode radiation hardness assessment by IBIC microscopy. 2023 , 537, 14-22	О
109	Induction of DNA strand breaks and oxidative base damages in plasmid DNA by ultra-high dose rate proton irradiation. 1-8	0
108	Significantly improved strength and plasticity of a refractory high-entropy alloy at small length scale. 2023 , 867, 144729	O
107	Proton Bragg peak imaging by colour centre radiophotoluminescence in lithium fluoride thin film radiation detectors on silicon. 2023 , 34,	0
106	Flexible fully organic indirect detector for megaelectronvolts proton beams. 2023, 7,	1
105	Response of Bilayer and Trilayer Graphene to High-Energy Heavy Ion Irradiation. 2023, 16, 1332	O
104	Surface Characterization and Electrical Properties of Low Energy Irradiated PANI/PbS Polymeric Nanocomposite Materials. 2023 , 11, 74	O
103	Low energy irradiation induced effects on the surface characteristics of polydimethylsiloxane polymeric films. 2023 , 31, 53-63	0
102	Searches for Massive Neutrinos with Mechanical Quantum Sensors. 2023 , 4,	O

101	\Box ray emission in proton-induced nuclear reactions on natC and Mylar targets over the incident energy range, E = 30 \Box 200 MeV. Astrophysical implications. 2023 , 1032, 122622	О
100	Photoluminescent properties of the SiO2/Si system with ion-synthesized hexagonal silicon of the 9R-Si phase: Effect of post-implantation annealing. 2023 , 537, 60-64	О
99	Cyclotron production of 103Pd using a liquid target. 2023 , 118-119, 108328	О
98	A new high parallel-field spectrometer at TRIUMFEENMR facility. 2023 , 94, 023305	O
97	Electroluminescence of negatively charged single NV centers in diamond. 2023, 122, 072101	0
96	Simulation of the Irradiation Cascade Effect of 6H-SiC Based on Molecular Dynamics Principles. 2023 , 14, 455	O
95	Investigation of proton-induced excitation functions on natural tungsten up to 18 MeV. 2023 , 537, 88-94	О
94	Solar wind H+ fluxes at 1 AU for solar cycles 23 and 24. 2023 ,	O
93	Heavy Ion Displacement Damage Effect in Carbon Nanotube Field Effect Transistors. 2023 , 15, 10936-10946	0
92	Energy-efficient physical vapor deposition of dense and hard Ti-Al-W-N coatings deposited under industrial conditions. 2023 , 227, 111753	O
91	Cyclotron-Based Production of 67Cu for Radionuclide Theranostics via the 70Zn(p, № 7Cu Reaction. 2023 , 16, 314	0
90	Ion-Beam Synthesis of Structure-Oriented Iron Nanoparticles in Single-Crystalline Rutile TiO2. 2023 , 13, 355	O
89	Topography of high-speed steel substrates sputter cleaned by an Ar/Ti cathodic arc plasma. 2023 , 458, 129344	О
88	Effect of electronic stopping in molecular dynamics simulations of collision cascades in gallium arsenide. 2023 , 7,	Ο
87	Secondary particle predictions in quasifree proton scattering reactions in the 100\(\textit{\Pi}\)50 MeV energy range. 2023 , 107,	О
86	Ion Irradiation Effects on Two-Dimensional MXene Ti2C for Applications in Extreme Conditions: Combined Ab Initio and Monte Carlo Simulations. 2023 , 6, 3463-3471	О
85	The Effect of Black-Dot Defects on FeCrAl Radiation Hardening. 2023 , 13, 458	0
84	Analysis of single event effects by heavy ion irradiation of Ga2O3 metalBxideBemiconductor field-effect transistors. 2023 , 133, 085701	O

83	First application of Markov chain Monte Carlo-based Bayesian data analysis to the Doppler-shift attenuation method. 2023 , 839, 137801	0
82	Multiple Tin-Vacancy Centers in Diamond with Nearly Identical Photon Frequency and Linewidth. 2023 , 19,	O
81	Accelerator techniques and nuclear data needs for ion beam analysis of wall materials in controlled fusion devices. 2023 , 10,	O
80	The SHI irradiation induced transition to negative dielectric constant phase in K2Bi4Ti4WO18. 11,	O
79	Investigations on tissue equivalence of selected biomaterials through radiological parameters. 2023 ,	0
78	A Methodology for the Discrimination of Alpha Particles from Other Ions in Laser-Driven Proton-Boron Reactions Using CR-39 Detectors Coupled in a Thomson Parabola Spectrometer. 2023 , 2023, 1-12	O
77	141Pr(訣): New Cross-Section Data With Special Reference to 140Nd Production for Medicine. 1-12	О
76	Fabrication and characterization of high-resolution 4H-SiC epitaxial radiation detectors for challenging reactor dosimetry environments. 2023 , 278, 01003	O
75	Effects of vapor hydration and radiation on the leaching behavior of nuclear glass. 2023, 578, 154368	О
74	Tuning electrical properties in Ga2O3 polymorphs induced with ion beams. 2023 , 133, 095701	O
73	Measuring the cross sectionውf the N15(田)19F reaction using a single-fluid bubble chamber. 2023 , 107,	O
72	Online monitoring of a proton beam with perfluorinated polymer optical fibre. 2023,	O
71	Structural Properties of He-Irradiated Zr/Nb Multilayer Investigated by Grazing Incidence X-ray Diffraction. 2023 , 13, 451	0
70	Study of a planar cascaded GEM TEPC with sealed chamber for the radiation detection in microdosimetry. 2023 , 18, T03001	O
69	Dislocation density transients and saturation in irradiated zirconium. 2023, 164, 103590	О
68	Fractal characterizations of MeV ion treated CaF2 thin films. 2023 , 33, 033110	Ο
67	External Beam IBA Measurements for Cultural Heritage. 2023, 13, 3366	0
66	The contribution of inner electron excitation to the electronic stopping power of palladium for protons. 2023 , 25, 9043-9050	O

65	Structural mechanisms of enhanced mechanical properties in amorphousBanocrystalline ZrCu alloys under irradiation. 2023 , 58, 5061-5071	0
64	Hyperdoped Si nanocrystals embedded in silica for infrared plasmonics.	O
63	Neutron-induced damage simulations using MCNP6 and SRIM codes: Beyond neutron transmutation doping of silicon. 2023 , 187, 109795	0
62	Radiation Response of Large-Area 4H-SiC Schottky Barrier Diodes. 2023 , 16, 2202	О
61	Optimization for Ion Detection and Recognition From Laser-Generated Plasma Using SiC Detectors Connected in Time-of-Flight Acquisition. 2023 , 51, 747-753	0
60	Cross sections of the Rb83(p, DSr84 and . 2023 , 107,	O
59	The deposition of Ir/YSZ double-layer thin films on silicon by PLD and magnetron sputtering: Growth kinetics and the effects of oxygen. 2023 , 47, 106357	O
58	Bombardment of CO Ice by Cosmic Rays. I. Experimental Insights into the Microphysics of Molecule Destruction and Sputtering. 2023 , 944, 181	O
57	Effects of Proton Irradiation on Optocouplers with Bipolar and MOSFET Technologies, a Comparison of In-Situ and Ex-Situ Results. 2023 , 661-670	0
56	Elastic Modulus of a Carbonized Layer on Polyurethane Treated by Ion-Plasma. 2023 , 15, 1442	О
55	Atomic Delocalization in Solar Flare Heavy-Ion Tracks and Its Impact on the Plastic Deformation of CE-5 Lunar Soil.	0
54	Controlled Surface Modification to Revive Shallow NVICenters. 2023, 23, 2563-2569	O
53	Micromechanical properties of spherical and facetted He bubble loaded copper. 2023, 61, 102007	0
52	Structure Evolution of NanocrystallineAmorphous TiAl Biphase Films during Helium Ion Implantation. 2023 , 13, 632	O
51	Energetic laser-driven proton beams from near-critical-density double-layer targets under moderate relativistic intensities. 2023 , 30, 033107	0
50	Calorimetric low temperature detectors for heavy ion physics and their application in nuclear and atomic physics. 2023 , 104031	O
49	Velocity distributions of particles sputtered from supported two-dimensional MoS2 during highly charged ion irradiation. 2023 , 107,	О
48	Dynamic reactions of defects in ion-implanted 4H-SiC upon high temperature annealing. 2023 , 56, 235102	Ο

47	New experimental study of the 3He(\square)7Be reaction around the Ecm = 3 MeV resonance. 2023 , 279, 11007	О
46	Directing Exfoliation, Slipping, and Corrugation in WS 2 through Bubbling with 15 keV He 2+ Ion Irradiation.	Ο
45	Novel flexible and conformable composite neutron scintillator based on fully enriched lithium tetraborate. 2023 , 13,	0
44	Shell effect driven fission modes in fragment mass and total kinetic energy distribution of Hg*192. 2023 , 107,	O
43	225Ac-Labeled Somatostatin Analogs in the Management of Neuroendocrine Tumors: From Radiochemistry to Clinic. 2023 , 15, 1051	0
42	The CMAM facility for proton-therapy pre-clinical studies: biomaterial irradiation experiments. 2023 , 18, C03025	O
41	Segmented silicon-based solid-state detector with thin dead layer for superheavy element research. 2023 , 62, 046001	0
40	Defect engineering of silicon with ion pulses from laser acceleration. 2023 , 4,	O
39	Determination of 170,172Yb(計)173,175Hf reaction cross sections间n a stacked-targe. 2023 , 107,	0
38	CoAl ₂ O ₄ Spinel Growth on SiO ₂ Substrates via Annealing of Magnetron Sputtered Thin Films. 943, 145-150	O
37	Dynamic range and dose linearity of the radiophotoluminescence intensity in lithium fluoride crystals irradiated with 2.3 and 26 MeV protons. 2023 , 259, 119833	0
36	New constraints on sodium production in globular clusters from the Na23(He3,d)Mg. 2023 , 107,	O
35	Unfolding reaction mechanisms in C12 fusion with Zr below 7 MeV/nucleon. 2023, 107,	0
34	Cross-section measurement of the Kr82(p, DRb83 reaction in inverse kinematics. 2023 , 107,	O
33	ZnS-Based Neutron and Alpha Radiation Detectors. 2023 , 75-108	0
32	Negative muons for the characterization of thin layers in Cultural Heritage artefacts. 2023 , 2462, 012003	O
31	Evolution and characteristics of defect clusters in H2+ irradiated Al-based Gd2O3IW composites used as spent fuel shielding materials. 2023 , 34, 101295	0
30	Near-surface dynamics of the ionic liquid EMIM-Ac above and below the glass transition. 2023 , 2462, 012051	О

29	Search for a space charge layer in thin film battery materials with low-energy muons. 2023, 2462, 012046	О
28	8Li MMR studies of Epitaxial Thin Films of the 3D topological Dirac semimetal Sr3SnO. 2023 , 2462, 012057	O
27	8Li Spin Relaxation as a Probe of the Modification of Molecular Dynamics by Inelastic Deformation of Glassy Polystyrene. 2023 , 2462, 012053	О
26	Dynamic evolution of polyhedral bubbles in Fe9Cr1.5W0.4Si F/M steel under 30keV H2+& He+synergetic irradiation. 2023 , 580, 154425	O
25	Simulation of ion optics in a gas-filled solenoid GASSOL. 2023 , 1052, 168263	О
24	Investigation of the effect of cement type on nuclear shield performance of heavy concrete. 2023 , 209, 110954	O
23	Post-Bragg Peak keV-Secondary Electron Radiolysis Revealed by Track-Ends Imaging of High-Energy Protons	O
22	An experimental study of proton implantation in olivine. 2023 , 50,	O
21	MARGE has new ModulAr Robotic Gas-jet targEt system for chemistry studies with homologues of superheavy elements. 2023 , 1052, 168280	О
20	Europium diffusion in ammonothermal gallium nitride. 2023 , 625, 157188	О
19	Cluster formation by the precise joining of iron oxide nanoparticles on low energy nitrogen ion irradiation. 1-14	О
18	Plasma-stimulated great reduction of diffusion activation energies for B, Al, and Ag in Si. 2023 , 98, 055929	О
17	Effects of Ion Irradiation on Modifying Surface Characteristics and Dielectric Properties of PVA Polymeric Materials. 2023 , 12, 043007	О
16	Tailoring the Angular Mismatch in MoS 2 Homobilayers through Deformation Fields.	O
15	Subsurface Characteristics of Metal-Halide Perovskites Polished by an Argon Ion Beam. 2023 , 127, 7461-7470	О
14	Non-destructive measurement of the beryllium thickness of the iBNCT neutron-generation target using negative muons. 2023 , 168291	О
13	Near infrared photoluminescence of Si1⊠Gex quantum dots fabricated by double hot Ge+/Si+ implantation into SiO2 layer. 2023 , 133, 145703	О
12	Defect annealing in heavy-ion irradiated tungsten: Long-time thermal evolution of saturated displacement damage at different temperatures. 2023 , 581, 154454	0

11	Relative In-flight Response of IBEX-Lo to Interstellar Neutral Helium Atoms. 2023, 266, 2	O
10	Recoil Proton Telescopes and Parallel Plate Avalanche Counters for the 235U(n,f) cross section measurement relative to H(n,n)H between 10 and 450 MeV neutron energy. 2023 , 18, P04024	Ο
9	Insights into nanoparticle shape transformation by energetic ions. 2023, 13,	О
8	Isotopically Enriched Layers for Quantum Computers Formed by 28Si Implantation and Layer Exchange.	O
7	Low-energy protons shallow spread-out Bragg peak imaging with a lithium fluoride crystal. 2023 , 540, 74-79	0
6	Ion irradiation induced direction of collapsed hard-magnetization axis in thin Co films. 2023, 107,	O
5	10Be at iThemba LABS using a silicon nitride membrane stack as absorber for isobar suppression. 2023 , 540, 102-109	О
4	Cyclotron production of 43Sc and 44gSc from enriched 42CaO, 43CaO, and 44CaO targets. 11,	O
3	Transport and trap states in proton irradiated ultra-thick EGa2O3. 2023, 41,	О
2	Ion beam engineering of implanted ZnO thin films for solar cell and lighting applications. 2023 , 15, 100501	Ο
1	Investigation of 22Mg levels via resonant scattering of 18Ne + ⊞11,	O